

THEORETICAL INVESTIGATION OF IRIDIUM (II) SULFIDES

$\text{Ir}_2(\mu\text{-S})_2(\text{PH}_3)_4$ AND $\text{Ir}_2(\mu\text{-S})_2(\text{PPh}_3)_4$

A Thesis

by

STELLA KRITIKOU

Submitted to the Office of Graduate and Professional Studies of
Texas A&M University
in partial fulfillment of the requirements for the degree of

MASTER OF SCIENCE

Chair of Committee,	Michael B. Hall
Committee Members,	Danny Yeager
	Simon North
	Dimitri Nanopoulos
Head of Department,	David H. Russell

May 2014

Major Subject: Chemistry

Copyright 2014 Stella Kritikou

ABSTRACT

Density functional theory results of the electronic structure of an iridium sulfide, $\text{Ir}_2\text{S}_2(\text{PPh}_3)_4$ (**2**), are presented here, along with a discussion of the reaction mechanism of dihydrogen activation on this sulfide. This Ir (II) sulfide shows unusual reactivity binding two equivalents of H_2 . The first reaction was believed to be a homolytic cleavage of one H_2 , between the two iridium centers, which would produce the dihydride complex $\text{Ir}_2(\text{PPh}_3)_2\text{H}_2(\mu\text{-S})_2$ (**3**), while the second-product was believed to arise from heterolytic cleavage by (**3**) of a second H_2 , between an iridium and a bridging-sulfur atom, which would produce $\text{Ir}_2(\mu\text{-S})(\mu\text{-SH})(\mu\text{-H})\text{H}_2(\text{PPh}_3)_4$ (**4**). Previously published crystal structures on (**2**) and (**3**) suggest that there is a strong metal-metal bond in the Ir(II) d^7 dimer, (**2**), and that this bond is surprisingly preserved in the first H_2 cleavage product, (**3**). We investigated the activation of H_2 by this Ir(II) complex, and the corresponding model complex $\text{Ir}_2(\mu\text{-S})_2(\text{PH}_3)_4$, in order to determine the details of this pathway. Our proposed mechanism suggests that the activation of the first equivalent of hydrogen can be either heterolytic or homolytic, leading to a species with a bridging hydride $\text{Ir}_2\text{H}(\mu\text{-S})_2(\mu\text{-H})(\text{PPh}_3)_4$ (**3-brid**) in which the metal-metal bond is preserved, while the second activation appears to be a heterolytic activation, which produces the final product (**4**).

To my brother, Parthenis.

ACKNOWLEDGEMENTS

I would first like to thank my committee chair, Dr. Hall for his guidance and support throughout these two years. He has been an incredible advisor, helping me in each step of graduate school and life. I would particularly like to thank him for his valuable advice during my decision to pursue a research program that fits my scientific interests; I would not be able to complete this transition without him.

I would also like to thank Dr. Yeager, for his moral and academic support during those 2 years. He has been an excellent mentor, encouraging me not to give up on my quest to become the best quantum chemist I can be.

A special thanks to Dr. North for being an amazing teacher. He taught me how to think practically, reminded me to think simply, and reignited my interest in experimental physical chemistry. (He also “introduced me” to one of the best coffee places in town; I will be eternally thankful for that!)

I would also like to acknowledge Dr. Nanopoulos, for letting me explore my deep appreciation of physics. I am honored to have attended his lectures for a year; he conveys irresistible enthusiasm for his research field.

Thanks to all my friends for always being here for me, even if they were thousands miles away. Also, thank you to all the group members of the Hall group, for helping me with everyday problems as well as in in times of computational crisis.

I would finally like to thank my family for their encouragement, endless support and love. I would have never completed this work without you.

NOMENCLATURE

MO	Molecular Orbitals
HF	Hartree-Fock
BSSE	Basis Set Superposition Error
CI	Configuration Interaction
CIS	Configuration Interaction Singles
MCSCF	Multi Configuration Self-Consistent Field
PT	Perturbation Theory
CC	Coupled Cluster
CCSD(T)	Coupled Cluster Singles Doubles and perturbative Triples
TS	Transition State
DFT	Density Functional Theory
KS	Kohn-Sham
LDA	Local Density Approximation
GGA	Generalized Density Approximation
LSDA	Local Spin-Density Approximation
ECP	Effective Core Potential

TABLE OF CONTENTS

	Page
ABSTRACT	ii
DEDICATION	iii
ACKNOWLEDGEMENTS	iv
NONMENCLATURE	vi
TABLE OF CONTENTS	vii
LIST OF FIGURES	ix
LIST OF TABLES	xi
1 INTRODUCTION	1
1.1 Hydrogen Activation	1
2 THEORETICAL METHODS	9
2.1 Schrödinger's Equation	9
2.2 Born-Oppenheimer Approximation	12
2.3 Variational Principle	13
2.4 Hartree-Fock Formulation	14
2.5 Basis Sets	16
2.6 Correlation Energy And Post Hartree-Fock Methods	24
2.7 Density Functional Theory	32
3 THEORETICAL INVESTIGATION OF $\text{Ir}_2(\mu\text{-S})_2(\text{PH}_3)_4$ and $\text{Ir}_2(\mu\text{-S})_2(\text{PPh}_3)_4$	38
3.1 Experimental Information	38
3.2 Computational Details	41
3.3 Model System $\text{Ir}_2(\mu\text{-S})_2(\text{PH}_3)_4$	43
3.4 Full Ligand System $\text{Ir}_2(\mu\text{-S})_2(\text{PPh}_3)_4$	49

4 SUMMARY AND CONCLUSIONS.....	78
REFERENCES.....	80
APPENDICES.....	87
Appendix A: Geometrical Parameters of Isomers of the Model System.	87
Appendix B: Geometrical Parameters of Isomers of the Full Ligand System.	97

LIST OF FIGURES

		Page
Figure 1.1	Orbital interactions between H ₂ and C ₂ H ₄	4
Figure 1.2	Orbital representation for H ₂ activation by transition metal catalysts.	5
Figure 1.3	Addition of H ₂ to the ML ₅ fragment.	6
Figure 1.4	Hydrogen activation schemes.....	7
Figure 1.5	Transition state geometries of H ₂ addition.....	8
Figure 2.1	Gaussian type orbitals (GTOs) – product.....	19
Figure 2.2	Gaussian type orbitals (GTOs) – cusp.....	20
Figure 2.3	Polarization of a p-orbital by mixing with a d-function.....	22
Figure 2.4	Oscillating behavior of results obtained with the MP method.....	29
Figure 3.1	Proposed mechanism for the H ₂ activation on iridium center.....	39
Figure 3.2	Optimized structures 2', 4' and 4*'.....	43
Figure 3.3	Five lowest energy isomers of 3'.....	45
Figure 3.4	Optimized structures for 2 (left) and 3-crst (right).....	49
Figure 3.5	Reported crystal structures for 2 (left) and 3 (right).	50
Figure 3.6	Optimized intermediates from a homolytic activation of H ₂ on 2.	53
Figure 3.7	Optimized intermediates from a heterolytic activation of H ₂ on 2.	54
Figure 3.8	First step of a possible scheme for homolytic H ₂ activation on 2.	57
Figure 3.9	Optimized isomer (3-dbIr) with the BP86 functional.	58
Figure 3.10	Possible reaction scheme for homolytic H ₂ activation on 2.....	58

Figure 3.11	Possible reaction scheme for heterolytic H ₂ activation on 2.	59
Figure 3.12	Optimized intermediates from the second activation of H ₂	62
Figure 3.13	Possible reaction schemes for H ₂ activation on 3-crst.	65
Figure 3.14	Possible reaction scheme for H ₂ activation on 3-brid.	67
Figure 3.15	Proposed mechanisms for H ₂ activation on Ir ₂ (μ-S) ₂ (PPh ₃) ₄	69
Figure 3.16	Electronic profile for the proposed mechanisms a, b and c.	73
Figure 3.17	Geometries of TS 1 (left) and TS 2 (right).	75

LIST OF TABLES

		Page
Table 1.1	Bond Dissociation Energies for H-X Bonds	2
Table 3.1	Relative Gas Phase Energies of Optimized Model System Structures	46
Table 3.2	Ir-Ir Bond Length for Optimized Model System Structures	47
Table 3.3	Absolute Gas Phase Electronic Energies of Optimized Model System Structures.....	48
Table 3.4	Geometrical Parameters for 2.....	50
Table 3.5	Geometrical Parameters for 3-crst.....	51
Table 3.6	Iridium-Iridium Bond Length in 2 and 3-crst.....	52
Table 3.7	Relative Gas Phase Energies of Reactant and First Product Isomers	55
Table 3.8	Absolute Gas Phase Energies of 3-brid.....	56
Table 3.9	Absolute Gas Phase Energies of 3-crst	56
Table 3.10	Relative Gas Phase Energies of 3-brid and 3-crst.....	61
Table 3.11	Relative Gas Phase Energies of Reactant and Second Product Isomers ...	64
Table 3.12	Iridium-Iridium Bond Length in 2 and 3-crst.....	72
Table 3.13	Geometrical Parameters for 3 (reported crystal structure) and 3-brid (optimized structure)	72
Table 3.14	Relative Solvated Energies of Full Ligand System Isomers	76
Table 3.15	Difference between Gas Phase Energies and Solvated Energies of Full Ligand System.....	77

1 INTRODUCTION

Hydrogen is the lightest and the most abundant element in the universe. In our environment, hydrogen atoms exist in chemical compounds such as hydrocarbons and water, rather than in its elemental form. Hydrogen gas can be produced commercially by many different methods, such as electrolysis of water, gasification of coal, and steam reformatting of natural gas¹. Hydrogen gas is utilized in industry, mainly for hydrogenation reactions (reaction between molecular hydrogen H_2 and another compound or element, usually in the presence of a catalyst). Recently, though, it has also been considered a secondary energy carrier that can be developed in tandem with electricity in order to get reliable and clean energy services².

1.1. Hydrogen Activation

The H_2 molecule is not very reactive under ambient conditions, as the H-H bond is one of the strongest single bonds with a bond energy of (436 kJ/mol)³. Comparing this to other H-X bonds (Table 1.1) we can see that the H-H bond is among the strongest single bonds⁴. We can therefore see that there will be little or no thermodynamic driving force for the cleavage of the H-H bond, since most new H-X bonds generated will be weaker than the original H-H bond itself.

Table 1.1 Bond Dissociation Energies for H-X Bonds

Bond Type	Average Bond Dissociation Energy (kcal/mol)
H-F	135(1)
H-O	109.60(4)
H-H	103.25(1)
H-Cl	102.3(1)
H-C	98.3(8)
H-N	92(2)

Error in last digit is given parenthetically

In addition, hydrogen molecule is non-polar and a very poor acid. The polarity of the reacting species can often enhance the rate of a chemical reaction. The fact that H₂ is non-polar makes it a poor target for attack from either electrophiles or nucleophiles, and this results in large activation energies for H₂. Even in cases when direct reaction with H₂ is thermodynamically feasible, the rates of reactions involving H₂ can be extremely slow.

Thus, the controlled splitting this molecule into two hydrogen atoms (or a hydride and a proton) usually requires the assistance of efficient catalysts. In industrial processes, metal-based catalysts are used to activate the H-H bond, under high-temperature and high-pressure conditions. For example, platinum catalysts are used as catalysts of fuel cells, however platinum is a very expensive metal, and has limited deposits. The main advantage to the oxidation of dihydrogen, either via combustion, or electrochemically, is

that it leads only to the production of water. H_2 could be electrochemically generated via hydroelectric, solar and wind power, stored, and then potentially be burned to produce thermal or electrical power. There are numerous industrial reactions such as hydroformylation and hydrogenation that utilize dihydrogen gas as atom source or reducing agent. Understanding and controlling the activation of dihydrogen could potentially help us control and optimize the reactions. Even a small improvement in the efficiency of these reactions will equate significantly lower cost for the whole process. This makes the search of new, high efficient H_2 -activating catalysts with high efficiency the focus of many ongoing research projects.

At this point we should consider the fact that the frontier molecular orbitals (MOs) of H_2 do not permit most direct concerted reactions between with other non-metal elements, and result in high activation energies. In frontier molecular orbital theory⁵, when the symmetry of the HOMO of one reactant does not match the symmetry of the LUMO reactant (and vice versa) the activation energy is predicted to be high. The frontier MOs of H_2 are the H-H bonding HOMO and the H-H antibonding LUMO. In most cases the HOMO of the alkene, for example ethylene is not a match for the LUMO of dihydrogen and vice-versa. Therefore, this direct interaction between H_2 and C_2H_4 is expected to have a large activation barrier (Figure 1.1).

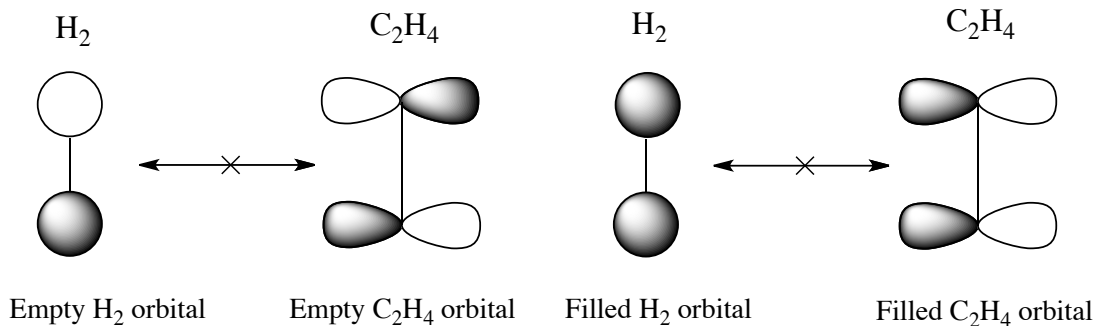


Figure 1.1 **Orbital interactions between H_2 and C_2H_4 .**
The frontier molecular orbitals of H_2 and C_2H_4 do not have the appropriate shape for a direct, concerted reaction.

Overall, we can summarize that the dihydrogen molecule is thermodynamically a powerful two-electron reductant⁶ but it's kinetically impotent due to the high H-H bond strength; ~ 104 kcal/mol.

Up to this point, we have discussed how difficult it is for a non-metal element to form a direct bond with dihydrogen. However metal centers react directly with H_2 in a concerted, direct way. The reason for this is the existence of low-lying d orbitals of the metals. According to this picture (Figure 1.2), H_2 donates a pair of electrons on the σ bonding orbital to the empty d orbital of the metal atom and the metal atom back-donates nonbonding d electrons to the antibonding orbital (σ^*) of H_2 , weakening the H-H bond.

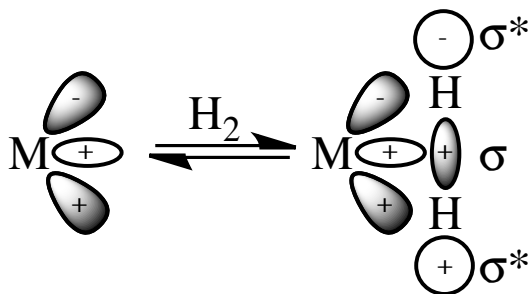


Figure 1.2 Orbital representation for H₂ activation by transition metal catalysts.

The low activation barrier of this type of direct reactions is due to the fact that the symmetry of the HOMO of H₂ matches the symmetry of the LUMO of the metal center. In addition a filled orbital of the metal center matches the symmetry of the LUMO of H₂ (Figure 1.3). The transition state for H₂ binding to the metal center is a synergistic flow of electron density from dihydrogen to the metal center and back. A low energy transition state is therefore expected for this reaction⁷.

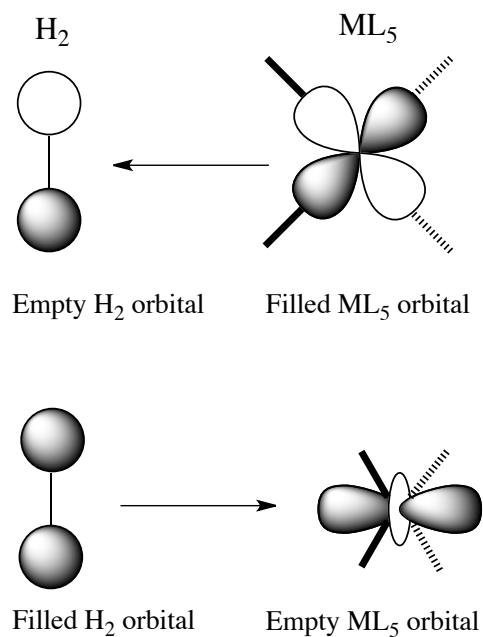


Figure 1.3 Addition of H_2 to the ML_5 fragment.

H_2 activation by transition metal compounds has been extensively studied both experimentally⁸⁻¹⁴ and theoretically¹⁵⁻²² over the last decades, and we now have a good understanding of dihydrogen activation by mononuclear transition-metal complexes. However, mechanistic studies of dihydrogen activation by multimetallic systems, which are known to exhibit striking reactivity due to cooperative functions of multinuclear metal centers, still remain rather unexplored²³⁻³⁷. The cleavage of H_2 at transition metal complexes usually occurs via two mechanisms, homolytic³⁸ or heterolytic³⁹ (Figure 1.4).

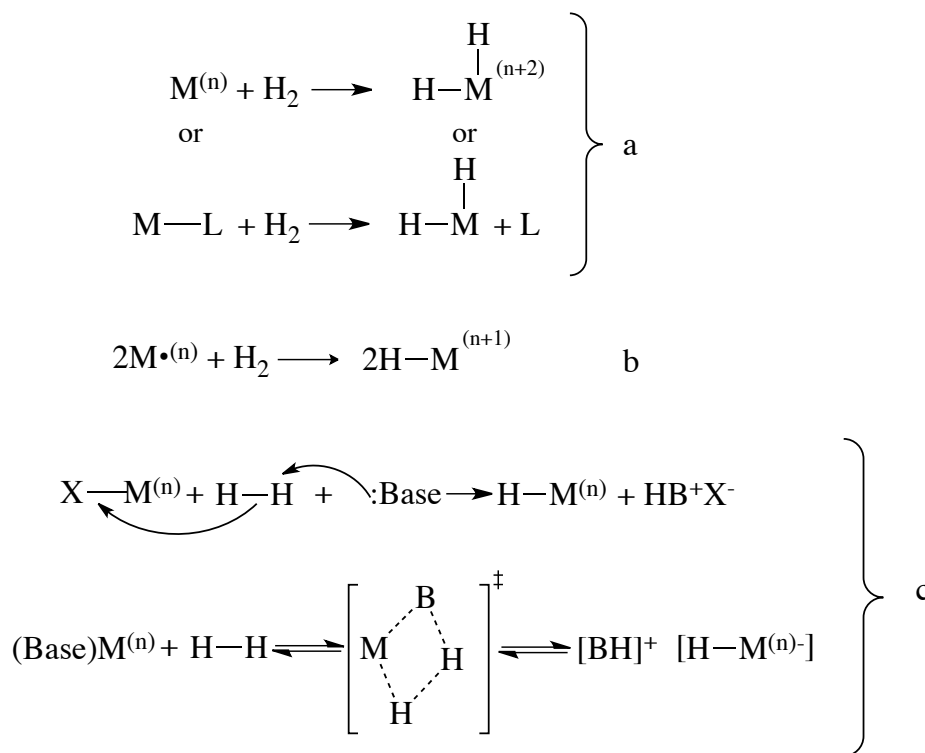


Figure 1.4 Hydrogen activation schemes.
Schemes a and b depict different oxidative addition paths and c shows two possible heterolytic hydrogen activation paths.

The homolytic cleavage involves oxidative addition at electron-rich transition metals, usually in low oxidation states, leading to two hydrides bound to the metal. Heterolytic activation is often associated with metals in higher oxidation state, and occurs with no formal change in the metal's oxidation state, giving rise to a hydride (H^- , attached to the metal), and proton (H^+ , attached to a Lewis base). Both reactions may involve a dihydrogen complex as an intermediate.

Density functional theory, along with localized molecular orbital energy decomposition analysis calculations were used in order to predict what determines the dihydrogen activation transition state geometries and reaction pathways. Those calculations revealed that the extent to which H₂ is activated in the transition state geometry depends only in back-bonding interactions and not forward-bonding orbital interactions, regardless of the mechanism and the nature of the metal (electrophile, ambiphile or nucleophile) towards H₂ (Figure 1.5)⁴⁰.

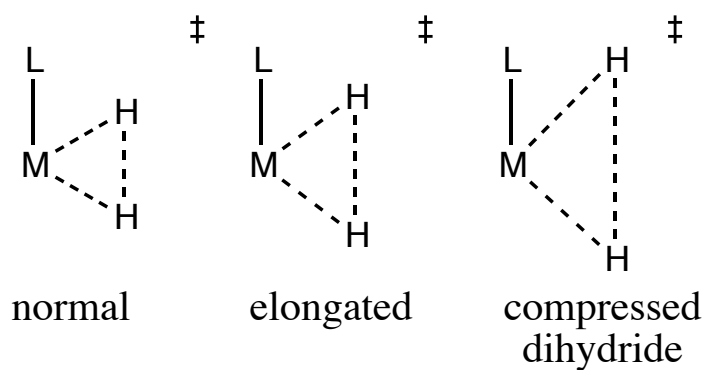


Figure 1.5 Transition state geometries of H₂ addition. Transition state geometries that correspond to different range of H-H bond lengths.

2 THEORETICAL METHODS

In the context of classical mechanics we use Newton's equation of motion in order to predict the future state of a system. The same general idea applies on quantum mechanics. We are trying to predict the future state of a system, based on the knowledge of its present state. Therefore we need an equation that can describe this temporal evolution in a quantum system of microscopic dimensions. In 1926, Erwin Schrödinger introduced the famous Schrödinger Equation that is one of the main tools of quantum mechanics. In the standard model, a wavefunction is the most complete and accurate description that can be given to a physical system.

2.1. Schrödinger's Equation

There are two forms of the Schrödinger's equation, the time dependent one, and the time independent one. In its most general form it can be written as

$$i\hbar \frac{\partial}{\partial t} \Psi(\vec{r}, t) = \hat{H} \Psi(\vec{r}, t) \quad (\text{eq. 2.1})$$

where \hat{H} is the Hamiltonian⁴¹ operator acting on the wavefunction $\Psi(\vec{r}, t)$, that describes the present state of the system. In many cases, the potential energy that is included in the Hamiltonian is time independent –something common in chemical

systems- then the equation takes the form of a standing wave, and thus it's common name, wave equation.

The wavefunction itself needs to meet some requirements: it needs to be continuous, single-valued, differentiable, and quadratically integrable and anti-symmetric⁴² since it describes fermions. In addition, its first derivative needs to be continuous as well. In order to give a physical meaning to the wavefunction we need to examine the following quantity

$$\langle \Psi(\vec{r},t) | \Psi(\vec{r},t) \rangle = \int_{\text{allspace}} |\Psi(\vec{r},t)|^2 dr \quad (\text{eq. 2.2})$$

which is the probability density, that describes the probability of the system to exist in space $[x, x + dx]$ at the moment t (Born interpretation⁴³).

In the case where there are no external forces acting on the system, the potential energy of the system is time independent, and therefore it only depends on the position r .

A way of solving this equation is to separate variables: we can express the wavefunction as a product of a spatial function and a time function, and then perform the appropriate substitutions:

$$\Psi(\vec{r}, t) = \psi(\vec{r})X(t) \quad (\text{eq. 2.3})$$

$$-\frac{\hbar^2}{2m}\nabla^2\psi(\vec{r}) + V(\vec{r})\psi(\vec{r}) = E\psi(\vec{r}) \quad (\text{eq. 2.4})$$

$$i\hbar\frac{\partial X(t)}{\partial t} = EX(t) \quad (\text{eq. 2.5})$$

$$X(t) = C \cdot e^{\frac{-iEt}{\hbar}} \quad (\text{eq. 2.6})$$

We are finally asked to solve the time independent equation, in other words to determine the spatial part of the function. As we already mentioned, the physical meaning of the wavefunction is reflected through the quantity $|\Psi|^2$.

We notice that this probability density does not depend on time, and is constant through time evolution of the system. Wavefunctions of this form, are called standing wavefunctions and the quantity $e^{\frac{-iEt}{\hbar}}$ describes the phase of the wavefunction. All systems where the potential energy is time independent are described by stationary wavefunctions.

2.2. Born-Oppenheimer Approximation

It is known for many years, that the mass difference between an electron and a proton is huge ($m_e = 0.00054897 \text{amu}$ and $m_p = 1.0072766 \text{amu}$). A proton is approximately 1827 times heavier than an electron. As a result, as the nuclei move, the electrons almost instantaneously adjust their positions, due to their almost negligible mass, comparing to that of the nuclei. This gives us the opportunity to approximate the following: The nuclei can be considered to be fixed in space, and the electrons can be considered to move due to the static potential created by the frozen nuclei. This approximation is called Born-Oppenheimer approximation. In the Hamiltonian of the system

$$\sum_{i=1}^n \frac{\hbar^2}{2m_e} \nabla_e^2 - \sum_{a=1}^N \frac{\hbar^2}{2m_n} \nabla_n^2 + \sum_{j>i} \sum_{i=1}^n k \frac{e^2}{r_{ij}} + \sum_{b>a} \sum_{a=1}^N k \frac{z_a z_b e^2}{r_{ab}} - \sum_{i=1}^n \sum_{a=1}^N k \frac{z_a e^2}{r_{ia}} \quad (\text{eq. 2.7})$$

the kinetic energy of the nuclei can be set equal to zero since the nuclei are frozen,

$$\sum_{a=1}^N \frac{\hbar^2}{2m_n} \nabla_n^2 = 0 \quad (\text{eq. 2.8})$$

and the nuclear-nuclear repulsion term

$$\sum_{b>a} \sum_{a=1}^N k \frac{z_a z_b e^2}{r_{ab}} \quad (\text{eq. 2.9})$$

can be considered a constant⁴⁴ that will be added later (with a discrete calculation) to the calculated, based on the electronic Hamiltonian energy, in order to improve the accuracy of the calculation.

The Born-Oppenheimer approximation is an essential step for solving the Schrödinger's equation due to the lack of an analytic solution for all cases other than the hydrogen and the hydrogen-like atoms. From now on the term Hamiltonian will refer to the electronic Hamiltonian of the system.

2.3. Variational Principle

The variational principle states that the energy calculated using any well-behaved trial wavefunction, will always be greater than the exact energy of the system.

$$\frac{\langle \Phi | \hat{H} \Phi \rangle}{\langle \Phi | \Phi \rangle} \geq E_0 \quad (\text{eq. 2.10})$$

In other words, the energy that we compute using an approximate wavefunction can only be an upper barrier to the true energy. In this context, the variational principle provides a criterion for evaluating wavefunctions. When we compare two trial wavefunctions, the one that produces the lower energy, provides a better result, and therefore is a better approximation. In most cases, the initial trial wavefunction is constructed using a linear

combination of two or more known functions, and the “best” wavefunction (that is still not exact) is found by systematically minimizing the energy, and changing the coefficients of the linear combination accordingly.

2.4. Hartree-Fock Formulation

The Hartree-Fock (HF) approximation is probably the most common one, when it comes to solving many-body problems in quantum mechanics, such as those encountered in electronic structure calculations. The significance of this method is even greater since it is the first step in higher-level calculations.

The factor that causes trouble in every calculation of electronic structure is the presence of the interaction cross-term (third term) in the electronic Hamiltonian of our system:

$$\hat{H} = -\sum_{i=1}^n \frac{\hbar^2}{2m_e} \nabla_e^2 - \sum_{i=1}^n \sum_{a=1}^N k \frac{z_a e^2}{r_{ia}} + \sum_{j>i}^n \sum_{i=1}^n k \frac{e^2}{r_{ij}} \quad (\text{eq. 2.11})$$

In the HF approach, this term is treated in a mean way: instead of the individual interaction between each electron, a mean interaction between each electron and the average potential created by the rest of the electrons is used.

This can be seen in the HF equations,

$$f\varphi_a(1) = \varepsilon_a\varphi_a(1) \quad (\text{eq. 2.12})$$

where ε_a is the spin-orbital energy, and f is the Fock operator.

$$f = h + \sum_u \{J_u(2) - K_u(2)\} \quad (\text{eq. 2.13})$$

In equation 2.4.3 h is the core Hamiltonian for electron 1, and the sum is over all spinorbitals $u = a, b, \dots, z$.

J_u and K_u are the Coulomb and exchange operators that are defined as

$$J_u(2)\varphi_a(1) = j_0 \left\{ \int \varphi_u^*(2) \frac{1}{r_{12}} \varphi_u(2) dx_2 \right\} \varphi_a(1) \quad (\text{eq. 2.14})$$

and

$$K_u(2)\varphi_a(1) = j_0 \left\{ \int \varphi_u^*(2) \frac{1}{r_{12}} \varphi_a(2) dx_2 \right\} \varphi_u(1) \quad (\text{eq. 2.15})$$

where

$$j_0 = \frac{e^2}{4\pi\varepsilon_0}. \quad (\text{eq. 2.16})$$

The Coulomb and exchange operators are defined in terms of spin-orbitals, and the coulomb operator accounts for the Coulombic repulsion between electrons, while the exchange operator represents the modification of the energy due to the effects of spin

correlation. Therefore, the sum in equation 2.4.3 represents the average potential energy of electron 1 due to the presence of the other $n - 1$ electrons.

Every spin orbital is the result obtained by solving a HF equation with a corresponding Fock operator. However, the Fock operator depends on the spinorbitals⁴⁵⁻⁵¹ of all electrons, so, in a way, we require the solution to the equation before hand.

These types of problems are solved using a self-consistent field approach (SCF). In an SCF approach, we start from a trial set of spinorbitals, which are used to form the Fock operator, solve HF equations and then obtain new spin orbitals and so on. The cycle of calculation and reformulation is repeated until a convergence criterion is satisfied.

2.5. Basis Sets

In the vast majority of systems, excluding small highly symmetric systems, all calculations use a basis set expansion to express the unknown MOs in terms of a set of known functions. There are many different types of basis functions that can be used, such as exponential, Gaussian, polynomial and many more, however, the basis set that one selects needs to fulfill some requirements. First of all, the basis set used should have a behavior that agrees with the physics of the problem, ensuring most of the times the convergence of the calculation as we add more functions. In addition, the chosen

functions should make calculating all required integrals easy, reducing the total time required for the calculation.

There are two main types of basis sets that are usually used. The first choice of basis functions is the Slater-type orbitals (STOs) that are exact solutions⁵¹ for the orbitals of a hydrogen-like atom. STOs are constructed as follows. An orbital with the quantum numbers n , l and m_l , that belongs to a nucleus of an atom of atomic number Z can be written as

$$\psi_{nlm_l}(r, \theta, \varphi) = N r^{n_{eff}-1} e^{-Z_{eff} \rho / n_{eff}} Y_{lm_l}(\theta, \varphi). \quad (\text{eq. 2.17})$$

In this expression, N is the normalization constant, Y_{lm_l} is a spherical harmonic and

$$\rho = \frac{r}{a_0} \cdot Z_{eff} \quad (\text{eq. 2.18})$$

is the effective nuclear charge, and n_{eff} is the effective nuclear quantum number. n_{eff} scales the principal quantum number n , to account for the shielding of the nuclear charge by the electrons.

An accurate basis set of STOs will need to consist of a large number of STOs with a large number of permitted quantum numbers and a large number of orbital exponents ζ ⁵²⁻⁵⁵. The variational principle is employed, in order to determine what the best values of ζ are. STO basis functions for atoms are centered on the atomic nucleus, and for

polyatomic species are centered on each of the atoms. There is no analytical solution available for the general four-index integral when the basis functions are STOs. Such integrals can only be solved by numerical methods, and that limits their utility in molecular systems of significant size. High quality STOs however, have been developed and are used for atomic and diatomic calculations.

The problem arising from the impractical compute of two-electron integrals, was primarily solved by using a new type of basis functions called Gaussian-type orbitals⁵⁶ (GTOs). These new basis functions played a very important role in making ab initio calculations computationally feasible. Cartesian Gaussians are functions of the general form of

$$\theta_{ijk}(r_1 - r_c) = (x_1 - x_c)^i (y_1 - y_c)^j (z_1 - z_c)^k e^{-a|r_1 - r_c|^2} \quad (\text{eq. 2.19})$$

where (x_c, y_c, z_c) are the Cartesian coordinates of the center of the Cartesian function at r_c ; (x_1, y_1, z_1) are the Cartesian coordinates of an electron at r_1 . In addition, a is a positive exponent, and i, j, k are non-negative integers. Different values of i, j, k define different types of Gaussians, for example if $i + j + k = 0$ we are dealing with an s-type Gaussian, if $i + j + k = 1$ we have a p-type Gaussian and if $i + j + k = 2$ we have a d-type Gaussian.

The main advantage of Gaussians is that any product of two Gaussians at different centers is equivalent to a single Gaussian function centered at a point between the two centers⁵⁷ (Figure 2.1).

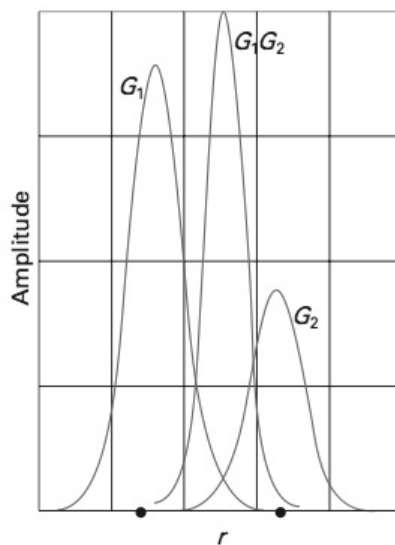


Figure 2.1 Gaussian type orbitals (GTOs) – product. The product of two Gaussians (G_1 and G_2) is itself a Gaussian (G_1G_2) centered between the two original functions. In this figure, the amplitude of the product has been multiplied by 100, for illustrative purposes (reprinted with permission from Ref. 57).

Therefore two-electron integral on three and four different atomic centers can be represented by integrals over two different centers, which are much easier to compute.

There is however a main disadvantage of GTOs, and that is the lack of cusp. A 1s atomic orbital has a cusp at the atomic nucleus, which is present at the n-1 STO but not at the GTO (Figure 2.2).

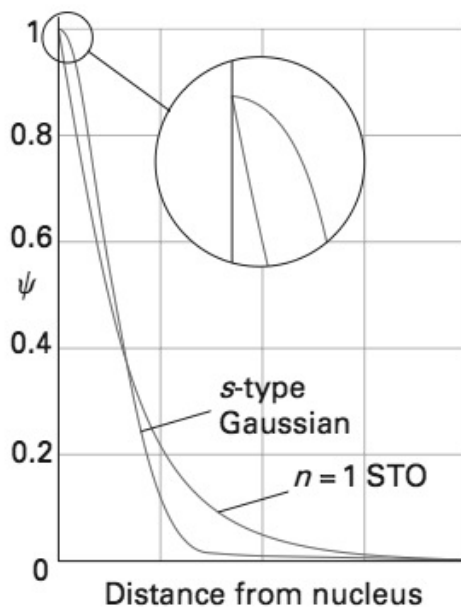


Figure 2.2 Gaussian type orbitals (GTOs) – cusp. A 1s-orbital is an exponential function, so there is a cusp at the nucleus. A GTO does not have a cusp at the nucleus (reprinted with permission from Ref. 57).

Therefore, since GTOs provide a poorer orbital representation we need a larger basis, in order to achieve comparable accuracy with that obtained using GTOs. To alleviate this lack of cusp, we group GTOs together to form the so-called contracted Gaussian functions⁵⁷. Each contracted Gaussian is a linear combination of the original or primitive Gaussian functions, centered on the same atomic nucleus. The replacement of primitive Gaussians by contracted ones reduces the unknown coefficients that need to be calculated by a HF scheme, making the calculation significantly faster.

The simplest type of basis set is called a minimal basis set. A minimal basis set includes one function for each representing orbital of elementary valence theory. Although possible, a minimal basis set would result in energies and wavefunctions that are far away from the HF limit. One can therefore add more functions to each atom, in order to significantly improve the calculated energies. This way we get a double-zeta basis set, in which each basis function in the minimal basis set is replaced by two basis functions, triple-zeta and so on. Finally, one can use a split-valence basis set as a compromise between an inadequate minimal basis set and the computationally demanding double and triple basis set. In this scheme valence atomic orbitals are represented by two basis functions, in the case of a double-zeta basis set- and each inner-shell orbital is represented by only one function.

In addition, one can add extra functions in order to have a better orbital representation. Diffuse functions are added in order to help describe the “tail” portion of the atomic

orbital, which are distant from the atomic nuclei. Usually, diffuse functions are added to light atoms and anions.

Further improvement of basis functions is achieved by adding d-orbitals to all heavy atoms. For typical organic compounds, these are not used in bond formation, as are the d-orbitals of transition metals. These d-orbitals are used to allow a shift of the center of an orbital away from the position of the nucleus. For example a p-orbital on a carbon can be polarized, by mixing it into a d-orbital of lower symmetry (Figure 2.3).

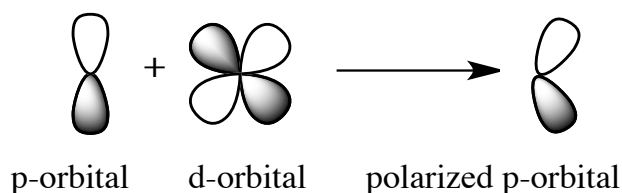


Figure 2.3 Polarization of a p-orbital by mixing with a d-function.

The selection and completeness of basis sets is very important since it gives rise to an error in the calculated energy, called Basis Set Superposition Error (BSSE). BSSE can be particularly important in cases of weakly bound systems. If we consider a dimer, then as the atoms of interacting molecules approach one another, their basis set overlap. As the two monomers approach each other, the dimer can be artificially stabilized as one monomer that utilized the extra basis functions from the other monomer. This

inconsistent treatment of the basis set of each monomer can be eliminated using the counterpoise correction⁵⁹, in which we calculate the amount by which one monomer is artificially stabilized by the extra basis functions from the other monomer. For example, if we consider the dimer AB , the interaction energy is computed as

$$\Delta E_{\text{int}}(AB) = E_{AB}^{AB}(AB) - E_A^A(A) - E_B^B(B). \quad (\text{eq. 2.20})$$

We can estimate the amount that each monomer is stabilized as

$$E_{BSSE}(A) = E_A^{AB}(A) - E_A^A(A) \quad (\text{eq. 2.21})$$

and

$$E_{BSSE}(B) = E_B^{AB}(B) - E_B^B(B) \quad (\text{eq. 2.22})$$

The corrected interaction energy can then be computed as

$$\Delta E_{\text{int}}^{\text{Corr}}(AB) = E_{AB}^{AB}(AB) - E_A^{AB}(A) - E_B^{AB}(B). \quad (\text{eq. 2.23})$$

Different methods can overestimate or underestimate the BSSE, and therefore in most cases it needs to be evaluated. Unfortunately, this would lead to $2N$ computations for a system containing N atoms, and this is not always computationally feasible.

2.6. Correlation Energy and Post Hartree-Fock Methods

So far we have discussed the basic method of quantum mechanics, the Hartree-Fock method. HF theory only accounts for the average electron-electron interactions, and consequently neglects the correlation between electrons. In a sufficiently large basis set, the HF wavefunction accounts for ~99% of the total energy, but the remaining ~1% is often very important for the description of chemical phenomena. Solving the HF equations with an infinite basis set provides an energy, which is defined as the HF limit. The energy difference between this HF limit and the exact, non-relativistic energy is called the electron correlation energy, and it corresponds to the motion of the electrons being correlated.

There are two main types of electron correlation, dynamical and non-dynamical (or static). The dynamical correlation includes the concept of electrons avoiding each other. This type of correlation is, for example, the main part of the electron correlation for the He atom, in which two electrons avoid each other, while occupying the same orbital. There is, however, another type of correlation, the non-dynamical, which reflects the inadequacy of a single reference in describing a given molecular state. This inadequacy is due to nearly degenerate states, or electrons with partially filled shells. Beryllium atom can be a system where non-dynamical correlation dominates, since the two different electronic configurations ($1s^2 2s^2$ and $1s^2 2p^2$) lie very close in energy. The two different types of correlation can also be explored by examining the hydrogen atom. If we pull the

molecule apart, we would expect that they electrons should not need to avoid each other as much, and the magnitude of correlation energy should decrease. In fact, the opposite is true, since the non-dynamical correlation is the dominating contribution. In contrast, when we examine short intermolecular distances the correlation that dominates is the dynamical term; in fact if we were to ignore electron repulsions, the electrons would stay in a bound state, like a He atom.

The HF method uses the variational principle in order to determine the best (the one with the lowest energy) single-determinant trial wavefunction. In order to improve the HF result and account for electron correlation, we need to start from a trial wavefunction that includes more than one determinant. Multi-determinant methods are much more computationally expensive, but can generate results that improve systematically, and can approach the exact solution of the Schrödinger's equation.

A generic multi-determinant wavefunction can be written as a linear combination of determinants,

$$\Psi = a_0 \Phi_{HF} + \sum_{i=1} a_i \Phi_i . \quad (\text{eq. 2.24})$$

In most cases a_0 is close to 1, and this is the reason why the Hartree-Fock method that accounts for the principle configuration of the system accounts for ~99% of the energy of the system. Different electron correlation methods, calculate the coefficients in front of other determinants in different ways.

The CI method, which is based in the variational principle, is somewhat analogous to the HF method. The trial wavefunction is written as linear combination of determinants with the expansion coefficients being determined by minimizing the total energy of the system. The MOs that are used for building the excited Slater determinants⁶⁰⁻⁶¹ are taken from a previous HF calculation. Full CI calculations that include all possible excitations are unfeasible for all but very small systems. However full CI calculations are used in method development, since they provide the best results for any given basis sets. CI methods can be truncated to include certain levels of excitations relative to the HF configuration, for example single (S), double (D), triple (T) etc. Truncated CIS, does not give any improvement over HF calculations, since all matrix elements between the HF wavefunction and singly excited determinants are zero. Therefore, in order to include electron correlation we must go beyond this CIS level of theory to at least CISD.

The Multi-Configuration Self-Consistent Field method (MCSCF) is another popular method that accounts for electron correlation. MCSCF method can be considered a variation of CI, where not only are the coefficients in front of the determinants optimized, but also the MOs used for constructing the determinants are optimized. MCSCF methods are rarely used for calculating large fractions of the correlation energy. It is more efficient to include additional determinants and keep the MOs fixed (which is the CI method that was previously discussed). In most cases, single determinant HF wavefunctions give qualitatively correct description of the electron structure, except a

few cases where the ground state of the system consists of many configurations (such as Beryllium atom).

Although CI provides a systematic way to improve the Hartree-Fock energies, it is not a size-consistent method. If A and B are two non-interacting systems with $E(A)$ the calculated energy of system A and $E(B)$ the calculated energy of system B , then a size consistent method will evaluate the energy of the supersystem $A - B$ to be equal to the sum of independent energies. In other words,

$$E(A - B) = E(A) + E(B). \quad (\text{eq. 2.25})$$

Size-consistency is a very important property of electronic structure methods, especially in order to obtain correctly behaving dissociation curves. Although CI is a variational method, only the full CI is size consistent. However, in most cases we are using truncated versions of this method, due to the size of the system, which is not size consistent.

Perturbation theory⁶²⁻⁶⁴ (PT) provides an alternative solution to finding the correlation energy. Perturbation theory partitions the Hamiltonian of the system into two parts, a known part and a perturbation.

$$\hat{H} = \hat{H}_0 + \lambda \hat{H}_1 \quad (\text{eq. 2.26})$$

Unfortunately, although perturbative methods are size consistent, they are not variational, meaning that the calculated energies are in many cases upper bounds to the exact energy of the system. In electronic structure calculations, the Møller-Plesset perturbation theory⁶⁵ is commonly used. The MP approach takes \hat{H}_0 to be the sum of the one-electron Fock operator

$$\hat{H}_0 = \sum_{i=1}^n f_i \quad (\text{eq. 2.27})$$

where n is the number of basis functions, and f_i the fock operator.

The perturbed part of the wavefunction, \hat{H}_1 is

$$\hat{H}_1 = \sum_i^{\text{occ}} \sum_{j>i}^{\text{occ}} \frac{1}{r_{ij}} - \sum_i^{\text{occ}} \sum_{j>i}^{\text{occ}} \left(J_{ij} - \frac{1}{2} K_{ij} \right) \quad (\text{eq. 2.28})$$

In order to apply perturbation theory and calculate the correlation energy, the unperturbed wavefunction must be selected. This unperturbed, zeroth-order wave function is the HF determinant, and the zeroth-order energy is the sum of MO energies. To include electron correlation we need to go at least to the second order MP2, since the energy up to the first order, MP1, is exactly the same as the HF energy. While developing this theory, we assume that the solutions to the unperturbed solutions form a complete set, which would require an infinite number of functions that of course is not computationally feasible. When we employ a finite basis set, we can only generate a

finite number of excited determinants. Therefore, this expansion of the many-electron wavefunction is truncated. In practice only low orders of perturbation theory are carried out, and in many cases the results of the HF and the MP2 calculations differ dramatically (Figure 2.4). MP2 usually overestimates the correlation energy, but often provides a better answer than MP3, especially in cases where a medium-sized basis set is used. Finally, in cases where the system has substantial multi-reference character, a perturbation expansion based on a single determinant will converge poorly.

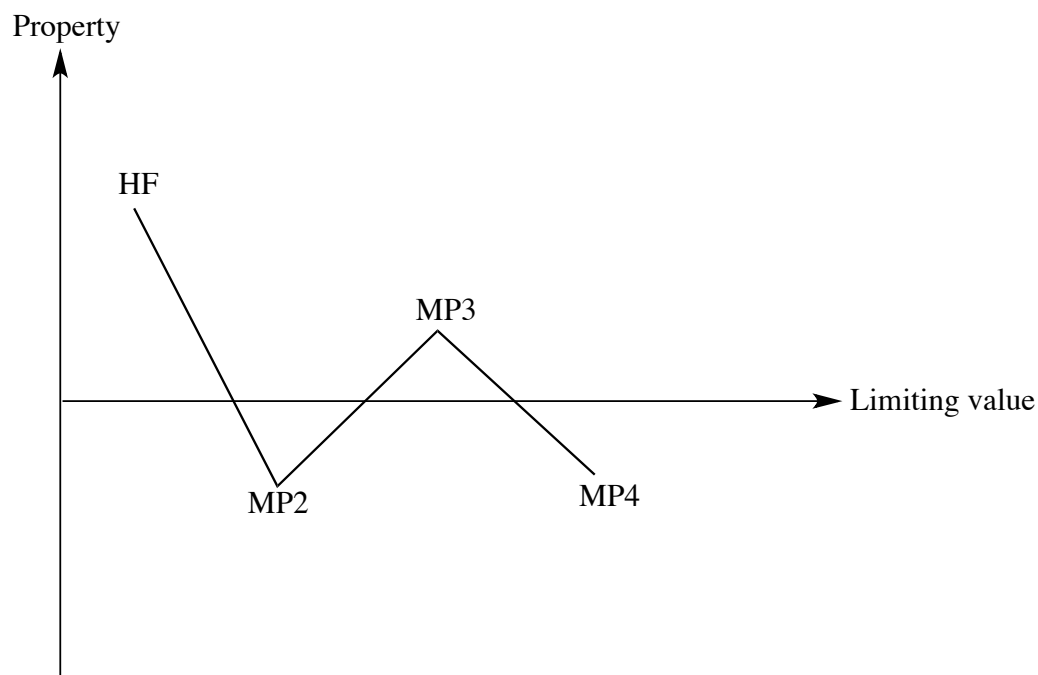


Figure 2.4 Oscillating behavior of results obtained with the MP method.

Last but not least, the last popular method that accounts for electron correlation is the Coupled Cluster method. The idea behind the CC method is to include all corrections of a given type to an infinite order*. The T operator is defined, and used to relate the exact electronic wavefunction to the HF wavefunction Φ_0 through $\Psi = e^{\hat{T}}\Phi_0$, and the exponential operator $e^{\hat{T}}$ is defined as

$$e^{\hat{T}} = 1 + \hat{T} + \frac{1}{2!}\hat{T}^2 + \frac{1}{3!}\hat{T}^3. \quad (\text{eq. 2.29})$$

When $e^{\hat{T}}$ acts on Φ_0 we get a linear combination of Slater determinants, where electrons from occupied spinorbitals have been excited to virtual ones. The \hat{T} operator generates all excited Slater determinants, upon acting on the HF wavefunction:

$$\hat{T}_1\Phi_0 = \sum_i^{\text{occ}} \sum_a^{\text{vir}} t_i^a \Phi_i^a \quad (\text{eq. 2.30})$$

or

$$\hat{T}_2\Phi_0 = \sum_{i < j}^{\text{occ}} \sum_{a < b}^{\text{vir}} t_{ij}^{ab} \Phi_{ij}^{ab}. \quad (\text{eq. 2.31})$$

This way we generate singly (\hat{T}_1) or doubly -connected in this case- (\hat{T}_2) excited states.

By comparing the CC wavefunction with the CI one, we can see that the CC wavefunction contains additional terms arising from products of excitations. Up to this point, this method has been exact, in the sense that all cluster operators up to \hat{T}_N are

included in \hat{T} and therefore all possible excited determinants are generated and the CC wavefunction is equivalent to the full CI wavefunction. Of course, in the same way that is inefficient to do a full CI calculation, in most cases the CC calculations are truncated. When we truncate the \hat{T} operator, some of the terms in the amplitude equations become zero and then the energy calculated becomes approximate. Of course we can improve the accuracy by including more terms in the \hat{T} operator. In most cases we include single and double excited states, and an estimate to the contribution of the connected triples, which is calculated non-iteratively using the MP methods. This method, denoted CCSD(T) is considered to be the “Gold Standard” of Quantum Mechanics, since it provides great results for a large variety of systems.

Overall, for typical equilibrium structures, the HF level of theory is sufficient to predict bond lengths that are slightly short. MP2 is considered an excellent level for geometry optimizations of minima. However this is not the case for transition state (TS) structures, where the accurate description of correlation usually requires correlation above the MP2 level. Considering the calculated energies, MP2 can again be considered a very efficient level of theory. However, the generally robust nature of MP2 does not work on TS calculations we need to use higher level of theory. Usually good agreement with experimental data and convergence with respect to treatment of electron correlation are the most used tools when evaluating different theories. We can roughly order theory levels as HF < MP2 ~ MP3 ~ CCD < CISD < CCSD < MP4 < CCSD(T). Of course, the selection of basis set, the nature of the system, and the scaling behavior of the various

levels of theory are parameters that need to be considered in order to decide what is the appropriate level of theory for each individual calculation.

2.7 Density Functional Theory

All the methods described above, called *ab initio* methods, start with solving the HF equations in order to find spinorbitals that can be then used to construct configuration state functions. As we already mentioned although these methods are powerful and accurate, they can only be employed in a limited number of systems. The computational difficulty of performing accurate calculations with large basis sets on molecules containing many atoms, especially heavy transition metals, is the biggest problem regarding these methods. An alternative to these methods is density functional theory (DFT). DFT has become one of the most popular methods nowadays, since it does account for electron correlation, while being less demanding computationally. Therefore, it can be used in large systems that contain many atoms and electrons.

DFT is based on the concept of electron probability density. There are two ingeniously simple theorems⁶⁶ stated and proven by Hohenberg and Kohn in 1964. The first one states, that for any system of interacting particles in an external potential, the density is uniquely determined. In other words, the external potential is a unique functional of the density. The second theorem is that there is a universal functional for the energy that can

be defined in terms of the electron density. The exact ground state of the system is the global minimum value of this functional.

In simple words, the basic idea behind DFT is that the energy of an electronic system can be written in terms of the electron probability density⁶⁷, ρ . For a system of n electrons, the total electron density at a particular point in space r , is denoted as $\rho(r)$. The electronic energy E is a functional of the electron density $E[\rho]$, in the sense that there exists a one-to-one correspondence between the electron density of a system and the energy. The significance of the Hohenberg-Kohn theorem is best illustrated when comparing it with the previously analyzed wavefunctions approach. A wavefunction for an N -electron system contains $4N$ variables, three spatial, and one spin coordinate for each electron. The electron density on the other hand only depends on three spatial coordinates, and it is independent of the number of electrons. While the complexity of a wavefunction increases exponentially, as we increase the number of electrons, the electron density is independent of the system size. Although appealing at first, DFT has one major downside: although it has been proven that each different density yields a different ground state energy, the functional connecting these two quantities is not known. The goal of DFT theory is to design functionals connecting the electron density with the energy. Early attempts of DFT models were not very successful, mainly because they tried to express all the energy components as a functional of the electron density. Recently though, this has changed, and this success is based on the suggestion by Kohn

and Sham that the electron kinetic energy should be calculated from an auxiliary set of orbitals that are used to represent the electron density.

Perhaps the most important step in DFT is the derivation of a set of one-electron equations from which we will obtain the electron density ρ . Kohn and Sham showed that the exact ground state electronic energy E of an n -electron system can be written as

$$E[\rho] = -\frac{\hbar^2}{2m_e} \sum_{i=1}^n \int \psi_i^*(r_1) \nabla_1^2 \psi_i(r_1) dr_1 - j_0 \sum_{I=1}^N \frac{Z_I}{r_{I1}} \rho(r_1) dr_1 + \frac{1}{2} j_0 \int \frac{\rho(r_1)\rho(r_2)}{r_{12}} dr_1 dr_2 + E_{XC}[\rho]$$

(eq. 2.32)

where the one-electron spatial orbitals $\psi_i (i = 1, 2, \dots, n)$ are the Kohn-Sham orbitals.

The first term of this equation is the kinetic energy of non-interacting electrons, the second term represents the electron-nuclear attraction, and the third the Coulomb interaction between the total charge distribution. The last term, denoted as $E_{XC}[\rho]$, is the exchange-correlation energy of the system, is also a functional of the electron density, and takes into account all non-classical electron-electron interactions and a correction for the kinetic energy. This term does not have an analytical form, and is the one that cannot be obtain directly. We therefore need to express this term in an approximate way in order to get the ground state energy of the system, which will correspondingly be approximate as well.

The ground-state electron density is given by

$$\rho(r) = \sum_{i=1}^n |\psi_i(r)|^2 \quad (\text{eq. 2.33})$$

and is considered to be known once these orbitals have been computed. These Kohn-Sham (KS) orbitals are found by solving the KS equation, which are derived by applying the variational principle to the electronic energy $E[\rho]$. The KS orbitals can either be computed numerically or expressed in terms of a set of basis functions. This set of calculated orbitals, can be used to compute the electron density and by using some approximate form for the exchange-correlation energy and compute an electronic energy. This procedure is repeated until the density and exchange-correlation energy have converged to the desired level.

There are many different schemes that one can employ in order to obtain an approximate form of the functional for the exchange-correlation energy. This exchange-correlation functional is often separated into an exchange functional and a correlation functional. The most basic approximation is the local density approximation (LDA) the exchange-correlation functional is expressed as

$$E_{XC} = \int \rho(r) \epsilon_{xc}[\rho(r)] dr \quad (\text{eq. 2.34})$$

where $\epsilon_{xc}[\rho(r)]$ is the exchange-correlation energy per electron in a homogeneous electron gas of fixed density. Although this approximation scheme is very basic, it can be surprisingly accurate, especially when it comes to predict structural properties.

However calculated binding energies have been found to be significantly larger than the experimental ones. To account for the inhomogeneity of the electron density, we can add a non-local correction that involves the gradient of the density. There are numerous different gradient-corrected functionals. The generalized gradient approximation (GGA), which is basically a gradient-corrected LDA, can produce accurate geometrical parameters and binding energies. DFT calculations, involving GGA procedures, are especially efficient for calculations that include d-metals⁶⁸.

Nowadays, there is an enormous number of functionals that has been developed, such as B3LYP⁶⁹⁻⁷¹, M05-2X⁷², M06L⁷³, ω B97X-D⁷⁴ etc. In many cases the name of the functional designates a particular pairing of an exchange and a correlation functional. In many cases there are functionals that contain some HF corrections in conjunction with density functional correlation and exchange. These functionals are called hybrid functionals, and they can contain different “amount” of HF correction. For example the M05-2X functional, from the well-known family of Minnesota functionals contains “twice” the amount of HF exchange; 56% of the overall exchange comes from the HF theory.

While DFT has already been noted to be computationally efficient, compared to other methods that account for electron correlation, it unfortunately doesn't work great in all cases. It usually fails to evaluate dynamical phenomena, such as multistate resonance effects, interference effects etc. that depend on matrix elements between different

wavefunctions. Excited state is another area where DFT is just starting to progress on. Although the density alone carries sufficient information to determine the excited-state wavefunctions, only recent research projects have been focused on applying DFT to excited states (with the exception of symmetric molecules). Other than the main limitations mentioned below, DFT is usually the method of choice in order to achieve a particular level of theory at lowest cost. New functionals, and new methods improve DFT results, for example incorporating dispersion corrections, are designed in order to provide as broad a coverage as possible in all different types of systems studied.

3 THEORETICAL INVESTIGATION OF Ir₂(μ-S)₂(PH₃)₄ AND Ir₂(μ-S)₂(PPh₃)₄

This research project is focused on a theoretical description of the Ir₂(μ-S)₂(PPh₃)₄ complex and its reaction with dihydrogen. Upon reaction of Ir₂(μ-S)₂(PPh₃)₄ with two equivalents of H₂, Ir₂(μ-S)(μ-SH)(μ-H)H₂(PPh₃)₄ is formed. Lack of evidence for the proposed mechanism, as well as some ambiguity in the experimental results, such as crystal structures of **2** and **3** being nearly identical, prompted interest in this reaction. A theoretical investigation of the proposed mechanism for this reaction scheme may validate it or invalidate it. Further, this exploration will uncover the details of the mechanism, intermediates and transition states, and will provide insight to this class of reactions.

3.1 Experimental Information

The Rauchfuss group has contributed in research areas revolving around applications of organometallic chemistry to basic issues related to sustainability, atom efficiency, and improved catalysts. More specifically, the bio-catalysis of small molecules and in particular H₂ has been one of their active research topics of the past decade. In this bio-catalysis, systems with metal sulfur bonds have a central role. In addition, enzymes are interesting from a synthetic perspective since many of these enzymes provide existence proofs for anticipated structures that challenge synthetic chemists.

Linck et al synthesized⁷⁵ an Ir(II) sulfide, $\text{Ir}_2(\mu\text{-S})_2(\text{PPh}_3)_4$ (**2**), and studied its reaction with dihydrogen in toluene. The noble metal reactant, $\text{Ir}_2(\mu\text{-S})_2(\text{PPh}_3)_4$ (**2**) is unusual because it is a five-coordinate Ir(II) complex, which would have been expected to be six coordinate. Furthermore, the Ir centers also appear to be electron deficient as each has 16 electrons, unless one invokes an Ir-Ir triple bond. This unprecedented structure prompted them to study its reactivity. Upon reaction with one equivalent of dihydrogen, H_2 appears to undergo a homolytic activation to form the first product, $\text{Ir}_2(\mu\text{-S})_2\text{H}_2(\text{PPh}_3)_4$ (**3**). Addition of another H_2 equivalent, converts (**3**) to $\text{Ir}_2(\mu\text{-S})(\mu\text{-SH})(\mu\text{-H})\text{H}_2(\text{PPh}_3)_4$ (**4**) apparently via a heterolytic activation. ^1H NMR as well as crystallographic studies showed no stable intermediate before (**3**), and one short-lived intermediate (**4***), after (**3**). The proposed mechanism is illustrated in Figure 3.1.

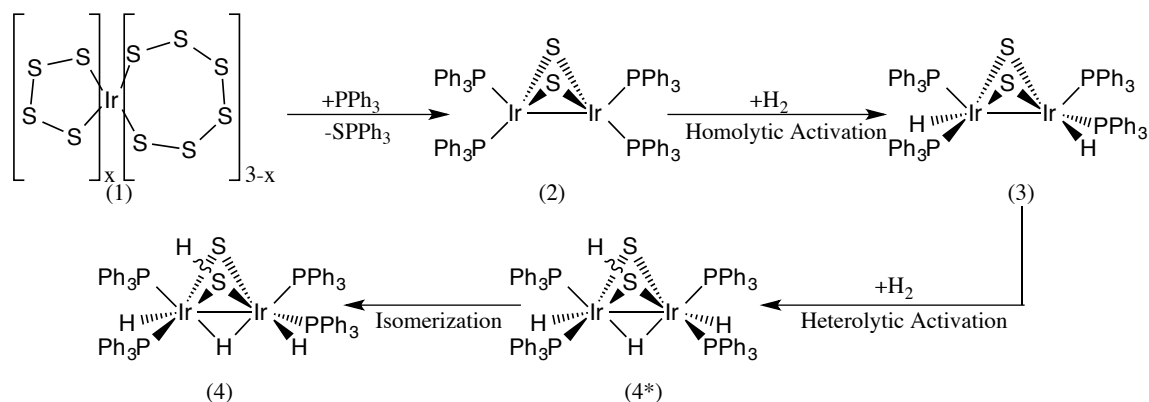


Figure 3.1 Proposed mechanism for the H_2 activation on iridium center.

The geometrical parameters that were reported in the crystal structures, regarding the first H₂ activation, were of particular interest. Specifically, the Ir-Ir bond reported for **(2)** and **(3)** only changes by 0.003 Å, preserving the metal-metal bond. This is unusual, considering that the classic 2-electron iridium-iridium bond would be expected to break upon addition of H₂, as two new metal-hydrogen bonds are formed. Although we usually cannot directly observe the hydrogen atoms in a crystal structure, their location is crucial, as their position determines the type of the hydrogen activation. In the experiment, the iridium hydrides were located on the difference Fourier map, therefore their location is expected to be valid. In addition, ¹NMR reveals only one peak in the hydride region at δ=-17.0, which indicates that both hydrogen atoms are equivalent on the NMR timescale. Therefore, the question remains: must oxidative addition of dihydrogen break the iridium-iridium bond in **(2)**?

The second part of the reaction, and more specifically the final product **(4)**, is in agreement with experimental data (crystal structure⁷⁶ and ¹NMR data) that were previously reported by Pignolet et al.

In order to clarify whether the metal-metal bond is preserved or broken, to verify the accuracy of the experiment, and to determine the reaction mechanism, we will investigate the system theoretically, using quantum chemistry, and more specifically DFT calculations. A theoretical investigation of the proposed mechanism for this reaction scheme may validate it or invalidate it. Further, this exploration will uncover the

details of the mechanism, intermediates and transition states, and will provide insight to this class of reactions.

3.2 Computational Details

The models used in this study are H_2 , $\text{Ir}(\mu\text{-S})_2(\text{PH}_3)_4$ and $\text{Ir}(\mu\text{-S})_2(\text{PPh}_3)_4$. The Gaussian 09 software suite⁷⁷ was utilized for all calculations presented herein.

For the model system, $\text{Ir}(\mu\text{-S})_2(\text{PH}_3)_4$ the functional used was a combination of the exchange functional of Tao, Perdew, Staroverov, and Scuseria with the τ -dependent gradient-corrected functional of Tao, Perdew, Staroverov, and Scuseria (TPSS⁷⁸). The basis set of the model system is as follows: the basis set on Ir is SDD⁷⁹ with effective core potential⁸⁰, the basis set on S and P is Pople's split-valence triple-zeta augmented with d polarization functions (6-311g*)⁸¹⁻⁸⁶, and the basis set on H is Pople's split-valence double-zeta augmented with d polarization functions (6-31g*)^{87,88}.

For the full ligand system $\text{Ir}(\mu\text{-S})_2(\text{PPh}_3)_4$, we used Head-Gordon's long-range exchange and dispersion corrected⁸⁹ functional ($\omega\text{B97X-D}$)⁹⁰. Tsuneda et al. have exhibited⁹¹ how a long-range correction scheme improves the reaction barrier energies in different chemical reactions, as well as the overestimated polarizabilities⁹². Additionally, the presence of twelve phenyl rings (some of which have parallel displacements) increases the dispersion interactions, and hence a dispersion corrected functional is expected to

perform better in this system than a functional that does not account for dispersion (e.g. the Becke three-parameter hybrid exchange functional and the Lee-Yang-Parr correlation functional, B3LYP⁹³). The basis set of the full ligand system is as follows: the basis set on Ir is SDD with effective core potential, the basis set on S and P is Pople's split-valence triple-zeta augmented with d polarization functions (6-311g*), the basis set on C and H atoms of the PPh₃ is Pople's split-valence double-zeta augmented with d-polarization functions (6-31g*), and finally the basis set on the incoming H atoms that are activated (denoted as H') is Pople's split-valence triple-zeta augmented with d polarization functions and diffuse functions (6-31++g**).

In order to examine the behavior of the full ligand system in solution, the SMD solvation model⁹⁵ was used, within the integral equation formalism variant (IEFPCM⁹⁵⁻¹¹⁴).

The spin study of the model system was performed using the more accurate CCSD¹¹⁵⁻¹¹⁸ method for calibration.

Finally, for the functional analysis of the full ligand system, the following 7 functionals were used: TPSS, TPSSh¹¹⁹, B3LYP, BP86^{120,121}, M06¹²², M06L, PBE1PBE^{123,124}.

All structures in this thesis were created using the graphical interface of Gaussian 09, and the Jimp 2 software¹²⁵⁻¹²⁷.

3.3 Model System $\text{Ir}_2(\mu\text{-S})_2(\text{PH}_3)_4$

In order to begin investigating the structures and reactivity of the system studied by Rauchfuss, we created a model system, by replacing each PPh_3 with a PH_3 . This change reduces the size of the system significantly (by 120 atoms and 480 electrons). Furthermore, it has been shown in different studies^{128,129}, that PH_3 is a good mimic for the electronic parameters of PPh_3 . Therefore we would expect this model system to provide a good starting point for our calculation on the full ligand system.

The optimized geometries for model structures (denoted with ') $2'$, $4'$ and 4^{*} were found to be in good agreement with the crystal structure of **2** and the proposed structures for **4** and 4^* (Figure 3.2).

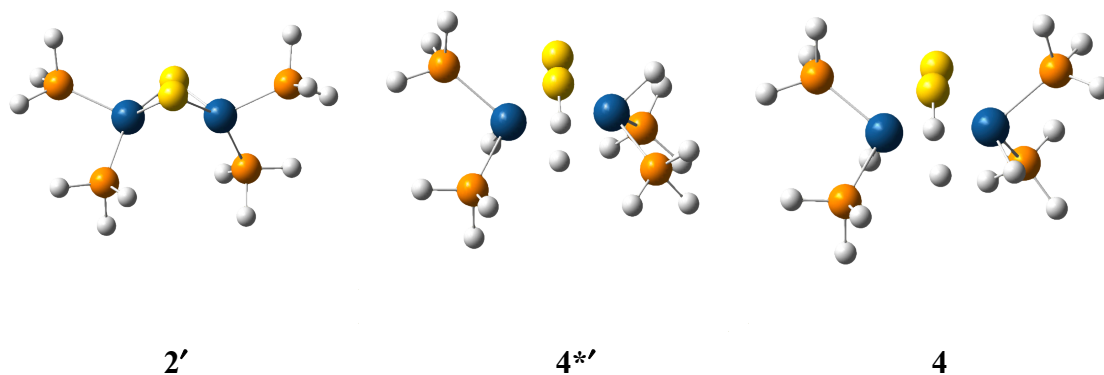


Figure 3.2 Optimized structures $2'$, $4'$ and 4^{*} .

Despite the agreement for structure **2'**, the lowest energy structure for **3'** does not correspond to the crystal structure, as the iridium-iridium bond is elongated by approximately ~ 0.2 Å. Since this error is beyond the usual error for either the experiment or the calculation, we began searching for other possible arrangements for structure **3'** that could potentially have a preserved metal-metal bond. In a previous study¹³⁰, Hua-Jun Fan had performed an exhaustive search for other hydrogen atoms arrangements that could provide agreement for the heavy atom positions of the experimental structure of **3'**. Hydrogen addition to **2'** could produce 43 different arrangements (generally denoted as **3x'**) that can be classified in five classes of structures: (i) one H is bound to each Ir, (ii) both H are bound to one Ir, (iii) one bridging Ir-H-Ir and the other H either on Ir or S, (iv) one H on Ir and the other on S, (v) one H on each S. All possibilities were re-examined in the current study, and the five lowest energy isomers were optimized (Figure 3.3). Three of these isomers (**3a'**, **3b'**, **3c'**) are products of a homolytic activation, and remaining two (**3i'**, **3k'**) are products arising from a heterolytic activation of H₂. The only case where the Ir-Ir bond is preserved is when this first H₂ activation is a heterolytic one.

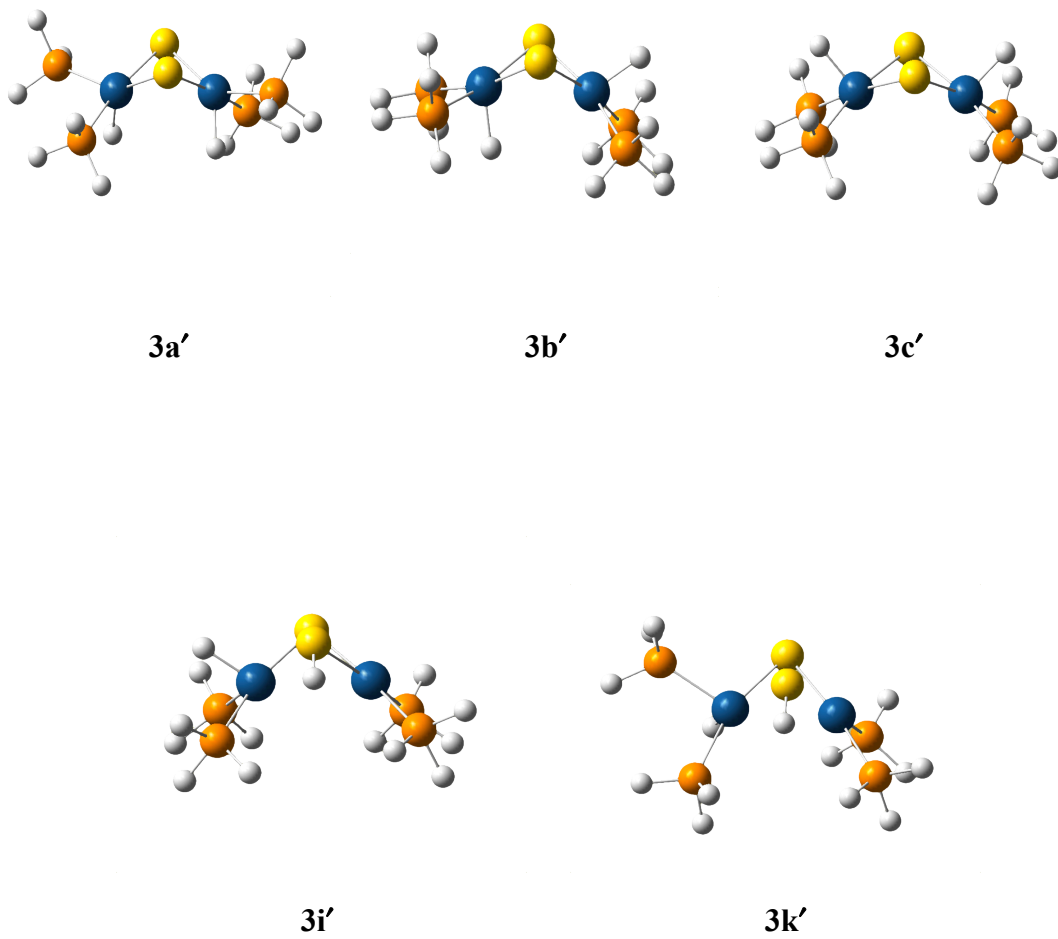


Figure 3.3 Five lowest energy isomers of 3'.

Examining the gas-phase calculated energies of the model system (Table 3.1) we can see that the geometrically equivalent structure for **3**, which is **3a'**, is not the lowest energy product of first H₂ activation. On the contrary, the lowest energy isomer, seems to be **3b'** followed by the almost isoenergetic **3c'**. In fact **3a'** appears to be the highest energy isomer, even compared to the isomers that rise from a heterolytic activation of H₂ (**3i'** and **3k'**).

**Table 3.1 Relative Gas Phase Energies of Optimized Model System Structures
(in Kcal/Mol)**

Structure	ΔE	ΔG
2'	0.00	0.00
3a'	-20.36	-9.64
3b'	-25.73	-14.64
3c'	-25.41	-15.41
3i'	-22.59	-11.26
3k'	-20.82	-9.13
4*'	-44.41	-21.10
4'	-44.97	-22.04

In all cases of homolytic-activated products (**3a'**, **3b'**, **3c'**) the metal-metal bond appears to be broken, as the bond length between each iridium center is significantly elongated

(Table 3.2). The only model system structure that seems to match the reported bond length for **3** (2.754 Å) seems to be **3k'**, which corresponds to a heterolytic cleavage of H₂ and is also quite high in energy.

Table 3.2 Ir-Ir Bond Length for Optimized Model System Structures (in Å)

Structure	Bond Length
2'	2.724
3a'	2.927
3b'	2.941
3c'	3.106
3i'	2.875
3k'	2.761

In all the results mentioned so far, we have assumed that all compounds **2'**, **3'**, **4*'** and **4'** have singlet ground states. This is a relatively safe assumption, since Ir is in most cases low-spin. However, in order to confirm this assumption, we looked at the energy difference between the singlet and the triplet configuration, by performing single point CCSD calculations in the **3'** class of isomers, since a triplet configuration could affect the iridium-iridium bond length. All previously optimized isomers of the model system (**3a'**, **3b'**, **3c'**, **3i'**, **3k'**) as well as two additional isomers were used for the single point CCSD calculations. The additional isomers (**3f'** and **3h'**) were obtained by the

optimized isomers of the full ligand system (**3-crst** and **3-heup** respectively) when each PPh₃ is replaced with PH₃. The calculated energies are shown in Table 3.3.

Table 3.3 Absolute Gas Phase Electronic Energies of Optimized Model System Structures (in Hartrees)

Structure	E
3' Singlet	-2373.87867
3' Triplet	-2373.845823
3a' Singlet	-2374.518947
3a' Triplet	-2374.437888
3b' Singlet	-2374.527705
3b' Triplet	-2374.459736
3f' Singlet	-2374.524291
3f' Triplet	-2374.463431
3h' Singlet	-2374.035303
3h' Triplet	-2374.004975

In all cases, the singlet configuration is lower in energy than the corresponding triplet, and therefore, as expected, we can exclude any spin crossing phenomena, and assume that all isomers will be singlet states.

Exploring the model system, although computationally feasible, does not provide the expected agreement with the experimental results for all of the structures. Hence, this

would be a poor starting point for a study of the mechanism. The lack of steric hindrance and dispersion interactions between the phenyl rings, which were neglected in the small model, can lead to numerous isomers, which do not have an equivalent structure at the PES of the full ligand system. Therefore, we need to examine the full ligand system in order to understand and fully explore the structures and mechanism of this reaction.

3.4 Full Ligand System $\text{Ir}_2(\mu\text{-S})_2(\text{PPh}_3)_4$

Investigation on the full ligand system began by optimizing **2** and **3-crst** (Figure 3.4) starting from the provided crystal structures (Figure 3.5).

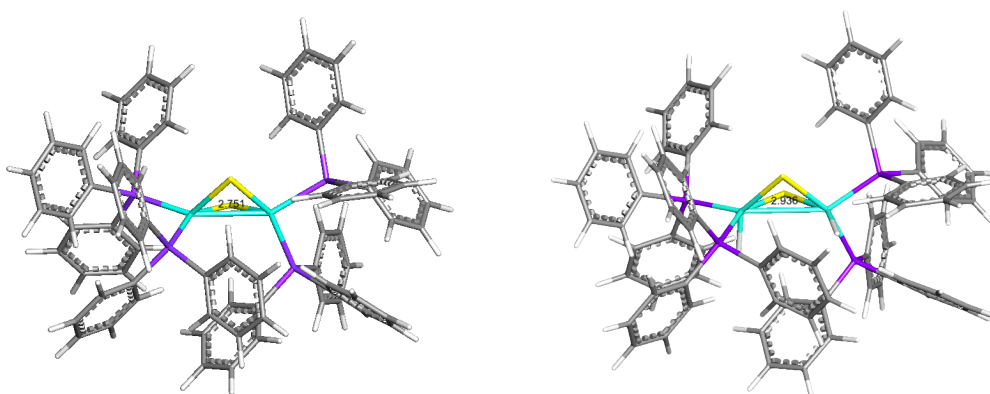


Figure 3.4 Optimized structures for **2** (left) and **3-crst** (right). The Ir-Ir bond length changes from 2.751 Å (in **2**) to 2.936 Å (in **3-crst**).

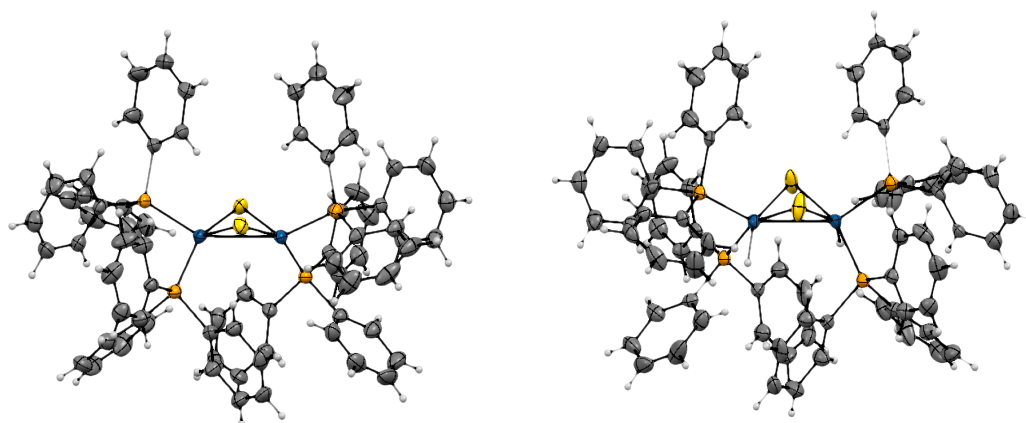


Figure 3.5 Reported crystal structures for **2** (left) and **3** (right). The Ir-Ir bond length changes from 2.757 Å (in **2**) to 2.754 Å (in **3**-crst).

Structure **2** was found to be in excellent agreement with the corresponding crystal structure (Table 3.4).

Table 3.4 Geometrical Parameters for 2

Structure / Bond	Crystal Structure	Calculated
2 / Ir-S [†]	2.2706(13) Å	2.293 Å
2 / Ir-S [‡]	2.3106(12) Å	2.340 Å
2 / Ir-P [†]	2.2606(12) Å	2.287 Å
2 / Ir-P [‡]	2.2705(13) Å	2.291 Å
2 / Ir-Ir	2.7575(30) Å	2.751 Å

[†] indicates “short” bond

[‡] indicates “long” bond

In contrast, our optimized structure that corresponds to the crystal structure **3**, which is **3-crst**, was not in agreement with the given crystal structure (Table 3.5). The homolytic cleavage of H₂ appears to break the metal-metal bond, indicating an elongated bond length between the two metals (by ~0.18 Å).

Table 3.5 Geometrical Parameters for 3-crst

Structure / Bond	Crystal Structure	Calculated
3-crst / Ir-S [†]	2.2907(18) Å	2.352 Å
3-crst / Ir-S [‡]	2.3619(17) Å	2.374 Å
3-crst / Ir-P [†]	2.2666(17) Å	2.254 Å
3-crst / Ir-P [‡]	2.2672(16) Å	2.310 Å
3-crst / Ir-Ir	2.7541(50) Å	2.936 Å

[†] indicates “short” bond

[‡] indicates “long” bond

In order to confirm that this result is independent of the functional used for the calculation, we performed geometry optimizations with 8 different functionals. The functionals that were used in order to test for a possible functional dependence were: B3LYP, BP86, M06, M06L, PBE1PBE, TPSS, TPSSh, and ωB97X-D. These functionals belong in different families, and are therefore expected to demonstrate different behavior and yield different geometrical parameters. The optimized Ir-Ir bond lengths in both **2** and **3-crst** that were obtained using these functionals are shown in Table 3.6.

Table 3.6 Iridium-Iridium Bond Length in 2 and 3-crst (in Å)

Functional	Bond length in 2	Bond length in 3-crst	Difference
BP86	2.87744	3.04118	0.16374
B3LYP	2.87703	3.12952	0.25249
TPSS	2.83228	2.98278	0.15050
TPSSh	2.81545	2.99236	0.17691
M06	2.80030	2.96806	0.16776
M06L	2.76211	2.89406	0.13195
PBE1PBE	2.80055	3.00125	0.20070
ω B97X-D	2.75096	2.93595	0.18499

As we can see, that although the iridium-iridium distance varies according to the functional used, the iridium-iridium bond length was elongated by ~ 0.18 Å and the metal-metal bond breaks, and the homolytic cleavage occurs as we move from **2** to **3-crst**. This is in agreement with our initial hypothesis: as the incoming dihydrogen molecule approaches the metal core, the 2-electron bond between the two metals breaks, in order for the two new metal-hydride bonds to form. In other words the homolytic cleavage of dihydrogen is expected to break the iridium-iridium bond and to leave the system as an Ir(III) d^6 dimer. Since this result is not supported by the experimental data, we need to examine the possibility of an alternative reaction mechanism: instead of a homolytic activation followed by a heterolytic one, we could have two heterolytic activations or a heterolytic followed by a homolytic one.

Starting from **2**, we examined all possible isomers for the “First Product” class of isomers **3-crst**, which could be obtained either by homolytic or heterolytic dihydrogen activation. Four stable isomers were found and are presented below. Two intermediates correspond to a homolytic activation of dihydrogen (Figure 3.6) and the other two are a result of a heterolytic activation (Figure 3.7).

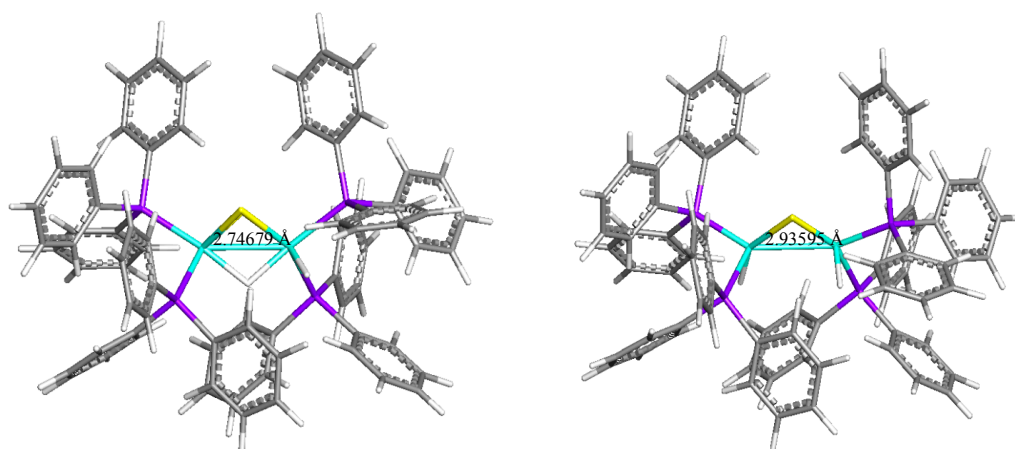


Figure 3.6 Optimized intermediates from a homolytic activation of H₂ on **2**.
3-brid (left) – with one bridging and one terminal H
3-crst (right) – with one terminal H on each Ir.

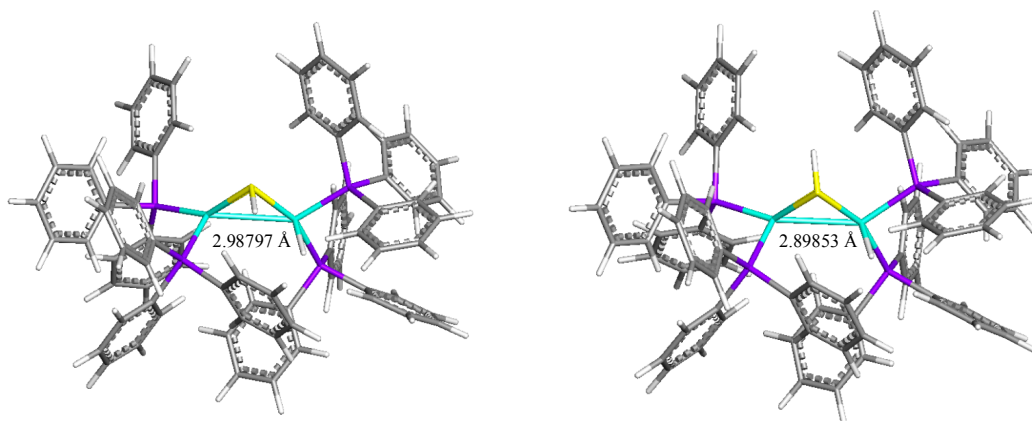


Figure 3.7 Optimized intermediates from a heterolytic activation of H₂ on **2**.
3-heup (left) – with S-H and Ir-H on same side of the Ir-S bond
3-hedo (right) – with S-H and Ir-H on opposite side of the Ir-S bond.

The lowest energy isomer of this class is **3-crst** (Table 3.7). This is in agreement with the previously proposed mechanism by Rauchfuss, if we disregard the broken metal-metal bond. In addition, ¹H NMR shows that in low temperatures (-60 °C) we have a triplet signal, indicating that each hydride is interacting with two PPh₃. This structure corresponds to structure **3-crst**. In higher temperatures (70 °C) a quintet signal was observed, which indicates that one hydride interacts with 4 PPh₃. This structure corresponds to our calculated structure **3-brid**.

**Table 3.7 Relative Gas Phase Energies of Reactant and First Product Isomers
(in Kcal/Mol)**

Structure	ΔE	ΔH	ΔG
2	0.00	0.00	0.00
3-heup	-17.51	-14.11	-4.96
3-hedo	-17.92	-14.75	-4.60
3-brid	-18.79	-16.20	-6.27
3-crst	-21.95	-18.29	-8.49

In addition, the gas phase electronic energy difference between **3-crst** and **3-brid** is only 3.16 kcal/mol, and the corresponding Gibbs free energy difference is only 2.22 kcal/mol. We therefore decided to perform a functional analysis with the same 10 functionals used before (BP86, B3LYP, M05-2X, M06, M06L, TPSS, TPSSh, PBE0, mPW3PBE, ω B97X-D) in order to confirm this energy difference, and understand if the second activation happens at **3-crst** or at **3-brid** compounds. Tables 3.8 and 3.9 show the absolute gas phase energies of **3-brid** and **3-crst** respectively, and Table 3.10 shows the relative gas-phase energies of **3-brid** and **3**, with respect to **2**.

Table 3.8 Absolute Gas Phase Energies of 3-brid (In Hartrees)

Functional	E	S	G
BP86	-5151.731507	-5150.551353	-5150.748922
B3LYP	-5151.328615	-5150.115729	-5150.309418
TPSS	-5151.929186	-5150.733534	-5150.929579
TPSSh	-5151.535233	-5150.325114	-5150.519181
M06	-5149.018641	-5147.808227	-5147.992067
M06L	-5151.033019	-5149.816546	-5150.002691
PBE1PBE	-5147.114048	-5145.891597	-5146.082344
ω B97X-D	-5150.463916	-5149.235763	-5149.421105

Table 3.9 Absolute Gas Phase Energies of 3-crst (In Hartrees)

Functional	E	S	G
BP86	-5151.746037	-5150.565687	-5150.760323
B3LYP	-5151.339161	-5150.125548	-5150.322481
TPSS	-5151.939293	-5150.743069	-5150.941145
TPSSh	-5151.543981	-5150.333315	-5150.529238
M06	-5149.024486	-5147.812967	-5147.998398
M06L	-5151.040257	-5149.821353	-5150.005253
PBE1PBE	-5147.123178	-5145.899981	-5146.093330
ω B97X-D	-5150.468952	-5149.239090	-5149.424579

If we consider the first reaction to be a homolytic activation of H_2 , then one would expect the first step of the reaction (Figure 3.8) to be the addition of molecular hydrogen to one of the metal centers, denoted as **3-dbIr**.

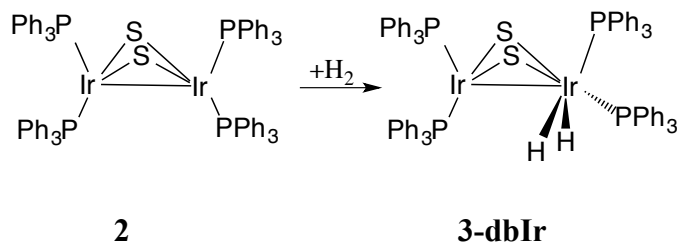


Figure 3.8 First step of a possible scheme for homolytic H_2 activation on **2**.

Although this isomer (shown in Figure 3.9) appears to be stable intermediate when optimized in some functionals, such as BP86 that doesn't account for dispersion interactions, it has a small imaginary frequency when optimized under normal criteria in ω B97X-D. However, the heavy atom arrangement is almost identical between the two optimized structures, and therefore we believe that this structure is a suitable candidate for an intermediate of the first H_2 activation.

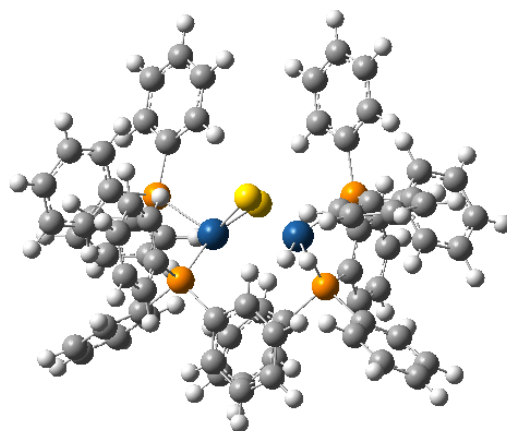


Figure 3.9 Optimized isomer (**3-dbIr**) with the BP86 functional.

We can then consider the following mechanism for the first reaction (Figure 3.10): The first H₂ addition is an oxidative addition on one of the iridium centers (producing **3-dbIr**) followed by a migration of one hydrogen atom to the bridging site between the two metal centers (**3-brid**). The bridging hydride can then migrate to the other metal, forming the final product that was observed by Rauchfuss (**3-crst**).

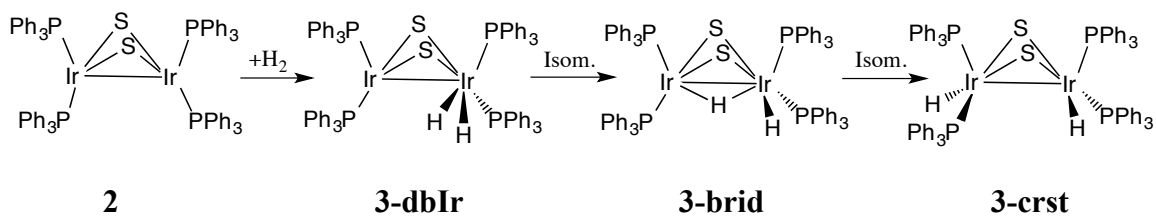


Figure 3.10 Possible reaction scheme for homolytic H₂ activation on **2**.

Since we have already examined the case of the first activation to be a homolytic one (Figure 3-0), we need to examine the possibility of the first activation to occur along the iridium-sulfur bond (Figure 3.11).

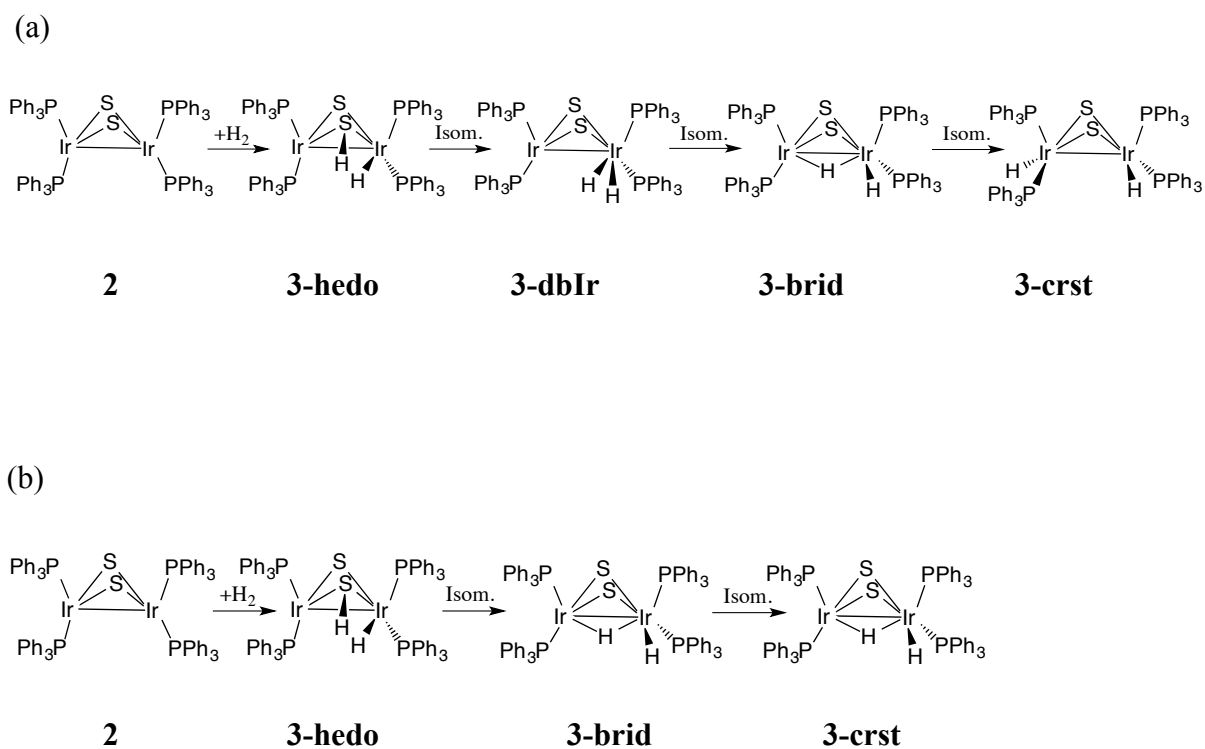


Figure 3.11 Possible reaction scheme for heterolytic H₂ activation on **2**.

Two possible pathways are examined. In both pathways the first step is the cleavage of H₂ along the Ir-S bond (**3-hedo**).

In the first considered mechanism shown in Figure 3.11 (a), the hydrogen of the sulfhydryl group migrates towards the metal hydride forming the previously examined dihydrogen intermediate **3-dbIr**, and then follows the same mechanism as before, producing **3-brid** and finally **3-crst**. In the second plausible mechanism shown in Figure 3.11 (b), the protonated sulfur rotates downwards, forming the bridging species (**3-brid**), which then isomerized to the final product (**3-crst**). A direct comparison of the calculated gas-phase electronic and Gibb's free energies (Table 3-.0) of the first-product class reveals that the first step is more likely to be a heterolytic activation (producing **3-hedo**), however a transition state that corresponds to a direct transition from **3-hedo** to **3-brid** has not been found.

Therefore, the first H₂ activation can occur through three possible pathways, one homolytic and two heterolytic ones, as shown in Figure 3-10 and 3-11 and described in the paragraph above.

Functional	2		3-brid		3-crst		$\Delta\Delta E^\dagger$	$\Delta\Delta G^{\dagger\dagger}$
	ΔE	ΔG	ΔE	ΔG	ΔE	ΔG		
BP86	0.00	0.00	-10.90	+0.20	-20.02	-6.96	-9.12	-7.15
B3LYP	0.00	0.00	-11.39	+1.03	-18.01	-7.16	-6.62	-8.99
TPSS	0.00	0.00	-12.67	-2.30	-19.02	-9.64	-6.34	-7.26
TPSSh	0.00	0.00	-14.84	-2.93	-20.33	-9.24	-5.49	-6.31
M06	0.00	0.00	-9.06	+1.85	-12.73	-2.12	-3.67	-3.97
M06L	0.00	0.00	-11.24	-0.21	-15.78	-1.82	-4.54	-1.61
PBE1PBE	0.00	0.00	-12.64	-0.56	-18.37	-7.46	-5.73	-6.89
ω B97X-D	0.00	0.00	-18.79	-6.45	-21.95	-8.63	-3.16	-2.18

\dagger $\Delta\Delta E$ refers to the electronic energy of 3-crst minus the electronic energy of 3-brid
 $\dagger\dagger$ $\Delta\Delta G$ refers to the Gibbs free energy of 3-crst minus the Gibbs free energy of 3-brid

Table 3.10 shows that **3-crst** is always the lowest energy isomer for the first-product class. The electronic energy as well as the Gibbs free energy of **3-crst** is always lower than **3-brid**; this result seems to be independent of the functional. However, the relative difference between the respective electronic ($\Delta\Delta E$) or Gibbs free energy ($\Delta\Delta G$) varies according to the functional used for the calculation, and it can be as low as 1.61 kcal/mol. This result is in agreement with the ^1H NMR results that predict **3-crst** to be the stable structure in low temperatures, but not in higher temperatures.

We can therefore conclude that isomer **3-crst** is in equilibrium with **3-brid** near room temperature, and we need to examine both cases: the case where H_2 is activated on **3-crst** and the case where the second activation occurs at **3-brid**. Before exploring the mechanism of the second activation, all possible isomers for the second-product were examined. The low-energy intermediates that were found using the ω B97X-D functional, are shown on Figure 3.12.

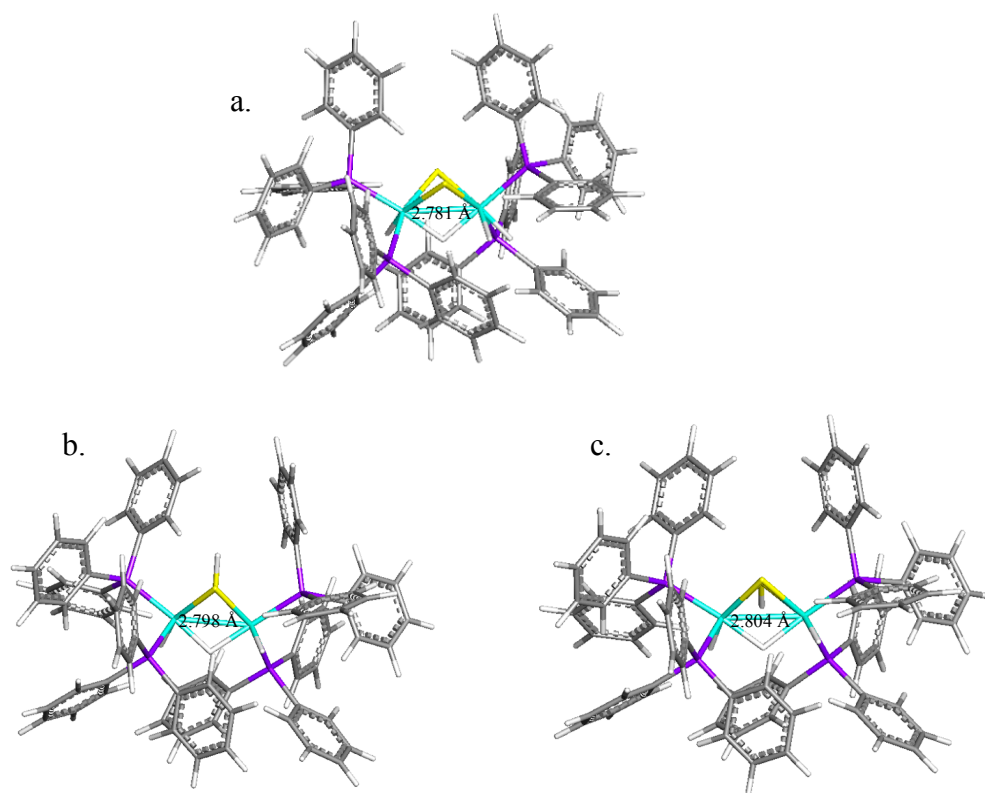
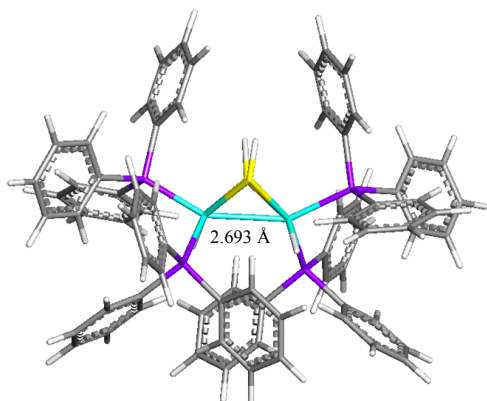
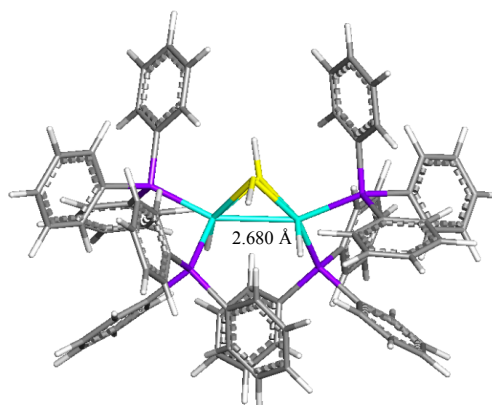


Figure 3.12 Optimized intermediates from the second activation of H_2 . 4-dbIr-brid (a.), 4-up (b.), 4-do (c.), 4-dbS-up (d.), 4-dbS-do (e.), 4*-up (f.), 4*-do (g.), 4-dbS-br-up (h.) and 4-dbS-br-do (i.).

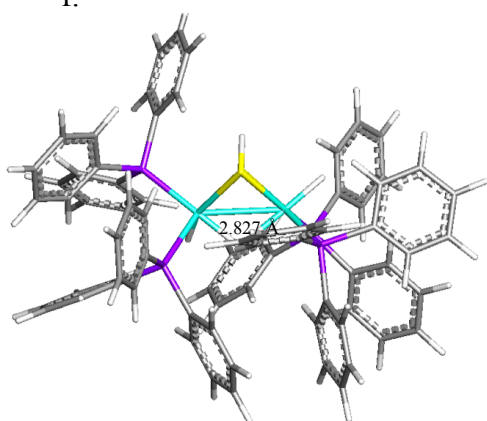
d.



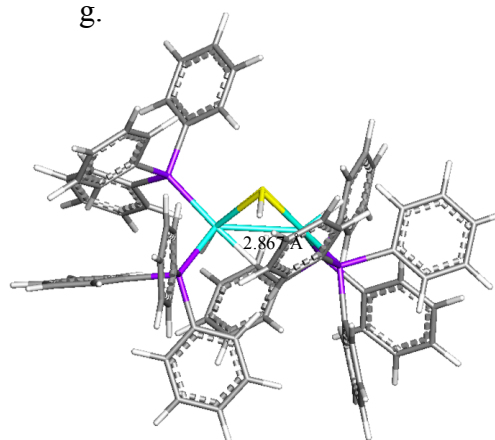
e.



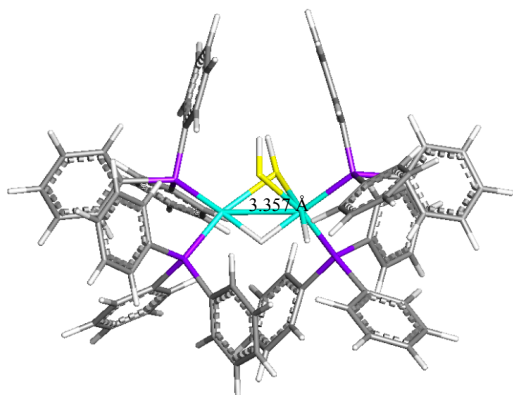
f.



g.



h.



i.

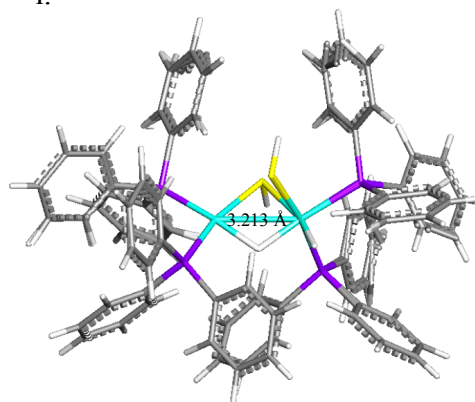


Figure 3.12 (cont.)

**Table 3.11 Relative Gas Phase Energies of Reactant and Second Product Isomers
(in Kcal/Mol)**

Structure	ΔE	ΔH	ΔG
2	0.00	0.00	0.00
4-dbIr-brid	-28.74	-23.63	-4.41
4-up	-56.52	-50.55	-32.35
4-do	-55.33	-48.51	-29.26
4-dbS-up	-52.09	-46.16	-28.73
4-dbS-do	-50.57	-44.09	-25.80
4*-up	-50.17	-43.11	-22.56
4*-do	-51.85	-44.73	-23.65
4-dbS-br-up	-41.33	-35.19	-18.70
4-dbS-br-do	-39.69	-33.13	-14.96

The relative energies of the second-product isomers are shown in Table 3.11.

All isomers presented above are lower in energy than **3-crst** and than **3-brid** and therefore could be suitable intermediates for the second dihydrogen activation. Other isomers were also optimized, however they are not presented here, since they appear to be really high in energy.

However, the system is very crowded, due to the presence of the four triphenylphosphines, and therefore we need to examine how the geometry of the system

will promote the second activation. In order to do so we will try to connect each isomer of the second-product class with **3** and with **3-brid**, and examine all the possible mechanisms. Assuming that the second activation occurs at **3-crst**, and considering geometric constraints of the system, the following possible reactions should to be examined (Figure 3.13):

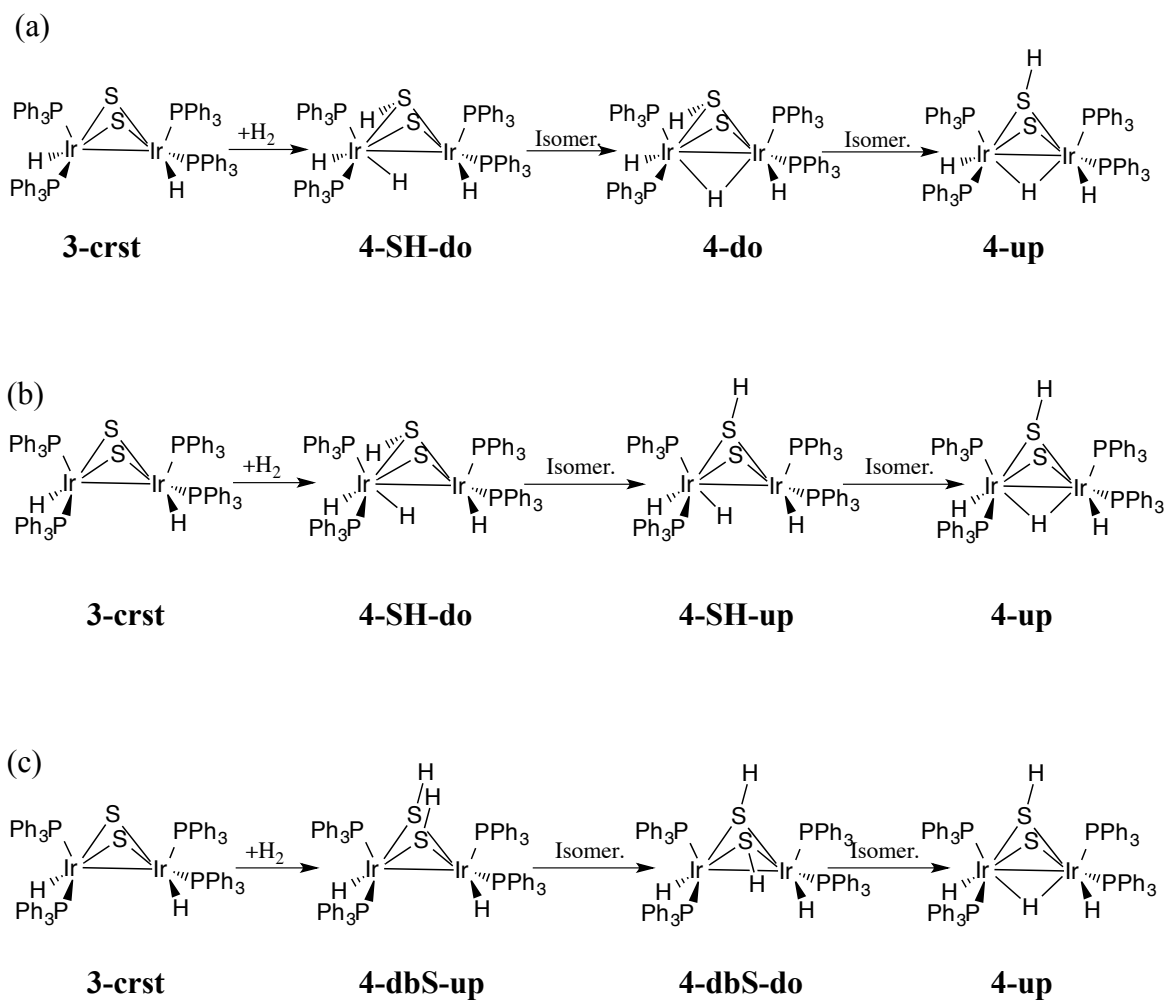


Figure 3.13 Possible reaction schemes for H_2 activation on **3-crst**.

In the first and second possible reactions Figure 3.13 (a) and (b), H₂ is activated on the S-Ir bond giving **4-SH-do**. In (a) the terminal hydride migrates to bridging position to give **4-do**, and then the sulfhydryl group rotates “up” in order to get the final product, **4-up**. In (b) the sulfhydryl group rotates first to give **4-SH-up**, and then the terminal hydride migrates to the bridging site, to isomerize in the final product, **4-up**. These two pathways could be possible, however the exhaustive search that was performed in both ωB98X-D, BP86 and M06L functionals failed to locate an intermediate that corresponds to **4-SH-up** and **4-SH-do**.

In the third reaction scheme (c), H₂ is activated homolytically at each S. This reaction, although possible due to the geometry and the energy of the isomers, cannot occur, since it is symmetry forbidden. Each S atom acts like a Lewis base, since it has a lone pair of electrons. As the H₂ approaches the core of the sulfide, S cannot provide an orbital of the correct symmetry that would accept the electron pair of the σ orbital of dihydrogen. Therefore this reaction will not proceed via this mechanism. That being the case, the reaction will not proceed via this mechanism.

Hence, we can see that the second activation cannot occur on **3-crst**, and we need to examine the possibility that the second activation occurs at **3-brid**, which as already mentioned seems to be in equilibrium with **3-crst**.

When we examine the activation of dihydrogen that occurs in **3-brid** we need to consider the following reaction mechanisms (Figure 3.14), which are in accordance with the energetics and the steric hindrance of the system:

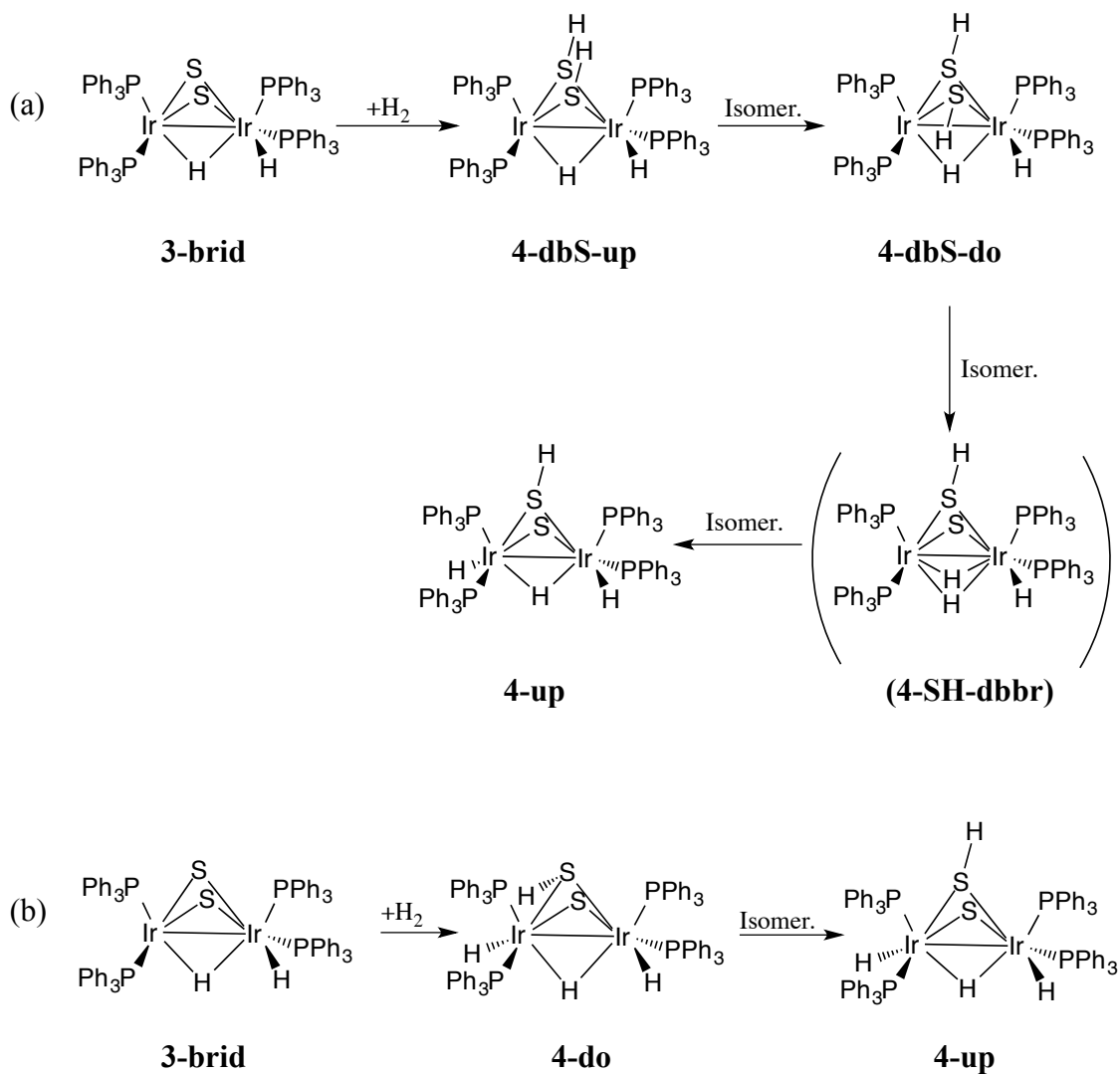


Figure 3.14 Possible reaction scheme for H_2 activation on **3-brid**.

In the first mechanism, illustrated in Figure 3.14 (a), H₂ is homolytically activated at each S. This pathway cannot be followed, since this reaction is symmetry forbidden. The second possible pathway, shown in Figure 3.14 (b), involves heterolytic activation of dihydrogen along the Ir-S bond, to give **4-do** which is further isomerized to **4-up**. This mechanism is symmetry allowed, and quite possible to occur due to geometric and energetic constraints. This heterolytic cleavage produces the final product that was observed by Rauchfuss, however the intermediate does not have a structure similar to the one supposed to be **4*** (**4*-up** or **4*-do**, not specified by the experiment).

All optimized second-product isomers have a similar phenyl ring arrangement, except from **4*** (**4*-up**, **4*-do**). In **4*** (**4*-up**, **4*-do**) the phenyl rings are arranged completely different; we could get to that arrangement by a two-fold rotation on one of the metal centers on **4**. However, this isomer does not appear to be on the same potential energy surface of our reaction for two reasons: the steric hindrance caused by the rings does not allow the dihydrogen to approach the metal-center in many directions, as there are only 3 possible directions of the H₂ to approach. This determines the position of the hydrogen atoms on the second-product, and the only possible way for the dihydrogen to be introduced leads to **4-do** isomer. The possibility that the rotation occurs after the second-activation is abandoned, due to the fact that **4*-do** is ~ 10 kcal/mol higher in energy. The rotation could potentially occur before the second activation (resulting in a “rotated” **3-brid** species, however we were not able to locate any stable intermediates of that structure.

Combining the two parts of the reaction, we can propose a mechanism for the dihydrogen activation on **2** (Figure 3.15).

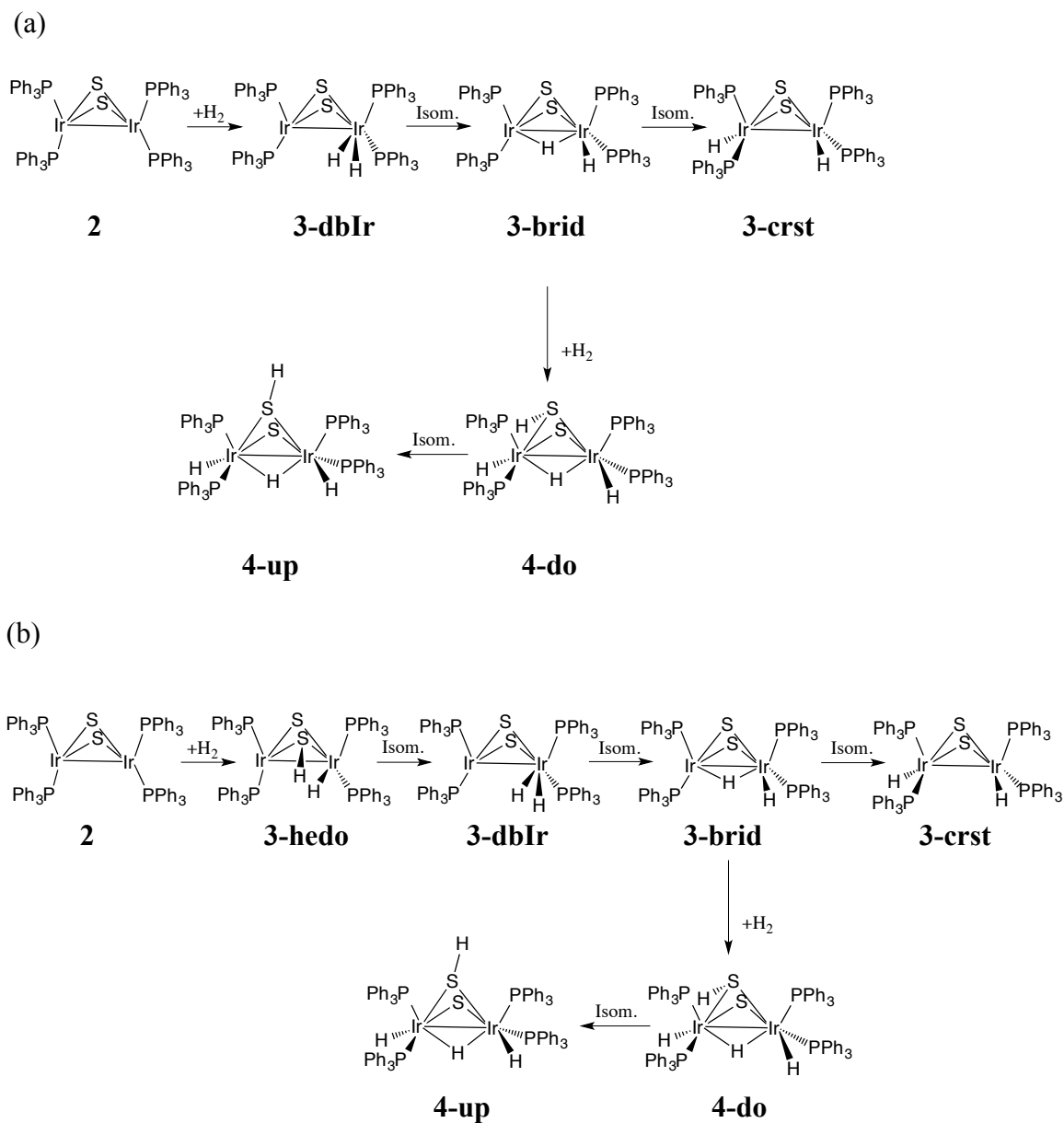


Figure 3.15 Proposed mechanisms for H_2 activation on $Ir_2(\mu-S)_2(PPh_3)_4$.

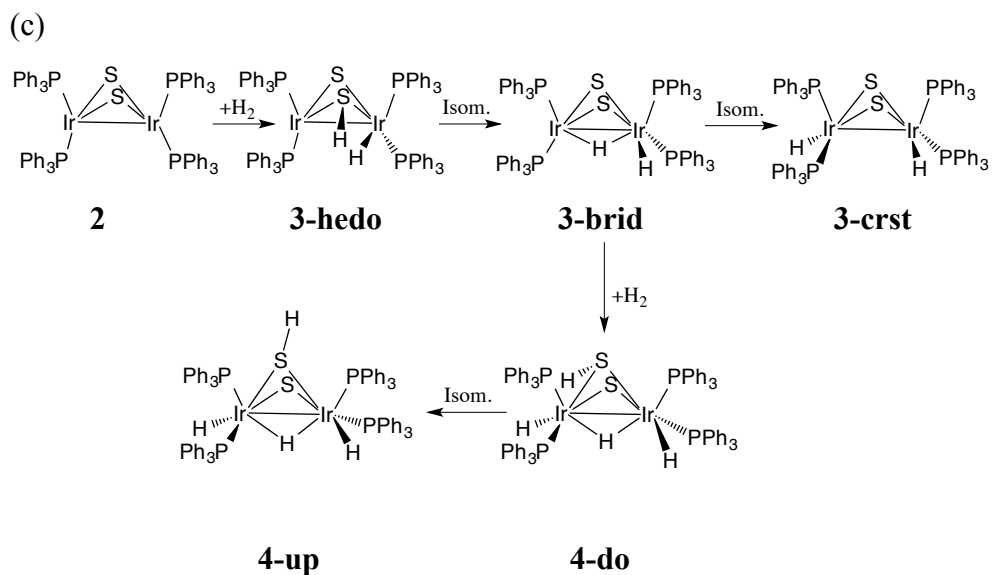


Figure 3.15 (cont.)

The first step of the reaction is the dihydrogen activation on **2**, which can be either homolytic (Figure 3.15 (a) - from now on described as “mechanism a”) or heterolytic (Figure 3.15 (b) and (c) - from now on described as “mechanism b” and “mechanism c”).

In the homolytic case, the dihydrogen is added directly on the iridium forming **3-dbIr**, and then one hydrogen atom migrates to the bridging site between the two metals (**3-brid**). Finally the bridging H migrates to a terminal position, giving rise to **3-crst**.

In the two heterolytic cases, the incoming H₂ is cleaved between the Ir-S bond, forming **3-hedo**, which can then isomerize into either **3-brIr** or **3-brid** in order for the reaction to proceed as described above.

As mentioned earlier, although **3-crst** is the lowest energy isomer of the first –product-class, it appears to be in equilibrium with **3-brid**, which is where the second activation occurs. We therefore believe that what Rauchfuss crystallized as (**3**) is the isomer that corresponds to **3-brid**. If we examine the iridium-iridium bond in **3-crst** and **3-brid** (Table 3.12) we can see that the short metal-metal bond length that was observed in the experiment (2.757 Å), corresponds to the preserved bond that still exists in the bridging species (2.74671).

In addition if we examine the Ir-S bond lengths we can see a correlation between the reported crystal structure and the optimized **3-brid** structure (Table 3.13). The bond lengths predicted from **3-brid** are all within 0.08 Å of accuracy when compared to the crystal structure. We can therefore conclude that the crystal structure of (**3**) actually corresponds to **3-brid**, and that the crystal was most likely disordered, resulting in densities corresponding to hydrogen atoms on both Ir. Furthermore, it would be almost impossible to observe the bridging hydrogen atom of **3-brid** due to the high electron density of the two metals, and the proximity of the H to both Ir.

Table 3.12 Iridium-Iridium Bond Length in 2, 3-crst and 3-brid (in Å)

Functional	Bond length in 2	Bond length in 3-crst	Bond length in 3-brid
BP86	2.87744	3.04118	2.80062
B3LYP	2.87703	3.12952	2.81497
TPSS	2.83228	2.98278	2.79042
TPSSh	2.81545	2.99236	2.78092
M06	2.80030	2.96806	2.77890
M06L	2.76211	2.89406	2.76327
PBE1PBE	2.80055	3.00125	2.76372
ω B97X-D	2.75096	2.93595	2.74671

Table 3.13 Geometrical Parameters for 3 (reported crystal structure) and 3-brid (optimized structure)

Bond	Bond length in 3 crystal Structure	Bond length in optimized 3-brid
Ir-S [†]	2.2907(18) Å	2.36491 Å
Ir-S [‡]	2.3619(17) Å	2.43826 Å
Ir-P [†]	2.2666(17) Å	2.31355 Å
Ir-P [‡]	2.2672(16) Å	2.32573 Å
Ir-Ir	2.7541(50) Å	2.74671 Å

[†] indicates “short” bond

[‡] indicates “long” bond

The second activation is a purely heterolytic one, in which the H₂ molecule is cleaved through the iridium-sulfur bond, forming **4-do**. Finally, the hydrogen atom that bonded to the sulfur rotates upwards, providing the final product, **4-up**. Therefore the short-lived intermediate observed by Rauchfuss (**4***) seems to be our calculated **4-do** and the final observed product of the reaction (originally named **4**), seems to be our optimized **4-up**.

Relative electronic energies of intermediates and corresponding transition states are shown in Figure 3.16, and Figure 3.17 respectively.

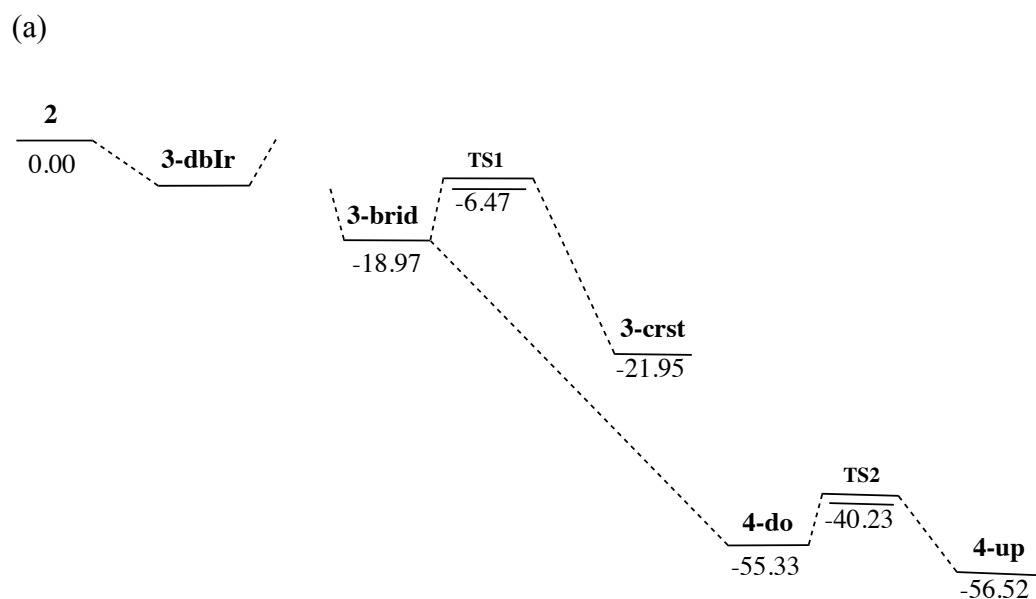


Figure 3.16 Electronic profile for the proposed mechanisms a, b and c. (all energies reported in kcal/mol)

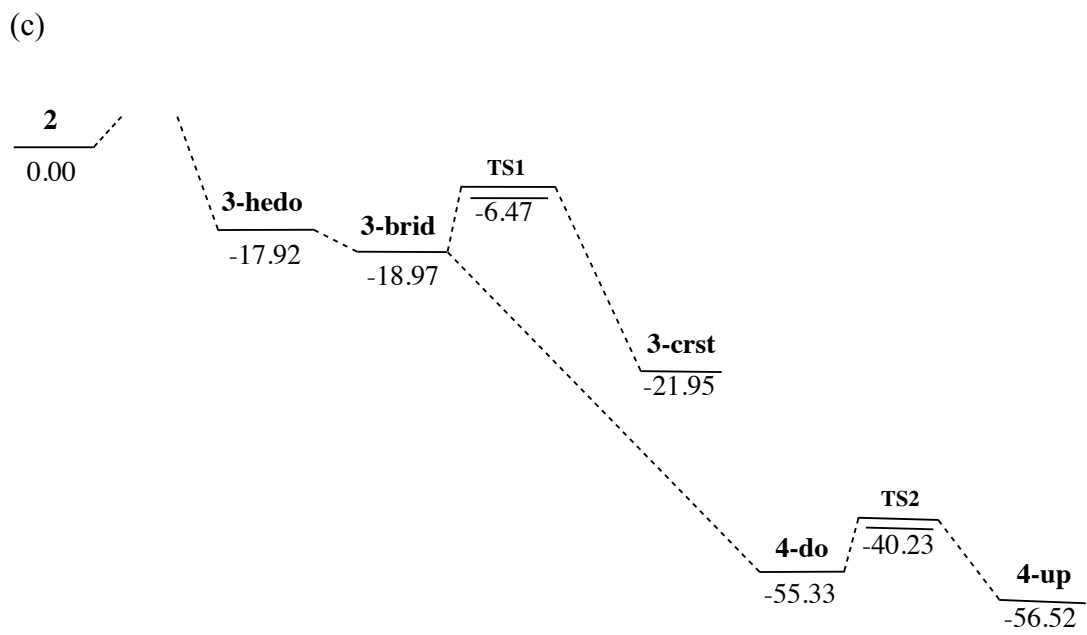
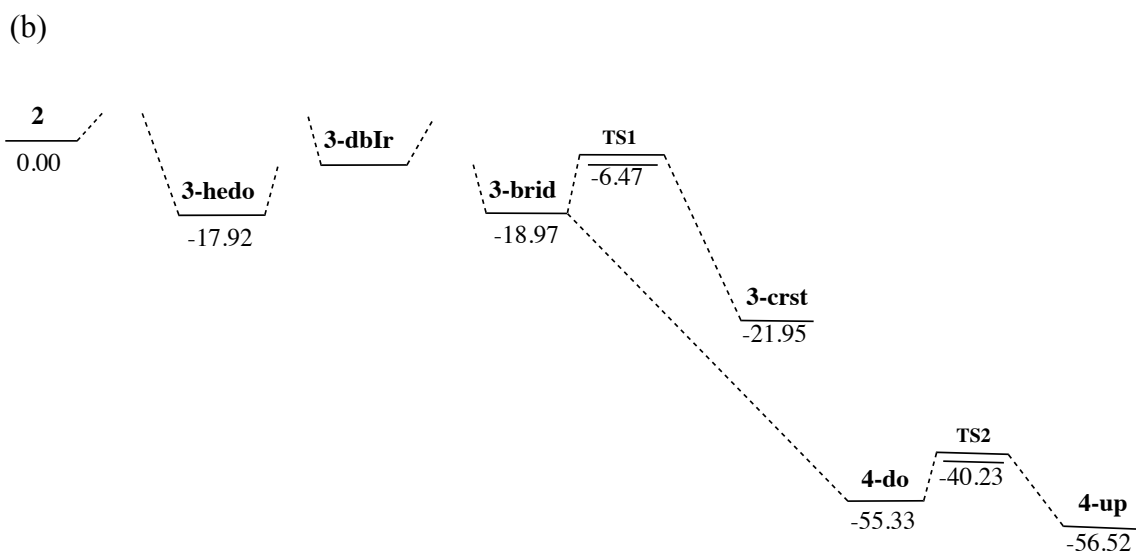


Figure 3.16 (cont.)

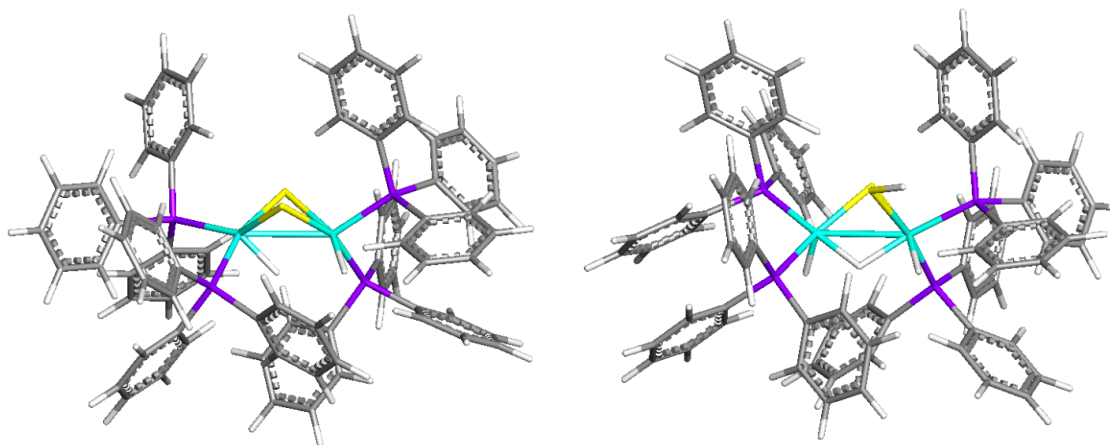


Figure 3.17 Geometries of TS 1 (left) and TS 2 (right).

From the energy diagram above, we can see that some transition states are missing. Although, it is unclear why, some were hard to calculate due to the fact that the PES is expected to be rather flat during most of the reactions. For example the transition state that corresponds to the rotation of the hydrogen between **3h-do** and **3-brid** can be calculated in functionals that lack dispersion, but cannot be located using ω B97X-D. The same applies to the transition state that connects **3-dblr** and **3-brid**. Future work that is not presented in this thesis would include locating the remaining transition states. This work will be completed before publication of this work.

All calculated energies mentioned so far correspond to gas phase calculations, yet the experiment was conducted in toluene solutions of the sulfides. We therefore need to account for the solvent, by performing single-point solvation corrections. Since all complexes in this study are neutral, and due to the protection of the metal core by the surrounding phenyl rings, as well as the non-polar nature of the solvent, we would not expect any major discrepancies on the geometries or the relative energy differences between the optimized intermediates. Table 3.14 shows the relative solvated energies of all complexes that participate in the reaction.

**Table 3.14 Relative Solvated Energies of Full Ligand System Isomers
(in Kcal/Mol)**

Structure	ΔE	ΔH	ΔG
2	0.00	0.00	0.00
3heup	-29.34	-29.70	-18.76
3hedo	-29.77	-30.67	-20.57
3-brid	-31.72	-33.77	-22.29
3-crst	-34.39	-36.04	-22.24
4-up	-80.41	-82.80	-61.64
4-do	-79.19	-80.73	-58.20
4*-up	-73.55	-74.86	-52.10
4*-do	-75.37	-75.87	-53.73

It is clear that **3-brid** and **3-crst** are indeed in equilibrium with each other, since they both have the same free energy, when in solution.

If we compare the difference between the calculated gas-phase energies and the calculated solvation corrections (Table 3.15) we can observe that there is a constant difference in energy of ~ 41 kcal/mol due to interactions with the solvent molecules.

Structure	$\Delta\Delta G$
2	-43.60
3-heup	-40.98
3-hedo	-43.15
3-brid	-43.21
3-crst	-40.94
4-up	-40.05
4-do	-39.71
4*-up	-40.32
4*-do	-40.86

$\dagger\dagger\Delta\Delta G$ refers to the solvated Gibbs free energy minus the gas phase Gibbs free energy

These results suggest that there is no further need to optimize each structure in solution, and that we can be fairly confident that the proposed reaction mechanism will not be changed in solution.

4 SUMMARY AND CONCLUSION

The electronic structure and mechanistic details of two consecutive hydrogen activations on an iridium (II) sulfide were successfully studied in this work with the aid of density functional theory. Calculations using the ω B97X-D functional and a moderate-sized basis set were performed for both model system structures, as well as full ligand system structures, in order to fully understand the way that the reaction proceeds.

The first reaction can be either homolytic or heterolytic in nature: the homolytic case produces a dihydrogen intermediate $\text{H}_2\text{Ir}(\text{PPh}_3)_2(\mu\text{-S})_2\text{Ir}(\text{PPh}_3)_2$ (**3-dbIr**) which then isomerizes to an intermediate with a bridging hydrogen (**3-brid**), leaving the bridging hydrogen to finally migrate on the other iridium, to produce a structure with two terminal hydrides (**3-crst**). The heterolytic activation occurs along the Ir-S bond, producing a reaction with a terminal hydride and a protonated sulfur (**3-hedo**). The hydrogen attached to sulfur, can either migrate to the protonated metal producing (**3-dbIr**) or it can rotate downwards, and occupy the bridging site between the two metals (**3-brid**). The reaction then proceeds as described above.

The second activation occurs on **3-brid**, and is purely heterolytic in nature. The activation occurs again along the Ir-S bond producing **4-do**, followed by a rotation of the sulfhydryl group, which produces the final product **4-up**.

The experimental data that were reported by Rauchfuss et al. reported that the metal-metal bond was preserved during the first reaction, something that is not validated on the present study. It is clear from our calculations that the metal-metal bond is broken in **3-crst** (indicated from the elongated Ir-Ir bond) yet it is preserved in the isomer with one bridging-hydrogen, **3-brid**.

We can therefore deduce, that the crystal observed by the experimental group that was believed to be **3-crst**, was actually a disordered crystal of **3-brid**. With regards to the second part of the reaction, the second hydrogen activation proceeds through the bridging isomer, since **3-brid** appears to be more stable in solution than **3-crst**. The final product of the reaction is $\text{Ir}_2(\mu\text{-S})(\mu\text{-SH})(\mu\text{-H})\text{H}_2(\text{PPh}_3)_4$ (**4**) which is in agreement with the result reported by Rauchfuss and in good agreement with the previously published crystal structure by Pignolet et al. The short-lived intermediate that was proposed by Rauchfuss (**4***), exists in the form **4-do**, but it appears to be geometrically different than the structure proposed.

The unusual reactivity of this system, which causes the system to bind two equivalents of hydrogen, could potentially be utilized in catalytic cycles, incorporating other transition metals that would provide a cheap but effective alternative to platinum-based catalysts.

REFERENCES

1. Arakawa, H.; Aresta, M.; Armor, J.N.; Barteau, M.A.; Beckman, E.J.; Bell, A.T.; Bercaw, J.E.; Creutz, C.; Dinjus, E.; Dixon, D.A.; Domen, K.; DuBois, D.L.; Eckert, J.; Fujita, E.; Gibson, D.H.; Goddard, W.A.; Goodman, D.W.; Keller, J.; Kubas, G.J.; Kung, H.H.; Lyons, J.E.; Manzer, L.E.; Marks, T.J.; Morokuma, K.; Nicholas, K.M.; Periana, R.; Que, L.; Rostrup-Nielson, J.; Sachtler, W.M. H.; Schmidt, L.D.; Sen, A.; Somorjai, G.A.; Stair, P.C.; Stults, B.R.; Tumas, W. *Chem Rev* **2001**, *101*, 953.
2. Winter, C.J. *Int J Hydrogen Energy* **2005**, *30*, 1371.
3. Zhang, X.M.; Bruno, J.W.; Enyinnaya, E.J. *Org. Chem.* **1998**, *63*, 4671.
4. Darwent B. *Nat. Stand. Ref. Data Ser.*, Nat. Bur. Stand. **1970**, (NSRDS–NBS 31).
5. Gordon, M.S.; Truong, T.N.; Pople, J.A. *Chem. Phys. Lett.* **1986**, *130*, 245.
6. Collman J.P. *Nature Structural Biology* **1996**, *3*, 213.
7. Kubas, G.J. *J. Organomet. Chem.* **2001**, *635*, 37.
8. Gunanathan, C.; Gnanaprakasam, B.; Iron, M.A.; Shimon, L.J.W.; Milstein, D. *J. Am. Chem. Soc.* **2010**, *132*, 14763.
9. Friedrich, A.; Drees, M.; Schmedt auf der Günne, J.; Schneider, S. *J. Am. Chem. Soc.* **2009**, *131*, 17552.
10. Heiden, Z.M.; Rauchfuss, T.B. *J. Am. Chem. Soc.* **2009**, *131*, 3593.
11. Iuliis, M.Z.D.; Morris, R.H. *J. Am. Chem. Soc.* **2009**, *131*, 11263.
12. Clapham, S.E.; Guo, R.; Iuliis, M.Z.D.; Rasool, N.; Lough, A. J.; Morris, R.H. *Organometallics* **2006**, *25*, 5477.
13. Webster, C.E.; Gross, C.L.; Young, D.M.; Girolami, G.S.; Scultz, A.J.; Hall, M.B.; Eckert, J. *J. Am. Chem. Soc.* **2005**, *127*, 15091.
14. Curtis, C.J.; Miedaner, A.; Ciancanelli, R.; Ellis, W.W.; Noll, B.C.; DuBois, M.R.; DuBois, D.L. *Inorg. Chem.* **2003**, *42*, 216.
15. Tao, J.; Li, S. *Dalton Trans.* **2010**, *39*, 857.

16. Kovacs, G.; Rossin, A.; Gonsalvi, L.; Lledo's, A.; Peruzzini, M. *Organometallics* **2010**, *29*, 5121.
17. Zeng, G.; Guo, Y.; Li, S. *Inorg. Chem.* **2009**, *48*, 10257.
18. Yang, X.; Hall, M.B. *J. Am. Chem. Soc.* **2009**, *131*, 10901.
19. Nagaraja, C.M.; Parameswaran, P.; Jemmis, E.D.; Jagirdar, B.R. *J. Am. Chem. Soc.* **2007**, *129*, 5587.
20. Hedberg, C.; Kallstroöm, K.; Arvidsson, P.I.; Brandt, P.; Andersson, P.G. *J. Am. Chem. Soc.* **2005**, *127*, 15083.
21. Bruschi, M.; Fantacci, P.; Gioia, L.D. *Inorg. Chem.* **2003**, *42*, 4773.
22. Belkova, N.V.; Besora, M.; Epstein, L.M.; Lledos, A.; Maseras, F.; Shubina, E. *J. Am. Chem. Soc.* **2003**, *125*, 7715.
23. Tard, C.; Pickett, C. *J. Chem. Rev.* **2009**, *109*, 2245.
24. Capon, J.F.; Gloaguen, F.; Petillon, F.Y.; Schollhammer, P.; Talarmin, J. *Coord. Chem. Rev.* **2009**, *253*, 1476.
25. Matsumoto, T.; Itakura, N.; Nakaya, Y.; Tatsumi, K. *Chem. Commun.* **2011**, *47*, 1030.
26. Matsumoto, T.; Nakaya, Y.; Itakura, N.; Tatsumi, K. *J. Am. Chem. Soc.* **2008**, *130*, 2458.
27. Morvan, D.; Capon, J.F.; Gloaguen, F.; Petillon, F.Y.; Schollhammer, P.; Talarmin, J.; Yaouanc, J.J.; Michaud, F.; Kervarec, N.J. *Organomet. Chem.* **2009**, *694*, 2801.
28. Capon, J.F.; Gloaguen, F.; Petillon, F.Y.; Schollhammer, P.; Talarmin, J. *Eur., J. Inorg. Chem.* **2008**, 4671.
29. Adams, R.D.; Boswell, E.M.; Hall, M.B.; Yang, X. *Organometallics* **2008**, *27*, 4938.
30. Cheah, M.H.; Borg, S.J.; Best, S.P. *Inorg. Chem.* **2007**, *46*, 1741.
31. Brown, S.D.; Mehn, M.P.; Peters, J.C. *J. Am. Chem. Soc.* **2005**, *127*, 13146.
32. Zhou, T.; Mo, Y.; Zhou, Z.; Tsai, K. *Inorg. Chem.* **2005**, *44*, 4941.
33. Justice, A.K.; Linck, R.C.; Rauchfuss, T.B.; Wilson, S.R. *J. Am. Chem. Soc.* **2004**, *126*, 13214.
34. Rauchfuss, T.B. *Inorg. Chem.* **2004**, *43*, 14.
35. Georgakaki, I.P.; Miller, M.L.; Darensburg, M.Y. *Inorg. Chem.* **2003**, *42*, 2489.

36. Startsev, A.N.; Zakharov, I.I.; Parmon, V.N. *J. Mol. Catal. A* **2003**, *192*, 113.
37. Aubart, M.A.; Chandler, B.D.; Gould, R.A. T.; Krogstad, D.A.; Schoondergang, M.F.J.; Pignolet, L.H. *Inorg. Chem.* **1994**, *33*, 3724.
38. Halpern, J. *Accounts of Chemical Research* **1970**, 386.
39. Brothers, P.J. (2007) Heterolytic Activation of Hydrogen by Transition Metal Complexes, in *Progress in Inorganic Chemistry, Volume 28* (ed S. J. Lippard), John Wiley & Sons, Inc., Hoboken, NJ, USA.
40. Devarajan D., Ess D.H. *Inorg. Chem.*, **2012**, *51*, 6367.
41. Schrödinger, E. *Ann. Physik.* **1926**, *79*, 361.
42. Pauli, W. *Z. Physik* **1925**, *31*, 765.
43. Born, M. *Proc. R. Soc. Lond. A* **1934**, *143*, 410.
44. Born, M.; Oppenheimer, R. *Ann. Physik.* **1927**, *84*, 457.
45. Hartree, D.R. *Proc. Cambridge Phil. Soc.* **1928**, *24*, 89.
46. Hartree, D.R. *Proc. Cambridge Phil. Soc.* **1928**, *24*, 111.
47. Hartree, D.R. *Proc. Cambridge Phil. Soc.* **1928**, *24*, 426.
48. Fock, V. *Z. Physik* **1930**, *62*, 795.
49. Slater, J.C. *Phys. Rev.* **1929**, *34*, 1293.
50. Slater, J.C. *Phys. Rev.* **1930**, *35*, 509.
51. Slater, J.C. *Phys. Rev.* **1930**, *36*, 57.
52. Boys, S.F. *Proc. Roy. Soc.* **1950**, *A200*, 542.
53. Davidson, E.R.; Feller, D. *Chem. Rev.* **1986**, *86*, 681.
54. Hehre, W.J.; Stewart, R. F.; Pople, J.A. *J. Chem. Phys.* **1969**, *51*, 2657.
55. Clementi, E. *IBM J. Res. Develop.* **1965**, *9*, 2.
56. Hehre W.J.; Steward R.F.; Pople J.A. *J. Chem. Phys.* **1969**, *51*, 2657.
57. Atkins, P.; Friedman, R. (2005) *Molecular Quantum Mechanics*, Oxford University Press Inc., New York, USA.
58. Pople J.A.; Hehre W.J. *J. Comp. Phys.* **1978**, *27* (2), 162.
59. Boys S.F.; Bernardi F., *Mol. Phys.* **1970**, *19*, 553.
60. Boys, S.F. *Proc. Roy. Soc.* **1950**, *A201*, 125.

61. Langhoff, S.R.; Davison, E.R. *Int. J. Quantum Chem*, **1974**, *8*, 61.
62. Pople, J.A.; Binkley, J.S.; Seeger, R. *Int. J Quantum Chem. Symp.* **1976**, *1*, 10.
63. Christiansen, O.; Olsen, J.; Jorgensen, P.L.; Koch, H.; Malmqvist, P.A. *Chem. Phys. Lett.* **1996**, *261*, 369.
64. Pople, J.A.; Binkley, J.S.; Seeger, R. *Int. J Quantum Chem. Symp.* **1976**, *1*, 10.
65. Møller, C.; Plesset, M. S. *Phys. Rev.* **1934**, *46*, 618.
66. Hohenberg, P.; Kohn, W. *Phys. Rev.* **1964**, *136*, 864.
67. Kohn, W.; Sham, L.J. *Phys. Rev.* **1965**, *140*, A1133.
68. Bray, M.R.; Deeth, R.J.; Paget V.J.; Sheen, P.D. *Int. J. Quantum Chem*, **1997**, *61*, 85.
69. Vosko, S.H.; Wilk, L.; Nusair, M. *Can. J. Phys.*, **1980**, *58*, 1200.
70. Lee, C.; Yang, W.; Parr, R.G. *Phys. Rev. B*, **1998**, *37*, 785.
71. Miehlich, B.; Savin, A.; Stoll, H.; Preuss, H. *Chem. Phys. Lett.*, **1989**, *157* 200.
72. Zhao, Y.; Schultz, N.E.; Truhlar, D.G. *J. Chem. Phys.* **2005**, *123*, 161103.
73. Zhao, Y.; Truhlar, D.G. *J. Chem. Phys.*, **2006**, *125* (2006), 1.
74. Chai, J.D.; Head-Gordon, M. *Phys. Chem. Chem. Phys.*, **2008**, *10*, 6615.
75. Linck, R.C.; Pafford, R.J.; Rauchfuss, T.B. *J Am Chem Soc.* **2001**, *123*(36), 8856.
76. Mueting, A.M.; Boyle, P.D.; Wagner, R.; Pignolet, L.H. *Inorg. Chem.*, **1988**, *27*, 271.
77. Gaussian 09, Revision D.01, Frisch, M.J.; Trucks, G.W.; Schlegel, H.B.; Scuseria, G.E.; Robb, M.A.; Cheeseman, J.R.; Scalmani, G.; Barone, V.; Mennucci, B.; Petersson, G.A.; Nakatsuji, H.; Caricato, M.; Li, X.; Hratchian, H.P.; Izmaylov, A.F.; Bloino, J.; Zheng, G.; Sonnenberg, J.L.; Hada, M.; Ehara, M.; Toyota, K.; Fukuda, R.; Hasegawa, J.; Ishida, M.; Nakajima, T.; Honda, Y.; Kitao, O.; Nakai, H.; Vreven, T.; Montgomery, J.A.; Peralta, J.E.; Ogliaro, F.; Bearpark, M.; Heyd, J.J.; Brothers, E.; Kudin, K.N.; Staroverov, V.N.; Kobayashi, R.; Normand, J.; Raghavachari, K.; Rendell, A.; Burant, J.C.; Iyengar, S. S.; Tomasi, J.; Cossi, M.; Rega, N.; Millam, N. J.; Klene, M.; Knox, J.E.; Cross, J. B.; Bakken, V.; Adamo, C.; Jaramillo, J.; Gomperts, R.; Stratmann, R.E.; Yazyev, O.; Austin, A. J.; Cammi, R.; Pomelli, C.; Ochterski, J.W.; Martin, R.L.; Morokuma, K.; Zakrzewski, V.G.; Voth, G.A.;

- Salvador, P.; Dannenberg, J.J.; Dapprich, S.; Daniels, A.D.; Farkas, Ö.; Foresman, J.B.; Ortiz, J.V.; Cioslowski, J.; Fox, D.J. Gaussian, Inc., Wallingford CT, 2009.
78. Tao, J.M.; Perdew J.P.; Staroverov, V.N.; Scuseria, G.E. *Phys. Rev. Lett.* **2003**, *91*, 146401.
79. Ditchfield, R.; Hehre, W.J.; Pople J.A. *J. Chem. Phys.* **1971**, *54*, 724.
80. Hehre, W.J.; Ditchfield, R.; Pople, J.A. *J. Chem. Phys.* **1972**, *56*, 2257.
81. Hariharan, P.C.; Pople J.A. *Theor. Chem. Acc.*, **1973**, *28*, 213.
82. Hariharan, P.C.; Pople J.A. *Mol. Phys.*, **1974**, *27*, 209.
83. Gordon, M.S. *Chem. Phys. Lett.*, **1980**, *76*, 163.
84. Francl, M.M.; Pietro, W.J.; Hehre, W.J.; Binkley, J.S.; DeFrees, D.J.; Pople J.A.; Gordon, M.S. *J. Chem. Phys.*, **1982**, *77*, 3654.
85. Binning, Jr R.C.; Curtiss, L.A. *J. Comp. Chem.*, **1990**, *11*, 1206.
86. Blaudeau, J.P.; McGrath, M.P.; Curtiss, L.A.; Radom, L. *J. Chem. Phys.*, **1997**, *107*, 5016.
87. Rassolov, V.A.; Pople, J.A.; Ratner, M.A.; Windus, T.L. *J. Chem. Phys.*, **1998**, *109*, 1223.
88. Rassolov, V.A.; Ratner, M.A.; Pople, J.A.; Redfern, P.C.; Curtiss L.A. *J. Comp. Chem.*, **2001**, *22*, 976.
89. Grimme, S., *J. Comp. Chem.*, **27** (2006) 1787.
90. Chai, J.D.; Head-Gordon, M. *Phys. Chem. Chem. Phys.*, **2008**, *10*, 6615.
91. Chiba, M.; Tsuneda, T.; Hirao, K. *J. Chem. Phys.*, **2006**, *123*, 144106.
92. Song, J.W.; Kamiya, M.; Tsuneda, T.; Hirao, K. *J. Chem. Phys.*, **2007**, *126*, 154105.
93. Becke, A. D. *J. Chem. Phys.* **1993**, *98*, 5648.
94. Marenich, A.V.; Cramer, C.J.; Truhlar, D.G. *J. Phys. Chem. B*, **2009**, *113*, 6378.
95. Miertuš, S.; Scrocco, E.; Tomasi, J. *Chem. Phys.*, **1981**, *55*, 117.
96. Miertuš, S.; Tomasi, J. *Chem. Phys.*, **1982**, *65*, 239.
97. Pascual-Ahuir, J.L.; Silla, E.; Tuñón, I. *J. Comp. Chem.*, **1994**, *15*, 1127.

98. Cossi, M.; Barone, V.; Cammi, R.; Tomasi, J. *Chem. Phys. Lett.*, **1996**, 255, 327.
99. Barone, V.; Cossi, M.; Tomasi, J. *J. Chem. Phys.*, **1997**, 107, 3210.
100. Cancès, E.; Mennucci, B.; Tomasi, J. *J. Chem. Phys.*, **1997**, 107, 3032.
101. Mennucci, B.; Tomasi, J. *J. Chem. Phys.*, **1997**, 106, 5151.
102. Mennucci, B.; Cancès, E.; Tomasi, J. *J. Phys. Chem. B*, **1997**, 101, 10506.
103. Barone, V.; Cossi, M. *J. Phys. Chem. A*, **1998**, 102, 1995.
104. Cossi, M.; Barone, V.; Mennucci, B.; Tomasi, J. *Chem. Phys. Lett.*, **1998**, 286, 253.
105. Barone, V.; Cossi, M.; Tomasi, J. *J. Comp. Chem.*, **1998**, 19, 404.
106. Cammi, R.; Mennucci, B.; Tomasi, J. *J. Phys. Chem. A*, **1999**, 103, 9100.
107. Cossi, M.; Barone, V.; Robb, M.A. *J. Chem. Phys.*, **1999**, 111, 5295.
108. Tomasi, J.; Mennucci, B.; Cancès, E. *J. Mol. Struct. (Theochem)*, **1999**, 464, 211.
109. Cammi, R.; Mennucci, B.; Tomasi, J. *J. Phys. Chem. A*, **2000**, 104, 5631.
110. Cossi, M.; Barone, V. *J. Chem. Phys.*, **2000**, 112, 2427.
111. Cossi, M.; Barone, V. *J. Chem. Phys.*, **2001**, 115, 4708.
112. Cossi, M.; Rega, N.; Scalmani, G.; Barone, V. *J. Chem. Phys.*, **2001**, 114, 5691.
113. Cossi, M.; Scalmani, G.; Rega, N.; Barone, V. *J. Chem. Phys.*, **2002**, 117, 43.
114. Cossi, M.; Rega, N.; Scalmani, G.; Barone, V. *J. Comp. Chem.*, **2003**, 24, 669.
115. Cížek, J. in *Advances in Chemical Physics*, Ed. P.C. Hariharan, Vol. 14 (Wiley Interscience, New York, 1969) 35.
116. Purvis, III, G.D.; Bartlett, R.J. *J. Chem. Phys.*, **1982**, 76, 1910.
117. Scuseria, G.E.; Janssen, C.L.; Schaefer, III, H.F. *J. Chem. Phys.*, **1988**, 89, 7382.
118. Scuseria, G.E.; Schaefer III, H.F. *J. Chem. Phys.*, **1989**, 90, 3700.
119. Tao J.M.; Perdew J.P.; Staroverov V.N.; Scuseria G.E. *Phys. Rev. Lett.*, **2003**, 91, 146401
120. Becke, A.D. *Phys. Rev. A*, **1988**, 38, 3098.
121. Perdew, J.P. *Phys. Rev. B*, **1986**, 33, 8822.
122. Zhao Y.; Truhlar D.G. *Theor. Chem. Acc.*, **2008**, 120, 215.
123. Perdew, J.P.; Burke, K.; Ernzerhof, M. *Phys. Rev. Lett.*, **1997**, 78, 1396.
124. Adamo, C.; Barone, V. *J. Chem. Phys.*, **1999**, 110, 6158.

125. Hall, M.B.; Fenske, R.F. *Inorg. Chem.* **1972**, *11*, 768.
126. Manson, J.; Bursten, B.E.; Jensen, J.R.; Fenske, R.F. *J. Chem. Phys.* **1978**, *68*, 3320.
127. Webster, C.E.; Pérez, L.M.; Hall, M.B. **2006**.
<http://www.chem.tamu.edu/jimp2/index.html>
128. Lin, Z.; Hall, M.B. *J. Am. Chem. Soc.* **1992**, *114*, 2928.
129. Song, J.; Hall, M.B. *J. Am. Chem. Soc.* **1993**, *115*, 327.
130. Fan, H.J.; Hall, M.B. (Unpublished communication, contact hall@science.tamu.edu).

APPENDICES

Appendix A: Geometrical Parameters of Isomers of the Model System

Cartesian Coordinates of 2'

Symbol	X	Y	Z
S	0.077524	-0.815656	1.70198
S	-0.077523	-0.815621	-1.701994
P	2.135477	1.674151	1.188963
P	3.367072	-0.929854	-0.593594
P	-3.367072	-0.929863	0.593575
P	-2.13548	1.674168	-1.188935
Ir	-1.355378	-0.01324	0.120857
Ir	1.355378	-0.013237	-0.120856
H	3.483786	1.737486	1.635216
H	2.082914	2.980567	0.643628
H	1.512443	1.957508	2.428348
H	3.891388	-0.986386	-1.911327
H	4.557148	-0.479458	0.033862
H	3.501947	-2.304686	-0.294065
H	-3.891381	-0.986438	1.91131
H	-4.557149	-0.479438	-0.033861
H	-3.501956	-2.304684	0.293998
H	-3.483795	1.737512	-1.635174
H	-2.082907	2.98058	-0.643588
H	-1.512456	1.957536	-2.428324

Cartesian Coordinates of 3f'

Symbol	X	Y	Z
S	0.063686	-1.616947	-0.890567
S	-0.051817	1.609436	-0.899231
P	-3.311531	-1.167617	-0.689161
P	-2.329964	1.616079	1.371733
P	3.288923	0.806233	-1.006692
P	2.371783	-1.372122	1.615911
Ir	1.461684	0.050574	0.047378
Ir	-1.472491	-0.021669	-0.023041
H	1.726432	1.185854	1.11981
H	-1.591168	-0.960843	1.222419
H	-3.157181	-1.777705	-2.415852
H	-4.866571	-0.192716	-0.786364
H	-3.766736	-2.685402	0.239141
H	2.930352	1.283648	-2.75007
H	4.146079	2.286748	-0.334327
H	4.645268	-0.412189	-1.251947
H	3.855425	-0.735964	2.504221
H	2.837337	-3.07885	1.140577
H	1.209651	-1.705762	3.001936
H	-3.51845	1.040591	2.664464
H	-3.131542	3.090989	0.647252
H	-0.964825	2.317529	2.384691

Cartesian Coordinates of 3h'

Symbol	X	Y	Z
S	-0.021235	1.556985	-0.986884
S	0.014482	-1.710984	-0.816394
P	3.353572	1.128893	-0.69212
P	2.297155	-1.402387	1.533401
P	-3.27195	-0.708631	-1.041017
P	-2.343615	1.431082	1.572923
Ir	-1.439163	-0.055402	0.096296
Ir	1.455183	0.008615	-0.045608
H	-1.741987	-1.168248	1.202669
H	0.128351	-1.35181	-2.108086
H	3.256763	1.56068	-2.480016
H	4.9482	0.20667	-0.627073
H	3.79585	2.735105	0.094154
H	-2.845653	-1.137128	-2.784619
H	-4.150479	-2.210144	-0.442303
H	-4.644156	0.491768	-1.29048
H	0.909488	-2.104253	2.516176
H	-3.850876	0.839685	2.457113
H	3.348676	-0.606372	2.819102
H	3.22884	-2.90871	1.050807
H	-1.237582	1.877762	2.96642
H	-2.798371	3.107234	0.97783

Cartesian Coordinates of 3a'

Symbol	X	Y	Z
S	-0.025803	1.633162	-0.911846
S	0.025648	-1.633741	-0.910972
P	-3.17693	-1.41234	-0.314909
P	-2.557396	1.760349	0.969123
P	2.558408	-1.759947	0.968831
P	3.1761	1.413376	-0.314768
Ir	1.463436	-0.004957	0.010671
Ir	-1.463444	0.004728	0.010862
H	-4.346337	-1.328898	0.481345
H	-3.8068	-1.399103	-1.580928
H	-2.949257	-2.803073	-0.215638
H	-2.822069	2.927179	0.219638
H	-3.853556	1.57867	1.517708
H	-1.967939	2.382845	2.093423
H	2.822324	-2.927182	0.219718
H	3.855154	-1.577858	1.515884
H	1.97026	-2.381871	2.094145
H	4.346421	1.32898	0.480046
H	3.804547	1.402381	-1.581503
H	2.948189	2.803887	-0.212999
H	-1.507173	-0.726756	1.426057
H	1.506575	0.726181	1.426011

Cartesian Coordinates of 3b'

Symbol	X	Y	Z
S	-0.008953	-1.610661	-1.056178
S	-0.008841	1.610475	-1.056398
P	2.547413	1.74441	0.833882
P	2.547015	-1.744418	0.834531
P	-2.777913	-1.762759	0.51698
P	-2.777408	1.763089	0.517559
Ir	-1.418202	0.000054	-0.020502
Ir	1.516274	-0.000086	-0.212991
H	3.691071	1.534388	1.649209
H	3.063726	2.810214	0.063132
H	1.799077	2.515835	1.751161
H	3.063071	-2.810665	0.064224
H	3.690712	-1.534336	1.649788
H	1.798481	-2.51527	1.752127
H	-2.450414	-2.61781	1.595704
H	-4.133329	-1.53786	0.87
H	-2.98905	-2.759404	-0.459802
H	-4.132998	1.538489	0.870096
H	-2.449909	2.617389	1.596887
H	-2.987904	2.760398	-0.458681
H	2.731872	-0.000447	-1.219041
H	-1.047928	-0.000348	1.51106

Cartesian Coordinates of 3c'

Symbol	X	Y	Z
S	0.000005	1.604425	-0.953477
S	0.000005	-1.60443	-0.953469
P	-2.709275	-1.732377	0.776313
P	-2.709273	1.732381	0.776306
P	2.709266	-1.732377	0.776341
P	2.709266	1.732381	0.776332
Ir	1.55296	-0.000001	-0.170162
Ir	-1.552958	0	-0.170177
H	-3.999327	-1.526634	1.330652
H	-3.022712	-2.861116	-0.014483
H	-2.150435	-2.427432	1.874805
H	-3.02271	2.861117	-0.014495
H	-3.999324	1.526642	1.330648
H	-2.150431	2.427441	1.874795
H	3.022713	-2.861116	-0.014451
H	3.99931	-1.526635	1.330697
H	2.150411	-2.427434	1.874826
H	3.999309	1.526641	1.330692
H	3.022716	2.861114	-0.014468
H	2.15041	2.427446	1.87481
H	-2.636048	-0.000001	-1.313119
H	2.636061	-0.000004	-1.313093

Cartesian Coordinates of 3i'

Symbol	X	Y	Z
S	-0.049922	-1.543067	-1.386381
S	0.048059	1.547561	-1.260748
P	2.373508	1.756559	0.804369
P	2.398463	-1.676999	1.106422
P	-2.291631	1.782162	0.886682
P	-2.648724	-1.548366	0.905312
Ir	-1.433685	0.006005	-0.176538
Ir	1.441021	-0.047536	-0.170728
H	3.504722	1.592163	1.644947
H	2.877616	2.776176	-0.028234
H	1.603043	2.559025	1.674265
H	3.271716	-2.641649	0.541747
H	3.233096	-1.321244	2.19668
H	1.578844	-2.593344	1.814031
H	-2.733493	2.89446	0.130097
H	-3.423224	1.665342	1.736664
H	-1.474343	2.496611	1.795412
H	-3.227828	-1.2686	2.17213
H	-3.824779	-2.114032	0.333808
H	-2.058601	-2.789016	1.266627
H	2.729235	-0.151052	-1.09286
H	-0.065271	-2.679217	-0.633517

Cartesian Coordinates of 3k'

Symbol	X	Y	Z
S	0.115106	0.818239	1.864393
S	0.088046	-1.987394	0.437641
P	1.818068	1.944677	-1.154636
P	3.376778	-0.683879	0.325751
P	-2.353544	-1.354846	-1.376011
P	-2.626826	1.756162	-0.039469
Ir	-1.419623	-0.128065	0.270184
Ir	1.300922	-0.06048	-0.194447
H	3.161909	2.347718	-1.380611
H	1.354453	2.192947	-2.469763
H	1.374593	3.168391	-0.588727
H	3.723921	-2.043191	0.162945
H	4.497168	-0.114718	-0.330977
H	3.824408	-0.513357	1.657173
H	-2.742517	-2.687426	-1.104686
H	-3.52941	-0.939633	-2.057045
H	-1.559402	-1.60835	-2.516256
H	-3.209857	2.048769	-1.301237
H	-3.795907	2.034142	0.725247
H	-2.018825	3.023423	0.161056
H	1.556267	-0.774822	-1.599739
H	0.035567	2.15879	1.643786

Cartesian Coordinates of 4'

Symbol	X	Y	Z
S	-0.094629	-0.928373	-1.774047
S	0.204371	-1.316261	1.376224
P	-2.6119	1.651056	-0.948635
P	-2.951205	-1.441314	0.648676
P	3.194674	-1.047429	-0.690136
P	2.248139	1.298107	1.582818
Ir	1.382941	0.217538	-0.209242
Ir	-1.372111	0.09927	0.176987
H	-4.003597	1.460362	-1.14435
H	-2.693005	2.96915	-0.438654
H	-2.302398	2.007522	-2.286583
H	-3.044598	-1.904798	1.976085
H	-4.322493	-1.157693	0.429398
H	-2.889106	-2.685471	-0.01478
H	4.256614	-0.541374	-1.475065
H	3.975065	-1.590751	0.358509
H	2.949182	-2.236867	-1.408597
H	3.146298	0.611507	2.43116
H	2.980177	2.503925	1.455236
H	1.308975	1.708693	2.549086
H	-1.743884	0.815544	1.555113
H	-0.218627	-0.000737	-2.75938
H	-0.020966	1.306954	0.017715
H	1.836952	1.347684	-1.286959

Cartesian Coordinates of 4*'

Symbol	X	Y	Z
S	0.178537	0.760256	1.862996
S	0.036824	-1.984479	0.366858
P	2.254804	1.920973	-1.031447
P	3.181983	-1.011658	0.618348
P	-2.44924	-1.350819	-1.350739
P	-2.671483	1.826627	0.069385
Ir	-1.44629	-0.090066	0.23297
Ir	1.332741	-0.016412	-0.284119
H	3.657885	2.119038	-0.973702
H	2.087455	2.282211	-2.389549
H	1.890587	3.177117	-0.478934
H	3.489825	-2.329681	0.22079
H	4.473209	-0.450093	0.449328
H	3.225947	-1.200508	2.017395
H	-2.953227	-2.611178	-0.976872
H	-3.59246	-0.866909	-2.042535
H	-1.66935	-1.730378	-2.460987
H	-3.666974	1.96199	-0.932184
H	-3.470953	2.240834	1.161577
H	-2.036641	3.075746	-0.157272
H	1.673997	-0.683744	-1.696755
H	0.108176	2.109117	1.69222
H	-0.138002	0.527286	-1.049954
H	-2.522904	-0.611296	1.295015

Appendix B: Geometrical Parameters of Isomers of Full Ligand System

Cartesian Coordinates of 2

Symbol	X	Y	Z
Ir	-1.377808	0.338388	-0.078414
Ir	1.368985	0.334337	0.073456
S	-0.054008	1.140266	1.677673
S	0.053067	1.090134	-1.707188
P	3.297915	1.310631	0.818729
P	2.212442	-1.296771	-1.29749
P	-3.313166	1.255288	-0.883517
P	-2.209318	-1.230189	1.367703
H	-1.53073	3.254149	0.257908
H	-1.266238	5.685429	-0.084658
H	-2.574672	6.850741	-1.852289
H	-4.184161	5.56511	-3.241163
H	-4.50244	3.150347	-2.857297
H	-2.016816	-0.059475	-3.118381
H	-2.815284	-0.985259	-5.268657
H	-5.23996	-0.943596	-5.82235
H	-6.846218	0.088671	-4.231605
H	-6.04827	1.043841	-2.1063
H	-4.556713	3.364629	0.795279
H	-6.425438	3.327878	2.400578
H	-7.741379	1.24866	2.745473
H	-7.199391	-0.7847	1.411775
H	-5.363374	-0.739151	-0.218715
H	-2.389356	-2.072525	-1.339601
H	-4.002053	-3.394057	-2.654273
H	-5.984388	-4.412956	-1.53604
H	-6.308315	-4.105478	0.907327
H	-4.713238	-2.759106	2.213532
H	2.513133	6.93837	1.535719
H	4.177336	5.740125	2.937674
H	4.512141	3.313001	2.665015
H	2.042372	0.030485	3.098861
H	2.871203	-0.794275	5.278189
H	5.292345	-0.652948	5.828779

H	6.356597	3.270478	-2.582809
H	7.712456	1.202779	-2.824738
H	7.214532	-0.769938	-1.387561
H	5.381287	-0.677165	0.245872
H	2.388422	-2.024144	1.448264
H	4.022708	-3.251949	2.822975
H	6.031934	-4.275625	1.757515
H	6.363094	-4.064044	-0.695124
H	4.747507	-2.804012	-2.063483
H	3.039664	1.221614	-2.453256
H	4.16004	1.852548	-4.569684
H	4.712496	0.105731	-6.251943
H	4.124528	-2.265905	-5.804733
H	3.010801	-2.889503	-3.69029
H	0.109222	-1.217661	-3.305623
H	-1.539355	-2.86453	-4.130374
H	-1.603385	-5.156714	-3.164428
H	0.00894	-5.782246	-1.380812
H	1.652107	-4.140034	-0.559747
H	6.865093	0.374023	4.201122
H	6.037508	1.225711	2.043763
H	4.491302	3.352688	-0.97346
H	-3.058008	1.3359	2.396517
H	-4.198264	2.060373	4.471419
H	-4.750973	0.394029	6.232569
H	-4.1448	-1.993283	5.904588
H	-3.011463	-2.710632	3.831566
H	-0.246106	-1.105516	3.530259
H	1.439127	-2.689156	4.398986
H	1.695612	-4.934742	3.359584
H	0.247385	-5.573133	1.444926
H	-1.432589	-3.997136	0.577815
H	1.457237	3.232577	-0.369724
H	1.170114	5.672957	-0.135801
C	3.592962	5.197306	2.202412
C	3.781448	3.823394	2.046957
C	3.976474	0.692953	2.416558
C	3.096751	0.114154	3.343898
C	4.925123	-0.275442	4.880322
C	3.567555	-0.360413	4.56812

C	5.808698	0.299879	3.966192
C	5.33794	0.785095	2.745553
C	1.900459	5.160599	0.481073
C	2.656299	5.869677	1.416
C	4.784765	1.335423	-0.259975
C	6.903918	1.242603	-2.103014
C	5.084786	2.448987	-1.057276
C	-3.057337	3.036462	-1.255054
C	-4.154079	-3.275202	-1.587188
C	-4.533007	-2.918204	1.157463
C	-5.446649	-3.667767	0.414305
C	-3.01014	-0.739304	2.942678
C	-3.955501	1.013337	4.329219
C	-4.263474	0.078459	5.316179
C	-3.324975	0.607356	3.152166
C	-5.264245	-3.842235	-0.959493
C	-1.973093	5.134131	-0.695311
C	-2.709933	5.787454	-1.684745
C	-3.795159	3.699379	-2.245175
C	-3.971648	0.560861	-2.458427
C	-3.526534	-0.551847	-4.573021
C	-4.886087	-0.522151	-4.887488
C	-4.806522	1.307713	0.185146
C	-6.188448	2.432786	1.835342
C	-6.93132	1.267598	2.024633
C	-6.62754	0.127314	1.279147
C	-3.42496	-2.329894	0.53286
C	-5.579444	0.149482	0.361806
C	-3.241473	-2.527934	-0.844506
C	-5.334735	0.599223	-2.791079
C	-5.131888	2.454435	0.923336
C	-5.788289	0.056412	-3.994021
C	-3.073062	-0.020843	-3.365606
C	-0.965447	-2.437528	1.992838
C	-3.926441	-1.26505	5.13074
C	-0.812624	-3.70221	1.416047
C	0.808896	-2.977452	3.564213
C	0.953711	-4.239755	2.981037
C	0.142123	-4.597219	1.907339
C	3.02438	3.104352	1.111721

C	2.072538	3.783934	0.335249
C	-0.139309	-2.082666	3.074253
C	-3.297977	-1.670704	3.954905
C	-3.616333	5.066213	-2.463072
C	-2.13394	3.764252	-0.487578
C	5.57868	0.184273	-0.380576
C	3.44307	-2.332792	-0.407562
C	4.178502	-3.174766	1.752604
C	3.254145	-2.478404	0.975569
C	5.490254	-3.623583	-0.224749
C	4.566206	-2.923502	-1.002223
C	3.906991	-1.502901	-5.064922
C	4.233506	-0.167764	-5.317701
C	3.002976	-0.877215	-2.898483
C	3.307006	0.459736	-3.174916
C	3.926125	0.812018	-4.375002
C	0.958381	-3.852035	-1.340452
C	3.289181	-1.854883	-3.866353
C	0.995165	-2.55748	-1.868573
C	0.086025	-2.216252	-2.885592
C	-0.839224	-3.146756	-3.3509
C	-0.876667	-4.434638	-2.807841
C	0.02585	-4.784041	-1.806377
C	5.303544	-3.74421	1.154306
C	6.624505	0.135901	-1.299503
C	6.1388	2.401414	-1.971145

Cartesian Coordinates of 3-brid

Symbol	X	Y	Z
Ir	1.412679	0.110271	0.242939
Ir	-1.305161	0.176012	-0.148686
S	0.135283	1.162859	-1.67201
S	-0.194045	1.328716	1.56631
P	-3.110837	1.412296	-0.92007
P	-2.351153	-1.317953	1.308722
P	3.221258	1.404955	0.854041
P	2.295066	-1.490039	-1.181079
H	1.475457	3.068883	-0.79029
H	1.287142	5.504925	-1.114852
H	2.605172	7.068143	0.309096
H	4.137963	6.156437	2.04119
H	4.385428	3.721213	2.319958
H	1.72456	0.78706	3.282365
H	2.354665	0.523861	5.652005
H	4.737986	0.699822	6.343126
H	6.480218	1.179872	4.635804
H	5.853495	1.468961	2.271415
H	4.821911	3.141309	-0.983547
H	6.848479	2.703141	-2.32029
H	7.997028	0.50636	-2.169426
H	7.1054	-1.24724	-0.641878
H	5.085579	-0.813028	0.694107
H	2.348592	-2.718767	1.413143
H	3.861811	-4.28113	2.565535
H	5.930266	-5.08425	1.430495
H	6.430329	-4.324903	-0.882093
H	4.909225	-2.781993	-2.040757
H	-2.178609	6.957031	-1.917671
H	-3.78883	5.704163	-3.335492
H	-4.173018	3.298254	-2.94573
H	-1.840011	0.090328	-3.172914
H	-2.679558	-0.87995	-5.283821
H	-5.112899	-0.846659	-5.798422
H	-6.087683	3.757659	2.301398
H	-7.542426	1.779964	2.68709
H	-7.125518	-0.319454	1.412929

H	-5.276648	-0.440078	-0.195387
H	-2.522191	-2.078778	-1.426539
H	-4.219345	-3.185479	-2.819385
H	-6.310309	-4.062662	-1.780407
H	-6.660846	-3.821622	0.666008
H	-4.982725	-2.669887	2.05565
H	-3.000337	1.327186	2.355933
H	-4.096431	2.111065	4.425535
H	-4.826575	0.472085	6.146416
H	-4.428401	-1.954832	5.784912
H	-3.322304	-2.733336	3.719607
H	-0.133572	-1.116297	3.112908
H	1.441775	-2.750401	4.101767
H	1.271525	-5.163861	3.506776
H	-0.488418	-5.921885	1.928465
H	-2.07208	-4.291089	0.95601
H	-6.690732	0.223231	-4.203639
H	-5.858225	1.214716	-2.111325
H	-4.214879	3.631743	0.706971
H	3.082857	1.104646	-2.240822
H	4.19178	1.825787	-4.329415
H	4.762316	0.15064	-6.076549
H	4.210965	-2.245414	-5.713074
H	3.123631	-2.962123	-3.616694
H	0.454294	-1.312115	-3.439493
H	-1.360829	-2.762491	-4.282549
H	-1.897308	-4.895984	-3.121248
H	-0.606213	-5.551733	-1.102109
H	1.205582	-4.12155	-0.266797
H	-1.228725	3.337901	0.201379
H	-0.91651	5.763466	-0.133998
C	-3.24492	5.194196	-2.547652
C	-3.459279	3.83315	-2.328337
C	-3.789391	0.708367	-2.479643
C	-2.903335	0.114193	-3.3934
C	-4.74361	-0.411038	-4.876087
C	-3.379277	-0.436779	-4.583002
C	-5.629862	0.188008	-3.980386
C	-5.156414	0.749967	-2.794159
C	-1.628148	5.228551	-0.753113

C	-2.336554	5.89619	-1.753649
C	-4.592544	1.578841	0.151454
C	-6.727679	1.726664	1.973381
C	-4.846713	2.763789	0.856397
C	2.972701	3.221179	0.759882
C	4.090654	-3.964883	1.553457
C	4.655773	-3.122881	-1.044897
C	5.528297	-3.988423	-0.381655
C	3.082835	-0.979224	-2.753266
C	3.975628	0.775194	-4.171635
C	4.292023	-0.164199	-5.151016
C	3.365728	0.370303	-2.983058
C	5.248917	-4.41433	0.917094
C	1.966724	5.121897	-0.361573
C	2.704838	5.995279	0.437357
C	3.707249	4.105171	1.565873
C	3.742032	1.150626	2.602707
C	3.123508	0.726689	4.914095
C	4.460974	0.828743	5.302164
C	4.80113	1.19198	-0.055612
C	6.464506	1.932282	-1.660648
C	7.110159	0.69925	-1.575453
C	6.611802	-0.284839	-0.719531
C	3.491977	-2.662724	-0.414023
C	5.465891	-0.040558	0.034172
C	3.226146	-3.0907	0.897198
C	5.081931	1.2613	3.004422
C	5.318136	2.180666	-0.903262
C	5.438564	1.097076	4.344496
C	2.765349	0.882322	3.575209
C	0.983622	-2.623623	-1.809989
C	3.985772	-1.512466	-4.945803
C	0.660695	-3.816696	-1.152434
C	-0.793537	-3.06406	-3.40846
C	-1.096491	-4.261682	-2.756251
C	-0.372092	-4.629858	-1.624031
C	-2.752037	3.159674	-1.323162
C	-1.817571	3.861494	-0.546924
C	0.234134	-2.247369	-2.937904
C	3.380833	-1.916866	-3.757925

C	3.568999	5.483878	1.408169
C	2.086283	3.740876	-0.193274
C	-5.43853	0.477683	0.355875
C	-3.622793	-2.299433	0.418369
C	-4.383458	-3.09726	-1.751175
C	-3.424322	-2.465642	-0.961091
C	-5.752602	-3.44437	0.208056
C	-4.794348	-2.807053	0.99762
C	-4.135864	-1.235838	5.027211
C	-4.355298	0.128795	5.231468
C	-3.144387	-0.756451	2.861272
C	-3.340576	0.609095	3.089933
C	-3.94814	1.049039	4.266542
C	-1.309773	-3.951411	1.648222
C	-3.52521	-1.675118	3.854068
C	-1.222165	-2.597207	1.984462
C	-0.222286	-2.172586	2.875877
C	0.668397	-3.093025	3.421987
C	0.576019	-4.447082	3.082598
C	-0.410818	-4.872814	2.194773
C	-5.554211	-3.583294	-1.167962
C	-6.49415	0.549189	1.261471
C	-5.907195	2.834346	1.761594
H	1.812597	-0.729449	1.51933
H	0.054548	-0.96422	0.193887

Cartesian Coordinates of 3-hedo

Symbol	X	Y	Z
Ir	1.4581	-0.24221	0.209709
Ir	-1.513688	-0.269042	0.519128
S	0.06789	1.190246	1.512828
S	0.033181	-1.914981	1.164979
P	-3.285293	1.083048	1.067784
P	-2.435956	-1.583751	-1.088438
P	3.363948	-1.03406	1.095677
P	2.262976	1.413543	-1.149254
H	1.511042	-0.468323	3.295037
H	1.183441	-1.456932	5.530456
H	2.510763	-3.441676	6.232434
H	4.189111	-4.408714	4.677024
H	4.553138	-3.404446	2.462741
H	2.54642	-3.033938	-0.836265
H	3.730455	-4.79615	-2.090829
H	6.195489	-5.059597	-1.851093
H	7.442201	-3.577234	-0.294512
H	6.254494	-1.842229	0.987005
H	3.900632	0.500225	3.551192
H	5.43068	2.348061	4.07992
H	7.044273	3.168502	2.374627
H	7.131773	2.071591	0.141298
H	5.630497	0.204374	-0.38041
H	3.20235	-1.037268	-2.376805
H	5.28282	-1.698406	-3.522763
H	7.081025	-0.01627	-3.910612
H	6.755112	2.326318	-3.147665
H	4.696332	2.97125	-1.961536
H	-3.125381	2.729545	6.562266
H	-4.385498	4.077879	4.89742
H	-4.435418	3.395161	2.530457
H	-1.501698	3.234383	0.642391
H	-1.629712	5.430147	-0.484027
H	-3.75418	6.157918	-1.566427
H	-6.937409	-1.507814	3.210393
H	-8.169682	-1.938384	1.093013
H	-7.337288	-0.933584	-1.031066

H	-5.31365	0.433013	-1.040389
H	-2.492058	1.090152	-2.05882
H	-3.919118	2.356888	-3.635692
H	-5.814362	1.22161	-4.780821
H	-6.237807	-1.189965	-4.355772
H	-4.815754	-2.44435	-2.793143
H	-3.678636	-2.335487	1.359182
H	-5.104591	-4.235248	2.080529
H	-5.567077	-6.106746	0.50859
H	-4.613239	-6.054855	-1.784723
H	-3.228875	-4.14439	-2.510087
H	-0.995523	-4.211219	-1.287931
H	0.997892	-4.914547	-2.549476
H	2.0642	-3.361552	-4.177041
H	1.097287	-1.093368	-4.518222
H	-0.858538	-0.369229	-3.2342
H	-5.750595	4.682539	-1.462465
H	-5.634799	2.513041	-0.309878
H	-4.900097	-0.137507	3.205408
H	2.821112	2.307399	1.556751
H	3.362836	4.503671	2.549853
H	3.388889	6.541974	1.124425
H	2.886784	6.355095	-1.302452
H	2.375924	4.153845	-2.2966
H	-0.337417	2.608564	-1.088212
H	-1.91398	3.395352	-2.816568
H	-1.436209	2.967299	-5.226739
H	0.679849	1.840122	-5.877739
H	2.312477	1.172097	-4.150673
H	-1.935547	0.02012	3.443356
H	-1.909337	0.689117	5.827029
C	-3.856007	3.183737	4.585956
C	-3.881778	2.796849	3.246019
C	-3.546974	2.698117	0.215258
C	-2.429529	3.54971	0.171389
C	-3.696611	5.196777	-1.066502
C	-2.504439	4.789006	-0.460032
C	-4.815729	4.367185	-1.011053
C	-4.746019	3.129124	-0.364472
C	-2.467254	1.280466	5.108843

C	-3.148438	2.426242	5.520776
C	-4.936095	0.25385	1.079517
C	-7.276679	-1.322745	1.090517
C	-5.426043	-0.303713	2.272777
C	3.075881	-1.847357	2.725009
C	5.151157	-0.669823	-3.20453
C	4.804748	1.956144	-2.323556
C	5.978062	1.587209	-2.983702
C	2.60298	3.06847	-0.440086
C	3.160418	4.430879	1.487253
C	3.172854	5.57287	0.687285
C	2.869365	3.186493	0.927795
C	6.160031	0.272075	-3.415406
C	1.92824	-1.879259	4.864812
C	2.671569	-2.994234	5.257453
C	3.81889	-2.965225	3.127498
C	4.311431	-2.30511	0.161069
C	4.288098	-4.14878	-1.422325
C	5.669637	-4.296946	-1.286585
C	4.633355	0.222484	1.536347
C	5.471059	1.885758	3.099646
C	6.37865	2.343886	2.14401
C	6.42803	1.730403	0.892609
C	3.79457	1.013125	-2.087686
C	5.567287	0.675157	0.592323
C	3.975132	-0.298872	-2.553343
C	5.696088	-2.478207	0.309406
C	4.605179	0.834812	2.799332
C	6.370439	-3.462843	-0.414521
C	3.615089	-3.161932	-0.703502
C	1.10008	1.850148	-2.497623
C	2.890709	5.468499	-0.677256
C	1.37889	1.635267	-3.852523
C	-1.000284	2.892849	-3.116495
C	-0.727521	2.657679	-4.466187
C	0.459397	2.022512	-4.831255
C	-3.192967	1.651538	2.82094
C	-2.485795	0.896237	3.767547
C	-0.105542	2.469458	-2.137616
C	2.606249	4.224564	-1.238364

C	3.613578	-3.536856	4.385032
C	2.121024	-1.312975	3.606291
C	-5.657164	0.020495	-0.102504
C	-3.524791	-0.771361	-2.336743
C	-4.104116	1.30127	-3.470809
C	-3.291976	0.587268	-2.590243
C	-5.40732	-0.689613	-3.868668
C	-4.590025	-1.404677	-2.992346
C	-4.422948	-5.236944	-1.097731
C	-4.95681	-5.266891	0.193267
C	-3.384403	-3.088964	-0.628384
C	-3.905428	-3.142921	0.671017
C	-4.695933	-4.219569	1.076229
C	-0.477396	-1.374587	-3.09082
C	-3.644841	-4.154759	-1.507141
C	-1.086812	-2.239134	-2.168419
C	-0.538622	-3.518572	-1.987424
C	0.590142	-3.920681	-2.705761
C	1.185503	-3.051965	-3.620438
C	0.642236	-1.780796	-3.814338
C	-5.169759	0.665573	-4.108395
C	-6.812716	-0.760152	-0.097692
C	-6.582178	-1.084577	2.27667
H	1.700147	-1.212866	-1.030941
H	0.117459	-2.873393	0.223409

Cartesian Coordinates of 3-heup

Symbol	X	Y	Z
Ir	1.429301	-0.271645	0.030749
Ir	-1.458655	-0.322895	0.272741
S	0.062807	0.410891	1.888282
S	-0.015915	-2.161484	-0.133265
P	-3.323979	0.205601	1.504869
P	-2.36322	-0.572074	-1.803983
P	3.287146	-1.447181	0.526554
P	2.306986	1.800938	-0.346297
H	1.428711	-1.635597	2.773087
H	0.964812	-3.372977	4.458663
H	2.133859	-5.573048	4.347846
H	3.78819	-5.992007	2.542308
H	4.286444	-4.245847	0.881393
H	2.315761	-2.476086	-2.008615
H	3.366899	-3.710162	-3.871411
H	5.796009	-4.237069	-3.810181
H	7.152524	-3.556314	-1.841172
H	6.100087	-2.353104	0.032802
H	4.12688	-1.246442	3.366406
H	5.864497	0.070639	4.505153
H	7.41521	1.502956	3.192821
H	7.236654	1.550174	0.708384
H	5.533487	0.205104	-0.434177
H	3.102313	0.143974	-2.597575
H	5.072202	0.077979	-4.074861
H	6.908894	1.737854	-3.782696
H	6.728436	3.461718	-2.000694
H	4.777316	3.506813	-0.510179
H	-2.87758	-2.070189	6.749669
H	-4.073946	0.08491	6.447653
H	-4.267473	1.097465	4.206836
H	-1.702413	2.545056	1.799659
H	-2.168571	4.952285	2.186023
H	-4.519191	5.741726	2.408843
H	-6.941035	-3.227587	1.486039
H	-8.122844	-2.242207	-0.466214
H	-7.279721	-0.122193	-1.467883

H	-5.288435	0.972006	-0.547955
H	-2.406976	2.165528	-1.055219
H	-3.837748	4.11116	-1.595834
H	-5.726827	3.856619	-3.197644
H	-6.143992	1.651317	-4.262585
H	-4.730152	-0.281653	-3.711852
H	-3.487815	-2.659442	-0.191108
H	-4.831121	-4.689582	-0.673214
H	-5.354997	-5.300136	-3.025757
H	-4.524676	-3.873816	-4.883995
H	-3.198077	-1.850928	-4.396152
H	-0.819939	-2.719246	-3.124912
H	1.163563	-2.698728	-4.585839
H	2.137077	-0.538603	-5.34483
H	1.08305	1.59733	-4.636507
H	-0.886125	1.587371	-3.165023
H	-6.383062	4.103054	2.286803
H	-5.913262	1.71327	1.910089
H	-4.918148	-2.151767	2.387296
H	2.844614	1.166876	2.448573
H	3.584275	2.506242	4.386989
H	3.896961	4.963075	4.156754
H	3.460824	6.059487	1.968874
H	2.739584	4.714691	0.031215
H	-0.134839	3.006228	0.51648
H	-1.717632	4.626557	-0.483426
H	-1.345431	5.458134	-2.801747
H	0.652075	4.705368	-4.072134
H	2.26268	3.138842	-3.040037
H	-2.011501	-2.154627	2.53996
H	-1.859709	-3.201114	4.780895
C	-3.63408	-0.417437	5.592579
C	-3.743859	0.155182	4.323548
C	-3.770574	1.967974	1.802105
C	-2.724755	2.897373	1.891957
C	-4.309841	4.690059	2.243992
C	-2.991234	4.248434	2.113589
C	-5.356731	3.770725	2.172633
C	-5.090087	2.416858	1.958672
C	-2.388378	-2.261522	4.65862

C	-2.961059	-1.627025	5.763059
C	-4.930445	-0.52248	0.969398
C	-7.240577	-1.758893	-0.061075
C	-5.427157	-1.702831	1.542111
C	2.907556	-2.805532	1.71663
C	5.0042	0.843912	-3.309883
C	4.816727	2.771045	-1.303395
C	5.93345	2.736945	-2.139744
C	2.798566	2.830994	1.091673
C	3.418675	2.991733	3.431814
C	3.590182	4.368992	3.302611
C	3.017406	2.228448	2.334724
C	6.034356	1.770393	-3.141778
C	1.694729	-3.569762	3.680441
C	2.349795	-4.801439	3.616692
C	3.56159	-4.044004	1.661531
C	4.130103	-2.322419	-0.85482
C	3.96847	-3.409908	-3.020272
C	5.331517	-3.708132	-2.98477
C	4.67998	-0.599761	1.379802
C	5.786121	0.111238	3.424207
C	6.660201	0.91091	2.687438
C	6.560609	0.938756	1.29631
C	3.780511	1.838665	-1.455657
C	5.584615	0.184765	0.647236
C	3.886321	0.880729	-2.477017
C	5.496587	-2.64203	-0.820177
C	4.802799	-0.637835	2.776961
C	6.093518	-3.325244	-1.880319
C	3.371061	-2.721134	-1.964724
C	1.165564	2.960824	-1.192753
C	3.34717	4.98586	2.072762
C	1.384548	3.448863	-2.485032
C	-0.852705	4.299602	-1.051256
C	-0.641816	4.766642	-2.351159
C	0.477151	4.339815	-3.065647
C	-3.169418	-0.471377	3.210798
C	-2.484747	-1.683208	3.394474
C	0.036327	3.392823	-0.481443
C	2.948811	4.223449	0.976434

C	3.28031	-5.035618	2.604056
C	1.965604	-2.581041	2.735137
C	-5.630218	0.043476	-0.108451
C	-3.442913	0.811543	-2.362758
C	-4.023439	3.156841	-2.076139
C	-3.210705	2.064168	-1.776207
C	-5.319234	1.772133	-3.568003
C	-4.504974	0.679334	-3.267688
C	-4.31636	-3.602816	-3.854567
C	-4.779264	-4.406498	-2.809188
C	-3.2977	-2.088117	-2.249296
C	-3.740366	-2.918042	-1.213119
C	-4.48513	-4.065538	-1.489837
C	-0.458156	0.643523	-3.48659
C	-3.577868	-2.453654	-3.576971
C	-1.013423	-0.568691	-3.053831
C	-0.413962	-1.771163	-3.459088
C	0.713168	-1.759489	-4.281063
C	1.25727	-0.548626	-4.709785
C	0.664699	0.651128	-4.313119
C	-5.084408	3.012439	-2.970839
C	-6.768911	-0.572099	-0.623551
C	-6.573045	-2.314431	1.030209
H	1.686374	-0.541006	-1.523454
H	-0.087419	-2.613372	1.13209

Cartesian Coordinates of 3-crst

Symbol	X	Y	Z
Ir	1.438761	-0.167062	0.216498
Ir	-1.492448	-0.061203	0.344431
S	0.084001	1.324685	1.463125
S	-0.09197	-1.84723	0.887842
P	-3.301287	0.97429	1.235967
P	-2.397662	-1.404039	-1.31094
P	3.264339	-1.13127	1.087391
P	2.356018	1.502054	-1.081705
H	1.2619	-0.605474	3.183339
H	0.902121	-1.547912	5.439326
H	2.31494	-3.425725	6.255022
H	4.109749	-4.336549	4.798031
H	4.499041	-3.37867	2.565323
H	2.215369	-3.133626	-0.707503
H	3.227271	-5.002112	-1.977252
H	5.67605	-5.403905	-1.875439
H	7.103395	-3.949329	-0.451601
H	6.098432	-2.1081	0.837637
H	4.018959	0.234779	3.58214
H	5.719806	1.931573	4.124774
H	7.320867	2.701143	2.386664
H	7.224361	1.712057	0.103832
H	5.551446	-0.000678	-0.432454
H	3.072765	-0.98851	-2.397606
H	5.05503	-1.76916	-3.626811
H	6.961314	-0.217232	-4.04193
H	6.833634	2.126749	-3.224362
H	4.868741	2.896171	-1.961571
H	-2.831035	1.752145	6.890058
H	-4.2869	3.251024	5.54492
H	-4.472626	2.937167	3.105986
H	-1.661628	3.214753	0.618307
H	-2.085355	5.503203	-0.230507
H	-4.411555	6.234398	-0.736142
H	-6.709737	-2.137562	3.070853
H	-7.970834	-2.328819	0.937822
H	-7.261171	-0.981353	-1.033738

H	-5.31599	0.503875	-0.880648
H	-2.564119	1.310081	-2.33428
H	-4.130272	2.513957	-3.784129
H	-6.115648	1.34073	-4.732331
H	-6.469081	-1.066659	-4.223463
H	-4.903546	-2.273221	-2.771421
H	-3.344775	-2.40279	1.212065
H	-4.550171	-4.452006	1.907888
H	-5.057465	-6.222574	0.237187
H	-4.350394	-5.927222	-2.126339
H	-3.167813	-3.873431	-2.819317
H	-0.762319	-3.855853	-1.52239
H	1.142525	-4.482738	-2.946892
H	2.013505	-2.890221	-4.649646
H	0.908946	-0.680047	-4.935249
H	-1.013815	-0.062025	-3.545062
H	-6.304918	4.67774	-0.332654
H	-5.886828	2.411267	0.538961
H	-4.746309	-0.660878	3.224446
H	3.025774	2.213118	1.643159
H	3.797555	4.297102	2.726745
H	4.014191	6.385957	1.392932
H	3.456856	6.365825	-1.028086
H	2.71216	4.274103	-2.111948
H	-0.113134	2.965531	-0.884562
H	-1.768035	3.79791	-2.524529
H	-1.426597	3.376222	-4.959161
H	0.603225	2.165848	-5.722524
H	2.263891	1.365003	-4.081317
H	-1.704457	-0.353407	3.315895
H	-1.554833	-0.060501	5.767017
C	-3.733116	2.452458	5.062911
C	-3.836425	2.27451	3.68312
C	-3.739311	2.6427	0.605751
C	-2.675755	3.535961	0.395709
C	-4.224151	5.235467	-0.356603
C	-2.917421	4.823539	-0.078857
C	-5.286821	4.361044	-0.132699
C	-5.048607	3.073367	0.355812
C	-2.198587	0.592199	5.187226

C	-2.914953	1.610562	5.817737
C	-4.873049	0.023332	1.178753
C	-7.114772	-1.666615	1.007542
C	-5.292205	-0.72432	2.29018
C	2.918382	-1.911706	2.720517
C	5.011156	-0.740844	-3.284655
C	4.887392	1.883466	-2.34551
C	6.009566	1.443091	-3.04945
C	2.859373	3.08618	-0.311781
C	3.572662	4.29523	1.666088
C	3.691593	5.465686	0.917495
C	3.150115	3.113904	1.05611
C	6.079974	0.12802	-3.512119
C	1.69347	-1.946947	4.814081
C	2.485839	-3.000793	5.27152
C	3.713445	-2.967439	3.188819
C	4.08518	-2.478641	0.144244
C	3.856905	-4.362635	-1.368573
C	5.233217	-4.59093	-1.309541
C	4.646251	0.000105	1.528619
C	5.680143	1.514423	3.124325
C	6.581528	1.943968	2.149918
C	6.527887	1.390855	0.870392
C	3.816385	1.013943	-2.093664
C	5.572098	0.423902	0.563199
C	3.88708	-0.299453	-2.587311
C	5.463565	-2.729726	0.216695
C	4.719295	0.550722	2.817557
C	6.034456	-3.774766	-0.51154
C	3.284377	-3.31413	-0.649218
C	1.18336	2.100864	-2.365929
C	3.380689	5.454388	-0.444707
C	1.38007	1.887994	-3.734759
C	-0.889482	3.263246	-2.87202
C	-0.697219	3.026388	-4.236327
C	0.440469	2.343034	-4.664472
C	-3.114231	1.257806	3.042101
C	-2.290482	0.417364	3.806179
C	0.040936	2.799546	-1.944706
C	2.96456	4.272687	-1.056156

C	3.49439	-3.51189	4.454641
C	1.900234	-1.40689	3.544462
C	-5.609563	-0.072402	-0.012133
C	-3.590974	-0.583969	-2.459126
C	-4.297712	1.462135	-3.578442
C	-3.401806	0.77441	-2.761802
C	-5.606769	-0.546028	-3.820388
C	-4.706054	-1.235407	-3.006626
C	-4.148992	-5.150117	-1.396827
C	-4.543374	-5.316809	-0.066374
C	-3.217811	-2.972849	-0.853829
C	-3.593162	-3.162598	0.480637
C	-4.260702	-4.32445	0.870816
C	-0.561676	-1.038903	-3.413497
C	-3.488817	-3.987063	-1.788429
C	-1.05853	-1.931767	-2.455471
C	-0.422175	-3.170169	-2.288517
C	0.670292	-3.515606	-3.082093
C	1.15712	-2.623743	-4.038698
C	0.537502	-1.384857	-4.200373
C	-5.409262	0.80535	-4.10716
C	-6.718425	-0.912727	-0.097465
C	-6.403939	-1.562885	2.203166
H	1.668897	-1.092666	-1.048159
H	-1.608807	1.09049	-0.707883

Cartesian Coordinates of 4-up

Symbol	X	Y	Z
Ir	1.438898	0.065387	0.19476
Ir	-1.32654	0.077042	-0.228786
S	0.220165	1.33725	-1.622439
S	-0.132052	1.251675	1.605117
P	-3.125004	1.36008	-0.898304
P	-2.326956	-1.423972	1.190834
P	3.134973	1.365468	1.010289
P	2.407634	-1.407938	-1.322765
H	2.551777	3.094799	-1.252857
H	1.958933	5.475026	-1.472651
H	1.790145	6.911057	0.551635
H	2.226477	5.931933	2.793604
H	2.841443	3.554254	3.014362
H	1.582565	0.372065	3.296984
H	2.125389	0.034095	5.689409
H	4.389543	0.598295	6.54934
H	6.103153	1.511579	4.997775
H	5.569494	1.834457	2.613206
H	5.067152	3.264301	-0.35017
H	7.234212	2.86678	-1.45932
H	8.224389	0.589503	-1.493176
H	7.036306	-1.28722	-0.364656
H	4.87024	-0.893142	0.737607
H	2.141859	-2.967984	1.078677
H	3.483785	-4.717377	2.162137
H	5.645184	-5.444272	1.157109
H	6.413516	-4.412465	-0.969841
H	5.060602	-2.682585	-2.071696
H	-1.785873	6.907788	-1.431471
H	-3.182098	5.813269	-3.169414
H	-3.768518	3.429636	-2.975869
H	-1.926893	0.206963	-3.288782
H	-2.777984	-0.291773	-5.555954
H	-5.171215	0.095022	-6.105428
H	-6.261111	3.407399	2.399545
H	-7.669956	1.369473	2.585074
H	-7.154906	-0.615119	1.168409

H	-5.25164	-0.563208	-0.383977
H	-2.74583	-2.45934	-1.476276
H	-4.512203	-3.798137	-2.554302
H	-6.510504	-4.513377	-1.247928
H	-6.690109	-3.893392	1.153447
H	-4.924583	-2.567351	2.229729
H	-2.938332	1.239686	2.245708
H	-3.914131	2.040793	4.366632
H	-4.46413	0.422015	6.173685
H	-4.024141	-2.001135	5.830624
H	-3.073519	-2.796647	3.699845
H	-0.15169	-1.263215	3.051999
H	1.421232	-2.916983	4.019817
H	1.311709	-5.303475	3.309718
H	-0.342274	-6.00301	1.596138
H	-1.92664	-4.357787	0.653771
H	-6.69502	1.025796	-4.375874
H	-5.840952	1.560205	-2.129192
H	-4.331658	3.44948	0.867332
H	3.432852	1.222136	-2.020901
H	4.757066	2.096707	-3.918002
H	5.39772	0.581343	-5.784234
H	4.696396	-1.802172	-5.730911
H	3.385988	-2.667352	-3.826904
H	0.860664	-0.866569	-3.737949
H	-1.064106	-1.976377	-4.805797
H	-1.973935	-4.087765	-3.862753
H	-0.931462	-5.076923	-1.833004
H	0.993506	-3.980584	-0.767626
H	-1.505637	3.178182	0.683218
H	-0.957235	5.569408	0.5055
C	-2.831757	5.244433	-2.314906
C	-3.165481	3.892728	-2.203822
C	-3.821026	0.912191	-2.542632
C	-2.967839	0.39079	-3.527248
C	-4.794828	0.324423	-5.113871
C	-3.452283	0.103328	-4.80324
C	-5.650664	0.846951	-4.143725
C	-5.166044	1.145646	-2.86931
C	-1.590749	5.114467	-0.247887

C	-2.046526	5.858704	-1.338374
C	-4.633461	1.435905	0.148124
C	-6.830672	1.391045	1.898385
C	-4.944825	2.557718	0.928043
C	2.773006	3.15926	0.895939
C	3.828959	-4.283334	1.230427
C	4.69408	-3.136713	-1.159489
C	5.469759	-4.11065	-0.527101
C	3.360442	-0.786161	-2.760898
C	4.469056	1.051623	-3.89859
C	4.827027	0.20176	-4.943233
C	3.732145	0.559373	-2.819951
C	5.039411	-4.689684	0.666512
C	2.165118	5.061602	-0.491585
C	2.065324	5.865914	0.647
C	2.667589	3.971697	2.029661
C	3.540614	1.107555	2.784215
C	2.883831	0.420878	5.017505
C	4.152657	0.743401	5.500664
C	4.801295	1.209118	0.252433
C	6.716842	2.040674	-0.983059
C	7.275169	0.762962	-0.998351
C	6.609519	-0.290434	-0.367078
C	3.476363	-2.721856	-0.601507
C	5.383727	-0.068047	0.254684
C	3.059451	-3.302401	0.607869
C	4.811635	1.439786	3.28066
C	5.488729	2.266033	-0.355649
C	5.11527	1.256793	4.629577
C	2.57707	0.599598	3.667406
C	1.086619	-2.355914	-2.189558
C	4.43593	-1.140272	-4.912404
C	0.560983	-3.540323	-1.65802
C	-0.609245	-2.419993	-3.926468
C	-1.120864	-3.605423	-3.396885
C	-0.534498	-4.160939	-2.258984
C	-2.713823	3.139937	-1.111188
C	-1.918302	3.763635	-0.135414
C	0.484115	-1.797122	-3.326164
C	3.704513	-1.629692	-3.832154

C	2.313185	5.317253	1.904233
C	2.51057	3.718547	-0.365617
C	-5.45691	0.302772	0.234277
C	-3.684513	-2.438981	0.463011
C	-4.600959	-3.543843	-1.503019
C	-3.595007	-2.794215	-0.892896
C	-5.820838	-3.59407	0.577157
C	-4.810243	-2.852191	1.19121
C	-3.811697	-1.290473	5.038887
C	-4.054629	0.071561	5.232365
C	-3.002545	-0.83417	2.792078
C	-3.218189	0.529192	3.010336
C	-3.750562	0.979111	4.219107
C	-1.196681	-4.037569	1.388699
C	-3.283954	-1.739733	3.829915
C	-1.160857	-2.703984	1.808194
C	-0.202183	-2.307034	2.755342
C	0.684322	-3.238013	3.291074
C	0.630427	-4.574751	2.882681
C	-0.300295	-4.969167	1.922445
C	-5.720518	-3.942709	-0.771262
C	-6.542575	0.277868	1.106705
C	-6.036359	2.532916	1.798267
H	1.79527	-0.887389	1.389041
H	-1.622445	-0.875148	-1.471441
H	0.140379	2.528004	-1.004449
H	0.046639	-1.022292	-0.043178

Cartesian Coordinates of 4-do

Symbol	X	Y	Z
Ir	1.453946	0.081748	0.159679
Ir	-1.321348	0.084955	-0.239159
S	0.204738	1.344682	-1.651443
S	-0.103809	1.344234	1.517902
P	-3.142886	1.34722	-0.908747
P	-2.348104	-1.362038	1.215464
P	3.194765	1.311859	1.003523
P	2.412881	-1.404697	-1.352876
H	1.987999	3.138832	-0.899819
H	1.708661	5.584346	-0.975182
H	2.415341	6.983134	0.963403
H	3.429943	5.899699	2.955706
H	3.766576	3.456973	3.0056
H	1.559254	0.501578	3.277433
H	2.071821	-0.033141	5.63787
H	4.416839	0.068003	6.465288
H	6.241487	0.727325	4.911759
H	5.736052	1.258879	2.559263
H	5.01154	3.237391	-0.420795
H	7.118882	2.900332	-1.659402
H	8.153939	0.64568	-1.779271
H	7.072926	-1.269387	-0.609122
H	4.972858	-0.933399	0.630705
H	2.206228	-2.917152	1.069884
H	3.55174	-4.665814	2.150317
H	5.685554	-5.425446	1.108906
H	6.417145	-4.427506	-1.046169
H	5.05711	-2.702637	-2.143148
H	-1.908492	6.802697	-2.138298
H	-3.536935	5.564709	-3.548045
H	-4.063626	3.209309	-3.059594
H	-2.225046	-0.193736	-3.208045
H	-3.320671	-1.052898	-5.243335
H	-5.753877	-0.678938	-5.606652
H	-5.690364	3.869762	2.546208
H	-7.277278	2.011713	3.005085
H	-7.128197	-0.087288	1.673289

H	-5.415069	-0.327195	-0.06651
H	-3.0563	-2.180962	-1.473339
H	-5.034076	-3.242341	-2.488465
H	-6.96068	-3.917308	-1.058214
H	-6.86096	-3.526719	1.394349
H	-4.90138	-2.441491	2.399564
H	-2.825378	1.318907	2.302526
H	-3.650238	2.144268	4.473663
H	-4.13152	0.542612	6.316013
H	-3.773856	-1.891715	5.953082
H	-2.97082	-2.712877	3.773194
H	-0.008961	-1.358172	2.862966
H	1.511353	-3.121076	3.709572
H	1.14513	-5.499777	3.058878
H	-0.752693	-6.092627	1.573917
H	-2.295181	-4.333007	0.765779
H	-7.058423	0.617061	-3.934296
H	-5.95966	1.50154	-1.918032
H	-3.948322	3.618924	0.825848
H	3.296386	1.269318	-2.074869
H	4.573173	2.192872	-3.977629
H	5.3087	0.697852	-5.824574
H	4.743989	-1.721334	-5.749831
H	3.474481	-2.639447	-3.844614
H	1.07179	-1.169031	-3.995428
H	-0.947515	-2.209367	-4.933479
H	-2.117728	-4.0212	-3.693001
H	-1.222806	-4.778062	-1.499236
H	0.759552	-3.714289	-0.532327
H	-1.250723	3.261123	0.208944
H	-0.777758	5.634016	-0.247442
C	-3.050498	5.069452	-2.714337
C	-3.347776	3.733718	-2.436969
C	-4.009472	0.70944	-2.406904
C	-3.279358	-0.003235	-3.370271
C	-5.267057	-0.286077	-4.720414
C	-3.902703	-0.497551	-4.515327
C	-5.999572	0.439132	-3.780687
C	-5.375078	0.938505	-2.636521
C	-1.502123	5.111454	-0.862803

C	-2.133235	5.762865	-1.924441
C	-4.534358	1.616954	0.265739
C	-6.519703	1.905011	2.236394
C	-4.640226	2.804345	1.004473
C	2.932905	3.126404	1.040696
C	3.880093	-4.249545	1.204118
C	4.70204	-3.144558	-1.220979
C	5.483978	-4.114161	-0.589923
C	3.341519	-0.753487	-2.793319
C	4.346482	1.133148	-3.947629
C	4.757764	0.294504	-4.98174
C	3.635405	0.61215	-2.864919
C	5.074444	-4.673962	0.620671
C	2.168425	5.125582	-0.105845
C	2.561264	5.907896	0.983399
C	3.323935	3.916618	2.129163
C	3.61253	0.899347	2.746294
C	2.877396	0.240691	4.964672
C	4.192889	0.301813	5.429717
C	4.831363	1.172636	0.179612
C	6.649066	2.058118	-1.162665
C	7.231903	0.793357	-1.227477
C	6.626763	-0.281586	-0.571901
C	3.498419	-2.713543	-0.644903
C	5.437348	-0.09236	0.126962
C	3.106385	-3.271476	0.582417
C	4.929688	0.971929	3.225039
C	5.456789	2.249847	-0.460035
C	5.217375	0.671442	4.558005
C	2.585934	0.535345	3.632781
C	1.075961	-2.362158	-2.192747
C	4.444236	-1.067079	-4.938337
C	0.413483	-3.391122	-1.507554
C	-0.571584	-2.545683	-3.972584
C	-1.224277	-3.564289	-3.280564
C	-0.721128	-3.990121	-2.04986
C	-2.72157	3.075632	-1.370154
C	-1.783257	3.772859	-0.591018
C	0.572349	-1.952083	-3.435427
C	3.737865	-1.586336	-3.85564

C	3.133721	5.300216	2.100973
C	2.341913	3.743315	-0.072398
C	-5.455938	0.587364	0.511734
C	-3.817358	-2.249668	0.5387
C	-5.000155	-3.093343	-1.414664
C	-3.877844	-2.495123	-0.842252
C	-6.025392	-3.243041	0.76318
C	-4.90453	-2.640614	1.335543
C	-3.590532	-1.187215	5.14876
C	-3.787243	0.180576	5.35287
C	-2.903699	-0.753765	2.856788
C	-3.072751	0.614891	3.083826
C	-3.521054	1.078924	4.320968
C	-1.457085	-4.064624	1.399599
C	-3.146142	-1.650698	3.911795
C	-1.253733	-2.729735	1.760607
C	-0.17508	-2.398242	2.597256
C	0.68067	-3.391797	3.065736
C	0.477449	-4.725592	2.695328
C	-0.587808	-5.059145	1.859565
C	-6.08062	-3.465128	-0.613946
C	-6.4361	0.727776	1.492022
C	-5.62587	2.945264	1.982502
H	1.788818	-0.853852	1.368644
H	-1.599864	-0.929704	-1.435125
H	0.317869	0.521804	-2.707871
H	0.04949	-0.997986	-0.044845

Cartesian Coordinates of 4*-up

Symbol	X	Y	Z
Ir	-1.258295	-0.219546	-0.175219
Ir	1.484437	-0.432446	-0.829353
S	-0.137524	0.575958	-2.367974
S	-0.132929	-2.196911	-0.97886
P	2.455752	-1.955776	0.588169
P	2.850259	1.469633	-0.818242
P	-3.290841	-1.165242	-0.842379
P	-1.991701	1.658395	0.96517
H	-2.378712	-0.609323	-3.563398
H	-2.232528	-1.947692	-5.62083
H	-2.921603	-4.338892	-5.60708
H	-3.780587	-5.354525	-3.508443
H	-3.965256	-4.009441	-1.460402
H	-2.026533	-2.916042	1.114902
H	-2.889124	-4.518186	2.770773
H	-5.342407	-4.884299	3.010348
H	-6.915732	-3.65295	1.531193
H	-6.057383	-2.061181	-0.139682
H	-4.489968	-0.036937	-3.354673
H	-6.187016	1.679028	-3.754647
H	-7.428807	2.692257	-1.851566
H	-6.965905	1.900691	0.466801
H	-5.281782	0.172661	0.868451
H	-2.726066	-0.681867	2.551125
H	-4.586536	-1.229775	4.051827
H	-6.360765	0.460868	4.516898
H	-6.212942	2.707662	3.46187
H	-4.37316	3.242578	1.933524
H	-1.10252	-3.514146	4.806613
H	-0.202101	-5.237174	3.252785
H	1.324563	-4.589012	1.432181
H	2.092102	-3.184842	-2.101419
H	2.931025	-5.275601	-3.108959
H	4.338127	-6.832305	-1.77644
H	5.459717	-1.301103	4.562669
H	7.371856	-0.539238	3.173682
H	7.135935	-0.45075	0.69539

H	5.004318	-1.086441	-0.366812
H	3.379736	0.451964	-3.451668
H	5.423491	0.03925	-4.772468
H	7.66011	0.541614	-3.804012
H	7.821628	1.490382	-1.513133
H	5.78358	1.916704	-0.199118
H	2.727205	0.612966	1.964005
H	3.693708	1.482788	4.059929
H	4.883678	3.670857	4.063001
H	5.052132	4.978145	1.955375
H	4.133991	4.068215	-0.145464
H	0.269763	2.724703	-0.7111
H	-0.695088	4.791589	-1.654256
H	0.657426	6.196933	-3.201882
H	2.972537	5.507818	-3.783215
H	3.941593	3.460003	-2.811633
H	4.908426	-6.265168	0.577736
H	4.098822	-4.165397	1.574287
H	3.323891	-1.931524	3.500236
H	-2.729867	1.941886	-1.784871
H	-3.655116	3.779926	-3.15223
H	-3.972041	6.037191	-2.152884
H	-3.368366	6.424739	0.227008
H	-2.486145	4.578986	1.599337
H	-0.142664	4.065854	0.958653
H	1.454596	4.917945	2.603701
H	1.745007	3.772019	4.786919
H	0.45231	1.699811	5.267604
H	-1.137701	0.824208	3.607502
H	1.03265	-0.47771	2.65969
H	-0.453481	-1.134566	4.506966
C	0.084376	-4.196723	3.139749
C	0.959921	-3.832555	2.115985
C	3.029965	-3.522421	-0.192687
C	2.71294	-3.851356	-1.516308
C	3.972572	-5.911754	-1.333696
C	3.184642	-5.038376	-2.081599
C	4.293014	-5.594337	-0.01193
C	3.830131	-4.407093	0.551257
C	-0.058012	-1.894129	3.840561

C	-0.423327	-3.230556	4.009427
C	4.006374	-1.5345	1.490819
C	6.436245	-0.822492	2.703717
C	4.152072	-1.604774	2.881773
C	-3.211563	-2.197808	-2.362663
C	-4.532423	-0.239374	3.613028
C	-4.386804	2.27438	2.416317
C	-5.44528	1.964935	3.27185
C	-2.573433	3.113473	0.008619
C	-3.405218	3.95901	-2.112941
C	-3.58118	5.223078	-1.551945
C	-2.895414	2.91479	-1.339917
C	-5.527726	0.705073	3.866625
C	-2.621149	-2.399348	-4.714498
C	-3.00576	-3.741703	-4.705568
C	-3.594449	-3.544463	-2.365466
C	-3.98156	-2.342869	0.389786
C	-3.588695	-3.974496	2.145716
C	-4.963235	-4.180993	2.276284
C	-4.710313	-0.036352	-1.20263
C	-5.979122	1.36489	-2.737281
C	-6.680713	1.927835	-1.671937
C	-6.42117	1.487339	-0.374822
C	-3.388338	1.329701	2.139697
C	-5.451697	0.512547	-0.144107
C	-3.471603	0.074008	2.76365
C	-5.359004	-2.583231	0.504284
C	-5.006535	0.391411	-2.50632
C	-5.846823	-3.488773	1.447306
C	-3.097956	-3.063866	1.209998
C	-0.7737	2.37774	2.155758
C	-3.243385	5.441367	-0.213279
C	-0.574277	1.721466	3.380451
C	0.875238	4.031343	2.835781
C	1.043525	3.383719	4.057021
C	0.322669	2.218903	4.323399
C	1.338083	-2.49546	1.943718
C	0.807095	-1.527957	2.810022
C	-0.025108	3.533604	1.89306
C	-2.746491	4.39474	0.562277

C	-3.488687	-4.310176	-3.529071
C	-2.714574	-1.639735	-3.551477
C	5.100674	-1.128691	0.713306
C	4.4315	1.223586	-1.731584
C	5.504827	0.453827	-3.773641
C	4.35083	0.690137	-3.029861
C	6.851147	1.26823	-1.944576
C	5.693555	1.516093	-1.201374
C	4.559723	4.01144	1.958361
C	4.460414	3.278218	3.14432
C	3.406815	2.242157	0.755172
C	3.261488	1.550481	1.958666
C	3.801332	2.051002	3.143228
C	2.929064	3.746232	-2.550117
C	4.039005	3.497524	0.772248
C	2.178749	2.95704	-1.668591
C	0.869397	3.349434	-1.361552
C	0.323444	4.511367	-1.900669
C	1.081483	5.295201	-2.773052
C	2.380506	4.907674	-3.100373
C	6.760759	0.736573	-3.229801
C	6.305083	-0.772065	1.314229
C	5.360716	-1.245972	3.483572
H	-1.400463	-0.92241	1.211514
H	2.453609	-0.977747	-1.950987
H	-0.334576	-0.584077	-3.017029
H	0.289791	0.248519	0.472226

Cartesian Coordinates of 4*-do

Symbol	X	Y	Z
Ir	1.251748	0.278753	-0.059611
Ir	-1.525843	0.487134	-0.738104
S	0.175982	-0.437687	-2.25719
S	0.08356	2.251216	-0.774816
P	-2.421954	1.925767	0.807608
P	-2.961424	-1.364842	-0.913323
P	3.248129	1.23022	-0.849003
P	2.022526	-1.629064	0.985512
H	1.564095	1.44011	-3.251339
H	1.444626	3.044547	-5.104038
H	2.876079	5.082141	-5.094302
H	4.442125	5.468332	-3.203362
H	4.595994	3.847445	-1.369054
H	2.428361	2.78614	1.423296
H	3.627903	4.103967	3.135679
H	6.113871	4.214395	3.115264
H	7.380369	3.041473	1.327263
H	6.185311	1.755234	-0.399795
H	3.599052	0.233347	-3.58988
H	4.961025	-1.557855	-4.571842
H	6.585269	-2.816327	-3.166308
H	6.83998	-2.221421	-0.761318
H	5.493872	-0.424375	0.218135
H	3.139513	0.46058	2.613442
H	5.314738	0.820091	3.716827
H	7.087728	-0.926649	3.576184
H	6.644148	-3.029252	2.328595
H	4.484404	-3.366783	1.191667
H	1.332445	1.765991	5.103229
H	1.091533	3.847529	3.768372
H	-0.564527	3.968341	1.938856
H	-2.262232	3.356981	-1.790847
H	-2.794434	5.677838	-2.449846
H	-3.507163	7.331966	-0.736635
H	-5.956911	1.39789	4.338001
H	-7.739921	0.904944	2.680528
H	-7.199507	0.909228	0.248797

H	-4.896416	1.364878	-0.504425
H	-3.444714	0.130315	-3.363034
H	-5.459221	0.687688	-4.66812
H	-7.701365	-0.062134	-3.890723
H	-7.88927	-1.413566	-1.812972
H	-5.882798	-1.997069	-0.524485
H	-3.636829	-0.593494	1.816103
H	-4.813985	-1.693761	3.665825
H	-5.489542	-4.088374	3.460958
H	-4.959192	-5.333108	1.374649
H	-3.83311	-4.199577	-0.49744
H	-1.030042	-3.41865	-0.20552
H	0.103811	-5.19741	-1.445934
H	-0.422678	-5.587745	-3.847754
H	-2.122487	-4.166454	-4.975701
H	-3.277645	-2.386413	-3.731855
H	-3.715802	6.631542	1.639313
H	-3.230441	4.303535	2.290341
H	-3.647416	1.844779	3.584086
H	2.718877	-2.061719	-1.78013
H	3.282958	-4.05478	-3.115243
H	3.120348	-6.32577	-2.100891
H	2.365312	-6.568004	0.255069
H	1.821202	-4.569092	1.596692
H	-0.849261	-2.058537	1.355642
H	-2.197466	-3.104269	3.130038
H	-1.138617	-3.772791	5.277023
H	1.308592	-3.444079	5.590229
H	2.674131	-2.515022	3.773001
H	-1.803799	-0.052116	2.824425
H	-0.142782	-0.186124	4.620411
C	0.44414	2.998532	3.573831
C	-0.506404	3.078969	2.554517
C	-2.7036	3.666502	0.292903
C	-2.596484	4.066388	-1.044142
C	-3.287606	6.309096	-0.449635
C	-2.889763	5.380858	-1.411195
C	-3.402587	5.917036	0.885744
C	-3.121476	4.602359	1.252364
C	-0.253519	0.739351	4.064844

C	0.577935	1.830014	4.326017
C	-4.10773	1.624505	1.486266
C	-6.729381	1.114211	2.346431
C	-4.421469	1.64498	2.851331
C	3.116631	2.496675	-2.185575
C	5.132839	-0.106232	3.183189
C	4.652162	-2.456718	1.755067
C	5.879421	-2.262297	2.392002
C	2.250349	-3.168866	0.006834
C	2.963513	-4.175515	-2.086249
C	2.871356	-5.446098	-1.516664
C	2.649309	-3.045431	-1.331018
C	6.127428	-1.082894	3.096606
C	2.147077	3.216342	-4.295849
C	2.945215	4.360526	-4.287082
C	3.910578	3.652545	-2.184358
C	4.221345	2.146887	0.409697
C	4.191201	3.578644	2.371846
C	5.58624	3.643291	2.358591
C	4.432533	0.038182	-1.6044
C	5.07649	-1.316405	-3.520568
C	5.990331	-2.01927	-2.733542
C	6.135083	-1.685457	-1.387681
C	3.657203	-1.471521	1.816054
C	5.365579	-0.664864	-0.828902
C	3.904834	-0.304176	2.554039
C	5.619648	2.246956	0.383287
C	4.304625	-0.297456	-2.962476
C	6.297687	2.981916	1.356928
C	3.512353	2.839229	1.403924
C	1.0204	-2.248228	2.407455
C	2.449001	-5.582871	-0.191607
C	1.608325	-2.63105	3.622784
C	-1.133468	-2.969868	3.276678
C	-0.537198	-3.345176	4.481926
C	0.833869	-3.16401	4.655826
C	-1.343938	1.990434	2.287033
C	-1.206117	0.823342	3.052196
C	-0.364503	-2.408158	2.259101
C	2.137325	-4.45192	0.565707

C	3.823633	4.57737	-3.226782
C	2.223887	2.297168	-3.251053
C	-5.128492	1.377242	0.555874
C	-4.506793	-0.993504	-1.854805
C	-5.554011	0.097195	-3.763427
C	-4.413545	-0.227575	-3.030691
C	-6.917019	-1.082453	-2.162598
C	-5.773733	-1.419722	-1.434021
C	-4.67739	-4.290403	1.472914
C	-4.973538	-3.591586	2.646379
C	-3.651125	-2.300741	0.520248
C	-3.928132	-1.625227	1.711958
C	-4.59735	-2.253991	2.763089
C	-2.53927	-2.993432	-3.222558
C	-4.03159	-3.650277	0.415295
C	-2.243432	-2.761878	-1.874739
C	-1.283029	-3.575408	-1.247793
C	-0.638874	-4.590465	-1.949314
C	-0.933427	-4.804874	-3.297725
C	-1.884897	-4.006463	-3.929562
C	-6.812196	-0.324822	-3.327868
C	-6.42885	1.118713	0.982286
C	-5.726704	1.385818	3.277655
H	1.445909	0.931661	1.355944
H	-2.463775	1.144412	-1.819365
H	0.069608	-1.77007	-2.134518
H	-0.291739	-0.219323	0.549972